NTNU
Det skapende universitet

Modell for casing design

Marie Tøien

Petroleumsfag
Innlevert: juni 2015
Hovedveileder: Sigbjørn Sangesland, IPT
Medveileder: Bjørn Brechan, IPT

Norges teknisk-naturvitenskapelige universitet
Institutt for petroleumsteknologi og anvendt geofysikk

Abstract

Casing design is performed to evaluate all possible scenarios a well can be exposed to, making sure the casings can withstand the loads, temperatures and wear during the entire lifetime of the well. To approve a casing design the casings must have safety factors that are greater than the design factors. The goal of this study is to obtain a greater understanding of how casing design is performed and which assumptions and methods are most accurate. It is further desired to provide an indication of what methods and assumptions that are used in an industry leading software (ILS) for casing design.

The casing design model developed in present thesis consists of two main aspects; (1) evaluation and calculation of load cases and (2) temperature prediction. Both aspects are compared with results from the ILS. The load case calculation consists of pressure and resulting axial stress calculations of worst-case scenarios for a well. The load cases applied to the casing design model are during the production phase. The temperature prediction is based on methods found to be the most recognized in the literature.

The calculated pressure differentials under the conditions of the load cases are identical to the ILS results. The axial loads have similar trends and good match with the ILS axial loads. The ILS and the developed casing design model disagree on the philosophy behind the calculation of the axial load due to weight in the cemented part of the casing. It has been concluded that the greatest stress obtained from either bending or buckling should be applied if both occur at the same length of the casing. The ILS does not take this into consideration.

The wellbore temperature calculated by the casing design model has slightly lower temperatures than the ILS has calculated. The details in philosophy for calculating temperature in the ILS are not fully known. Since temperature logging data are not available, the true production temperature remains unknown. It is therefore difficult to conclude which model that predicts the most accurate results.

Sammendrag

Foringsrørdesign er utført for å evaluere alle mulige hendelser en brønn kan bli utsatt for. Foringsrørene må tåle lastene, temperaturene og slitasjen den kan bli utsatt for i løpet av brønnens levetid. For å godkjenne et foringsrørdesign må foringsrørene ha sikkerhetsfaktorer som er større enn designfaktorene. Målet med denne studien er å oppnå en bedre forståelse av hvordan foringsrørdesign er utført og hvilke antagelser og metoder som er mest korrekte å anvende. Videre er det ønske om at studien gir en indikasjon på hva slags metoder og antagelser som er tatt i en industriledende software (ILS) som utfører foringsrørdesign.

Modellen for foringsrørdesign, som er utviklet i denne masteroppgaven, består av to hovedaspekter; (1) evaluering og kalkulasjon av laster og (2) prediksjon av temperatur. Begge aspektene er sammenlignet med resultater fra ILS. Lastkalkulasjonene innebærer kalkulasjon av trykk og resulterende aksialspenning for de verst tenkelige hendelsene. Lasthendelsene som er anvendt i modellen for foringsrørdesign er under produksjonsfasen. Prediksjon av temperatur er basert på anerkjente metoder fra litteraturen.

Trykkdifferansen ved forhold under lasthendelsene er identiske som trykkdifferansen generert av ILS. De aksielle lastene fra foringsrørdesignet har lignende trender og matcher godt resultatene fra ILS. Modellen for foringsrørdesign og ILS er uenige i filosofien bak kalkulasjonene av aksielle laster forårsaket av vekten av foringsrøret i den sementerte delen. Det er konkludert med at den høyeste spenningen fra enten bøying eller buckling skal anvendes dersom begge forekommer ved samme sted i foringsrøret. ILS tar ikke dette i betraktning.

Brønntemperatur som er beregnet av modellen for foringsrørdesign har litt lavere temperaturer enn hva ILS beregner. Detaljene i filosofien for beregning av temperatur i ILS er ikke fullstendig kjent. De virkelige produksjonstemperaturene er ukjente ettersom temperaturlogger ikke er tilgjengelige. Det er dermed vanskelig å konkludere med hvilken modell som predikerer de mest korrekte temperaturresultatene.

Preface

This thesis is carried out at the Norwegian University of Science and Technology at the Department of Petroleum Engineering and Applied Geophysics, and is a final product of my specialization project and the course "TPG4520 – Drilling Engineering".

I would like to thank my supervisor Prof. Sigbjørn Sangesland for giving me the opportunity to write my master thesis under his guidance. A deep gratitude goes to my co-supervisor PhD student Bjørn Brechan for his expertise and follow-up throughout the last year at the university. I would also like to thank PhD student Jesus Alberto De Andrade Correia, who has been kind to share his knowledge of heat transfer in wellbores.

Table of Contents

List of Figures

1 Introduction

Motivation

Casing design is a complete set of calculations that models all the loads on the pipe and displays the resulting loads in an orderly manner. Casing design is calculated by simulation software that has built in assumptions based on theory behind each load case. These models and their assumptions are not always clear to the user.

State of the art

Simulation software makes it possible to combine advanced temperature prediction in the well with pressures and calculate resulting loads acting on the tubular strings in different scenarios.

Goals

The goals of this study were to establish a casing design model and through this obtain a greater understanding of how casing design is performed and which assumptions and methods that are the most accurate. The model was compared with a casing design model from an industry leading computer software (ILS) for high pressure high temperature (HPHT) wells. This provides an indication of what methods and assumptions the software uses and fuels the understanding of the philosophy in each case. It can detect unnecessary conservative or unlikely assumptions and theory. For simplicity, this thesis will focus on the production phase of the lifetime of the well.

Approach

A casing design model was developed to calculate temperature during production and the burst, collapse and axial load cases that work on the casing in a deviated oil-producing well. The theory of the casing limits, the design limit plot, and the different load cases is based on the theory presented in the specialization project by Tøien (2014). Specific production load cases have been chosen and will be analyzed in this thesis. Primarily, oil field units are used in the equations, but some equations are based on SI units when it is natural. All casing design models in the industry are applicable for both sets of unit systems, as the users could be from any company in the world. The results from the casing design model by present thesis and from the ILS model are compared and discussed. The burst, collapse and axial ratings of the

casing and the triaxial limits are calculated for the different casings in the well to find the safety factors. The risk of casing failure is detected in the casing design by comparing the safety factors with the design factors.

2 Theory

2.1 Casing Design Model

The casing design model evaluates all the scenarios, referred to as load cases, a well can be exposed to, and compare the results with the limit load the casing can withstand without failure. Casing failure depends on the differential pressure and the axial stress in the load cases and the casing limits. The theory is discussed closer in this chapter. Temperature prediction is performed to calculate the axial loads due to temperature changes.

2.1.1 Developing the Casing Design Model

The design limit plot and the safety factor plots are used to show if the casing will fail as a cause of any of the casing loads. The plots depend on the limits of the chosen casing and the resulting loads it is exposed to, as described in this chapter.

The potentially occurring differential pressure and the total axial loads on the casing for the different load cases are the input for the calculation behind the plots. The theory behind the axial loads and differential pressures acting on a casing are given in chapter 2.2.

The axial loads depends on several factors, among them are temperature. The temperature must be predicted for the condition of the well in each of the load cases. As only production loads are looked at in this casing design model, the temperature during production must be predicted. This theory is presented in chapter 2.3.

2.1.2 Assumptions and conditions of the wellbore

The casing design model is applied with three production loads acting on the intermediate and production casing. The buoyancy of the casing can be calculated in two different ways. The axial load due to weight of the casing is calculated by using the piston force acting upwards at the bottom of the casing to get the buoyancy. The wellbore properties are based on data from a real well. The well is horizontal in the reservoir section. It is chosen to have a deviated well with one-phase production with drilling mud in the annuli. Properties as drilling mud, casing shoe depth, casing grade, and the wellbore path are given in Appendix B.

In the temperature prediction it is assumed the annulus fluid is water for simplification of calculations. The temperature model used is applicable for two-phase flow, but lacks a model for the amount of gas that comes out of solution as the fluid flows up the well. It is therefore

valid for one-phase flow. The overall heat transfer coefficient in the calculations is based on the assumption that the conduction in the casing and tubing walls are negligible. To have equal values in both the casing design model and the ILS under the calculation of axial loads, it is chosen to use the wellbore temperature retrieved from the ILS (assuming drilling mud in the annulus) in the calculations.

2.1.3 Design Limit Plot and Safety Factor Plot

Both the design limit plot and the safety factor plot are graphical presentations of the loads and the limits of a specific casing and consists of two main elements; (1) the limit of the casing and (2) the load cases that acts on the casing during the lifetime of the well.

All scenarios the casing can be exposed to are calculated as different load cases. The casings have to withstand all the load cases throughout the lifetime of the well. The load cases occur during drilling and production. For simplicity this thesis will focus on three load cases that occur during production of the well. The load cases are defined as burst, collapse or axial load cases.

The burst, collapse, tension and compression limits must be calculated and depends on the properties of the chosen casing. The triaxial limits ellipse is defined by the Von Mises equivalent yield criterion. Tension in the casing reduces the collapse limit. The collapse pressure is calculated by accounting for the tension in the string.

The limits of the casing are plotted as an envelope consisting of burst, collapse, tension and compression limit depending on the properties of the chosen casing. The triaxial limits ellipse is also plotted in the design limit plot. The limits are divided by the design factors. The casing loads must be inside both the envelope and the ellipse to be sure the casing will not fail. The connection limits are marked by a red dotted line. The collapse pressure limit is calculated with different tension stresses, from zero to the maximum tension. The maximum tension is the yield strength of the casing divided by the design factor, which is the tension stress limit. As an example a design limit plot is given in Figure 2-1. The gas migration for the production casing is a collapse load. The tension in parts of the string causes the collapse pressure limit to reduce. The design limit plot gives a great overview of all load cases that act on the casing and whether or not casing failure is at risk. It is, however, not possible to know at which depths the loads are in the plot.

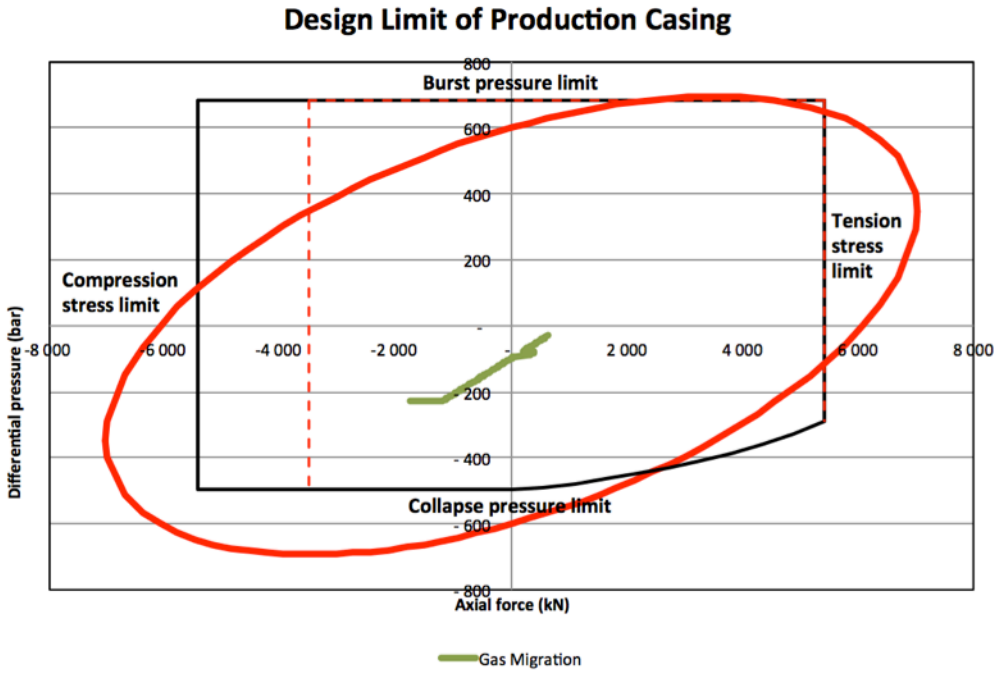

Figure 2-1 The figure is as an example of a design limit plot. The burst and collapse pressure is on the y-axis and the tension and compression stress is on the x-axis. The load case gas migration is plotted in the design limit plot and does not cause casing failure as it is inside the pressure limit, axial limit and the triaxial limit.

The load cases are also presented in a safety factor plot that shows the design factors of burst, collapse and the tension/compression limit as well as the safety factors of the burst or collapse pressure and the axial tension/compression of the different load cases evaluated. The safety factors of the load cases should be greater than the design factors to be certain there will be no casing failure. The safety factor plots allows an overview of the depth the casing is close to failure, and the type of failure. The figure below is used as an example of a safety factor plot.

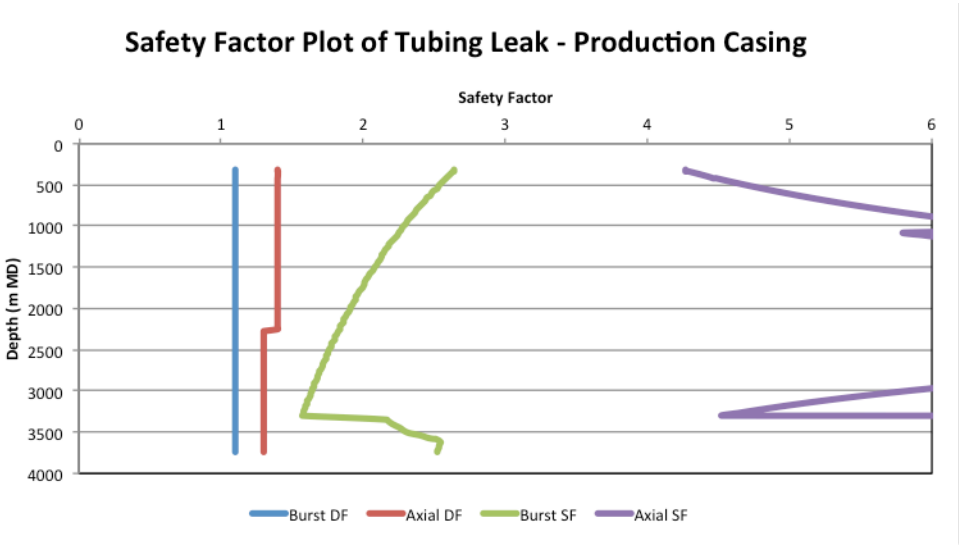

Figure 2-2 The figure is as an example of a safety factor plot. The plot is for the burst case of tubing leak acting on the production casing. As illustrated, there is no risk of casing failure because the safety factor of both the axial stress and the burst pressure is greater than the design factor.

The yield strength of the casing will be de-rated at higher temperatures. The default value in the ILS is that the yield strength de-rating factor is 1 at 68 °F and at 500 °F the de-rating factor will be 0.87. The ILS assumes a linear reduction in the yield strength as a function of temperature with a slope of 0.03 %/°F. In reality, the yield strength does not decrease linearly with the temperature increase. It is possible to insert values in the ILS to give a better estimate of the de-rating factor. The de-rating factors can be received from the producers of the casing. Instead of applying the temperature deration on the yield stress and producing several concentric ellipses for different temperatures, the temperature can be applied to the load case by plotting the pressure versus the axial load (Bellarby 2009, 518).

2.2 Casing Loads

The casing loads depend on both the differential pressure and the axial loads. This chapter will give the fundamental theory of loads acting on a casing.

2.2.1 Axial Loads

The axial loads are the sum of tension or compression forces due to the weight of the string, thermal extension or compression, ballooning effect, and bending of pipe due to dogleg in the wellbore or buckling. Axial load is defined as tension when positive and as compression when negative.

2.2.1.1 Weight of Casing

The weight of the casing contributes to axial stress. The stress is greatest in the top and decreases down the casing. There are two ways of calculating the buoyed weight of an object submerged in a fluid, either by the principles of Archimedes or by the piston forces. There is debate which method is correct. The ILS uses the piston forces when calculating the buoyancy. Aadnøy (2006, 40) states that the piston force gives the correct external axial loading, but that it is not suitable for failure calculations. The failure is not governed by the external stress alone, but depends on the three-dimensional stress. Below are both methods presented.

When a closed-ended string is submerged into a fluid with different density than the fluid inside the string, for instance when cementing a casing, the sum of forces by using the Archimedes principle yields a buoyancy factor expressed as follows:

$$\beta = 1 - \frac{\rho_o - \rho_i \left(\frac{d_i^2}{d_n^2}\right)}{\rho_s \left(1 - \frac{d_i^2}{d_n^2}\right)} \tag{1}$$

where

β = buoyancy factor

ρ_o = density outside the pipe (kg/m^3)

ρ_i = density inside the pipe (kg/m^3)

ρ_s = density of steel (7,83 kg/m^3)

d_i = inside diameter of pipe (in)

d_n = nominal outside diameter of pipe (in)

The force will be equal to zero in the bottom of the string and maximum at the top of the well in a vertical well for a free hanging casing. The tension of a deviated well is given as follows using the Archimedes principle of buoyancy (Hearn 1997, 2):

$$\sigma_z = \frac{L w_n \beta \cos\theta}{A_s} \tag{2}$$

where

σ_z = axial stress (psi)

L = length of pipe (ft)

w_n = nominal weight (lbm/ft)

θ = wellbore angle of inclination (radians)

A_s = cross-sectional area (in^2)

The piston force is the pressure that pushes the casing string upwards multiplied with the cross-sectional area. In cementing the float collar prevents flowback of cement. The piston force on the casing during cementing is expressed as (Aadnøy 2006, 44):

$$F_p = \left(\rho_i g Z \frac{\pi}{4} d_i - \rho_{cem} g (Z - Z_{TOC}) \frac{\pi}{4} d_n - \rho_o g Z_{TOC} \frac{\pi}{4} d_n\right) 14.50377 * 10^{-5} \quad (3)$$

where

F_p = piston force (lbf)

g = gravity coefficient (9.81 m/s^2)

ρ_{cem} = density of cement (kg/m^3)

Z = depth of casing (m)

Z_{TOC} = depth of TOC (m)

The axial load in the pipe when the piston force is used to calculate buoyancy is expressed as follows:

$$\sigma_z = \frac{L w_n \cos\theta + F_p}{A_s} \quad (4)$$

Both the Archimedes principle and the piston force will result in buoyancy that gives equal axial load at the top of the casing. The piston force will cause compression at the bottom of the casing, which will decrease upwards until a neutral point. Above the neutral point there will be tension.

2.2.1.2 Temperature Changes

Production of hot fluids causes compression and injection of cold fluids causes tension for a fixed pipe. The tension caused by the change in temperature from the initial temperature when the casing was set to production temperature is given as follows (Bellarby 2009, 489):

$$F_T = -c_T E \Delta T A_s \quad (5)$$

where

F_T = axial force due to temperature change (lbf)

c_T = coefficient of thermal expansion ($°F^{-1}$)

E = Young´s elastic modulus (psi)

ΔT = temperature change (°F)

Young´s elastic modulus for steel is assumed equal to 30 x 10^6 psi. The thermal expansion coefficient depends slightly on temperature and can vary from 5.5 x 10^{-6} -6 x 10^{-6} °F^{-1} for carbon steels and 13Cr pipes, while it is in the range of 7.5 x 10^{-6} -8.5 x 10^{-6} °F^{-1} for duplex steels.

2.2.1.3 Ballooning Effect

The ballooning effect is based on the changes in the average pressure inside and outside the pipe when comparing the initial conditions to conditions at the load case. The pressures at initial conditions are the pressure that acted on the casing when the well was completed (Lyons and Plisga 2011, 482). Pressure differential on a pipe can cause ballooning effects if the change in internal pressure times the inner area of the pipe subtracted by the change in external pressure times the area on the outside of the pipe gives a positive or negative answer. It is therefore not certain that a burst or collapse pressure in the pipe causes ballooning effect. Burst pressure may cause ballooning effect on the casing, while collapse pressure may cause negative ballooning effect. For a pipe that is fixed at the top and at the bottom, the ballooning effect induces tension, while negative ballooning effect induces compression. The force caused by ballooning effects is expressed as follows (Bellarby 2009, 487):

$$F_{bal} = 2\mu(A_i \Delta p_i - \mathrm{A_o} \Delta p_o) \quad (6)$$

where

F_{bal} = ballooning effect force (lbf)

μ = Poisson´s ratio (0.3 for steel)

A_i = area on the inside of the pipe (in^2)

A_o = area on the outside of the pipe (in^2)

Δp_i = change in internal pressure (psi)

Δp_o = change in external pressure (psi)

2.2.1.4 Bending and Buckling Effect

In deviated wells, the curved section has an increased axial tension on the convex side of the casing, and an increased axial compression on the concave side. Whether or not the axial load should be evaluated as tension or compression depends on the total sum of the axial loads. If the total sum of axial loads induced by weight, temperature and ballooning is positive, the

bending tension should be applied, but if the sum is negative the bending compression should be applied. The bending stress is expressed as follows (Bellarby 2009, 490):

$$\sigma_b = \pm \frac{E d_n \pi \alpha}{2 * 18000 * 12} \quad (7)$$

where

σ_b = bending stress (psi)

α = dogleg angle (°/100ft)

When a pipe is under sufficient compressional load, the initial configuration will become unstable. The pipe deforms by buckling to reach a more stable state. There are two types of buckling: sinusoidal and helical buckling. Buckling stress is a type of bending stress. The bending stresses caused by buckling are calculated by using a buckling-induced dogleg that is inserted in equation (7). The internal and external pressures have an effect on the buckling stresses. The effective buckling force is given as follows (Mitchell 2006, 305):

$$F_{eff} = -F_{tot} + p_i A_i - p_o A_o \quad (8)$$

where

F_{eff} = effective buckling force (lbf)

F_{tot} = total axial load (except bending forces) (lbf)

p_i = internal pressure (psi)

p_o = external pressure (psi)

Two processes induce buckling; mechanical buckling and pressure buckling (Lyons and Plisga 2011, 481). Mechanical buckling is due to axial stress in the casing. Pressure buckling occurs when the internal pressure is greater than the external pressure. The change in internal and external pressure affects the buckling force in two ways. First, a burst pressure with increased internal pressure compared with the external pressure, causes ballooning effect that decreases the buckling force. Second, a burst pressure will affect the p_iA_i - p_oA_o term that increases the buckling force. The second effect is greater than the first effect (Mitchell 2006, 305).

Buckling occurs when the effective buckling force is greater than a critical force, also called Paslay buckling force. The critical force is defined as follows:

$$F_c = \sqrt{\frac{EIw_c}{r_c}} \tag{9}$$

where

F_c = critical force (lbf)

I = moment of inertia (in^4)

w_c = casing contact load (lbf/in)

r_c = radial annular clearance (in)

The moment of inertia is expressed as follows:

$$I = \frac{\pi}{64}(d_n^4 - d_i^4) \tag{10}$$

The casing contact load in equation (9) is expressed as follows (Mitchell 2006, 305):

$$w_c = \sqrt{\left(w_e \sin\theta + F_{eff}\frac{d\theta}{dz}\right)^2 + \left(F_{eff}\sin\theta\frac{d\Theta}{dz}\right)^2} \tag{11}$$

where

w_e = distributed buoyed weight of casing (lbf/in)

Θ = wellbore azimuth angle (radians)

If the well does not change direction in the azimuth direction the casing contact load (w_c) in equation (9) is simplified to the buoyed weight of the casing, and the critical force F_c can be multiplied with the square root of sin(θ) (Bellarby 2009, 494). Whether there is sinusoidal or helical buckling depends on the relationship between the effective buckling force and the critical force. Sinusoidal buckling is approximated to occur when $2.8F_c > F_{eff} > F_c$, while helical buckling occurs when $F_{eff} > 2.8F_c$. If $F_{eff} < F_c$ no buckling occurs. The maximum helix angle, λ_{max}, of sinusoidal buckling is given by the following equation (Mitchell 2006, 306):

$$\lambda_{max} = \frac{1.227}{\sqrt{2EI}}F_{eff}^{0.04}\left(F_{eff} - F_C\right)^{0.46} \quad \text{for } 2.8F_c > F_{eff} > F_c \tag{12}$$

where

λ_{max} = maximum helix angle

The helix angle of helical buckling is defined as the following:

$$\lambda = \sqrt{\frac{F_{eff}}{2EI}} \qquad \text{for } F_{eff} > 2.8F_c \tag{13}$$

where

λ = helix angle

The buckling-induced dogleg can be calculated when the helix angle of either sinusoidal or helical buckling is defined:

$$\alpha = 68.755 r_c \lambda^2 \tag{14}$$

The corresponding bending stress for sinusoidal buckling using the equations above yields (Mitchell 2006, 307):

$$\sigma_b = \pm 0.3151 \frac{d_n r_c}{I} F_{eff}^{0.08} \left(F_{eff} - F_c\right)^{0.92} \tag{15}$$

$$\text{for } 2.8F_c > F_{eff} > F_c$$

Similarly, the helical buckling is expressed as:

$$\sigma_b = \pm 0.2500 \frac{d_n r_c}{I} F_{eff} \qquad \text{for } F_{eff} < 2.8F_c \tag{16}$$

2.2.2 Burst and Collapse Pressure Load Cases

The internal and external pressures of the casing are calculated in the case of tubing leak, gas migration and full evacuation. A burst load is calculated assuming the greatest possible pressure internally and the lowest possible pressure externally to the relevant casing, while opposite for a collapse load. On subsea wells each annulus has an initial wellhead pressure as a result of the mud column in the annulus and the offset of the rotary table and the wellhead. The assumptions of the load cases are described and illustrated with equations and drawings in this chapter. It is chosen to apply SI units in this chapter.

2.2.2.1 Tubing Leak

Tubing leak is a burst case scenario for the production casing assuming a tubing leak has occurred below and close to the wellhead into the A-annulus. Wellhead pressure in the A-annulus is set to maximum shut-in pressure, which is the reservoir pressure subtracted by the hydrostatic column of gas. This assumption is conservative for oil wells. It is assumed the A-

annulus is filled with packer fluid, while the B-annulus is filled with deteriorated mud. Below TOC in the B-annulus pore pressure is assumed.

The internal pressure is given by:

$$P_i = P_{i,WH} + \rho_m g Z \tag{17}$$

$$P_{i,WH} = P_{res} - \rho_{res} g Z_{res} \tag{18}$$

where

P_i = internal pressure (Pa)

$P_{i,WH}$ = internal wellhead pressure (Pa)

ρ_m = mud density (kg/m^3)

P_{res} = reservoir pressure (Pa)

ρ_{res} = reservoir fluid density (kg/m^3)

Z_{res} = reservoir depth (m)

The external pressure above TOC is given as follows:

$$P_o = P_{WH} + \rho_m g Z \tag{19}$$

where

P_o = external pressure (Pa)

P_{WH} = wellhead pressure (Pa)

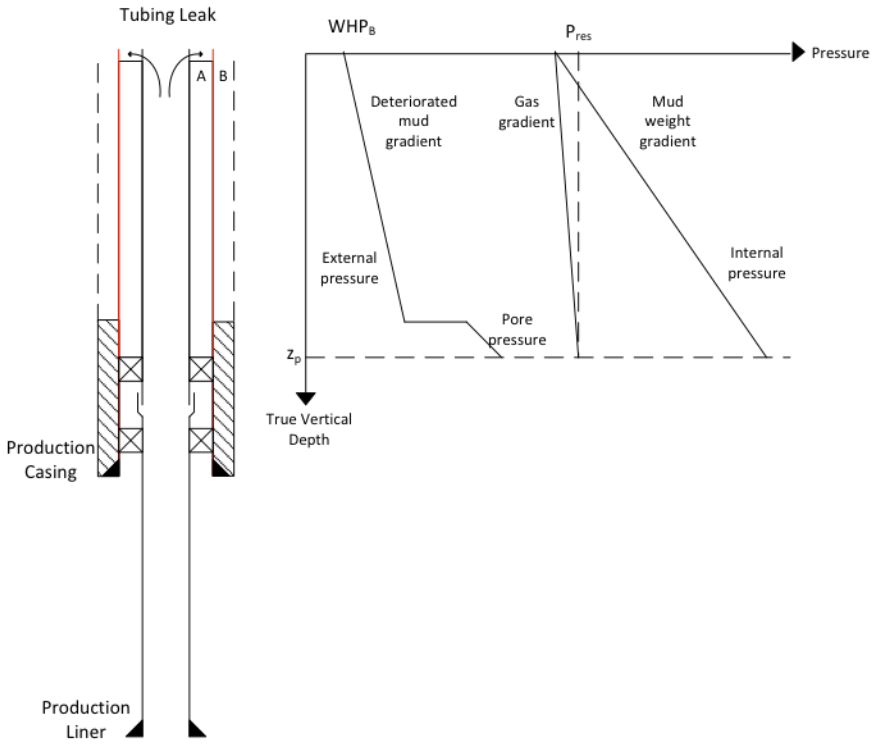

Figure 2-3 Illustration of tubing leak and the internal and external pressure on the production casing.

Figure 2-3 illustrates how the internal and external pressure depends on depth of the casing and the cement. The differential pressure for the conditions during tubing leak is greatest at TOC.

2.2.2.2 Gas migration

For subsea wells where a production liner has been run and where the option of B-annulus pressure monitoring is lacking and there is no possibility to bleed off pressure in the annulus, the production casing and the intermediate casing should be designed to withstand the gas migration case. Gas migration is the case when gas bubbles from the reservoir migrate up cement channels outside the liner and the production casing and gathers below the wellhead in B-annulus. The pressure in the annulus at wellhead is therefore assumed to be equal to the reservoir pressure. The annulus is filled with mud that contribute to hydrostatic pressure. However, the pressure at the intermediate casing shoe cannot exceed the fracture pressure at the same depth. The pressure in the annulus is determined by the lowest pressure of either the fracture pressure at the casing shoe of the intermediate casing or the reservoir pressure. The load from gas migration causes burst pressure to the intermediate casing and collapse pressure to the production casing. The pressure in the C-annulus is equal to the wellhead pressure and the hydrostatic column of deteriorated mud and pore pressure in the cemented area. This

pressure is used for the burst load of the intermediate casing. The collapse load of the production casing depends on the pressure in A and B annulus. The wellhead pressure and the hydrostatic pressure of the deteriorated packer fluid give the pressure in A-annulus. The external pressure below TOC is assumed to have a pressure gradient given by the density of brine.

The differential pressure of the intermediate casing due to gas migration causes burst pressure. The external pressure is calculated with the same assumptions as for the tubing leak in equation (19). The internal pressure at the casing shoe is the lowest value of the two equations:

$$P_i = P_{res} + \rho_m g Z \tag{20}$$

$$P_i = P_{frac,\ shoe} \tag{21}$$

where

$P_{frac,\ shoe}$ = fracture pressure at casing shoe (Pa)

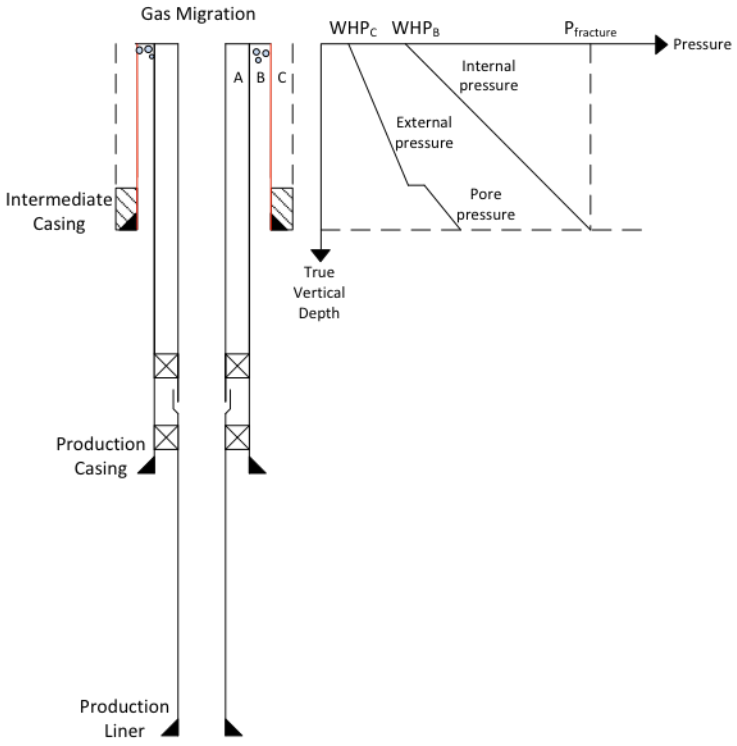

Figure 2-4 Illustration of the burst load case of gas migration and the internal and external pressure on the intermediate casing.

The gas migration causes collapse pressure on the production casing. The external pressure is expressed in equation (20) or (21). The internal pressure is given by:

$$P_i = P_{WH} + \rho_m g Z \tag{22}$$

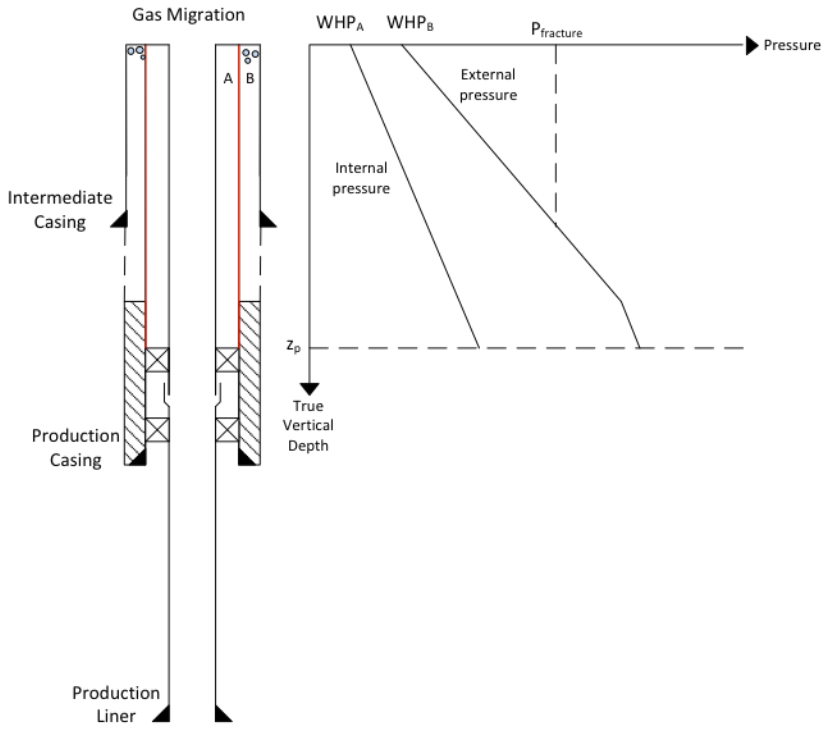

Figure 2-5 Illustration of the collapse load case of gas migration and the internal and external pressure on the production casing.

Figure 2-4 and Figure 2-5 illustrates the gas migration burst load case and collapse load case respectively. The figures explain how the internal and external pressures behave given by equation (20) to equation (22).

2.2.2.3 Full Evacuation

Full evacuation is a collapse load working on the production casing in wells with gas where the injection pressure is lost. The load may also be applicable for gas wells or wells in late life with high gas-oil ratio in the case of a leak in the production packer. The leak causes communication between the tubing pressure and the annulus pressure. The annulus may be partly or fully filled with gas, depending on the depth of the gas lift valve (below the gas lift valve there will be packer fluid) or the tubing pressure if there is a leak. In the casing design model the annulus is assumed fully evacuated of fluids, such that the annulus has a pressure

equal to the atmospheric pressure. The external pressure depends on the wellhead pressure and the hydrostatic pressure of mud weight above TOC and of brine below TOC.

The internal pressure is expressed as:

$$P_i = P_{i,WH} + \rho_m g Z \tag{23}$$

$$P_{i,WH} = P_{res} - \rho_{res} g Z_{res} \tag{24}$$

The external pressure is expressed as:

$$P_o = P_{WH} + \rho_m g Z \tag{25}$$

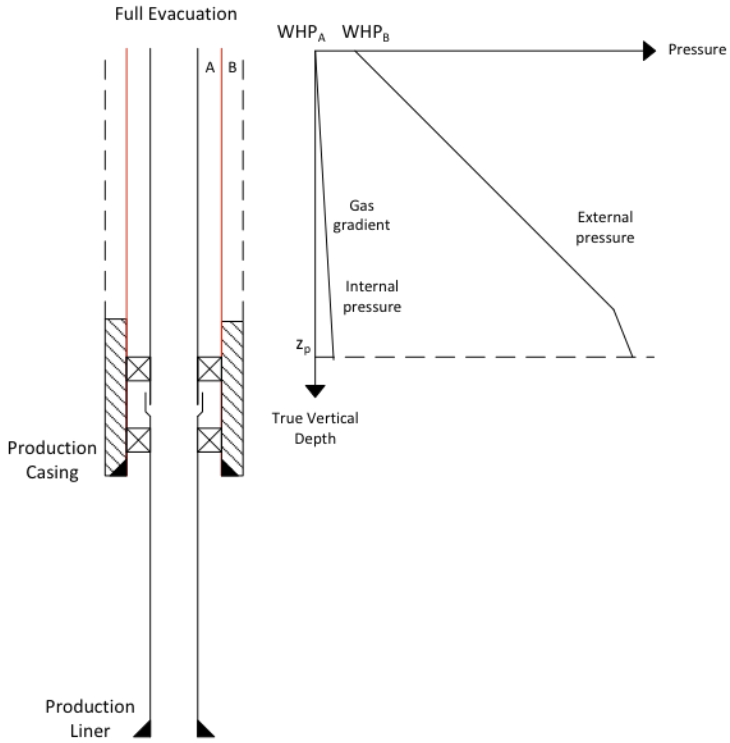

Figure 2-6 Illustration of the collapse load case of full evacuation and the internal and external pressure on the production casing.

Figure 2-5 illustrates the full evacuation load case acting on the production casing, supported by the equations.

2.3 Temperature Prediction

Temperature prediction is important for casing design as it affects the casing in two ways. Changes in temperature causes either expanding or compressing of the casing steel, and temperature also affects the casing by heating the annulus fluid, which can cause annular fluid

expansion. This chapter gives fundamental understanding of the theory behind temperature prediction for a flowing well with one-phase production.

2.3.1 Numerical Temperature Prediction Model

Temperature prediction during flowing of the wellbore or injection of gas or water must be performed for the entire well length. The heat flow in the wellbore is rapid, and can be viewed as steady state, while in the formation the heat transfer is time dependent. The models that are used assume steady-state heat transfer in the wellbore, while in the formation transient radial heat flow by conduction is assumed (Ramey 1962). The vertical heat transfer is neglected, and the geothermal gradient is used as the undisturbed temperature. The production and injection operations cause the highest temperature difference on the tubing and casings compared to the initial temperature when the pipe was installed. The temperature models are based on the total energy balance equation and radial transfer of heat in the wellbore (Sagar, Doty, and Schmidt 1991):

$$\frac{dH}{dL} = \frac{dQ}{dL} - \frac{v}{Jg_c}\frac{dv}{dL} - \frac{g_a \sin\theta}{g_c J} \tag{26}$$

$$\frac{dQ}{dL} = -\frac{2\pi r_{to} U_{to}}{w_t}\left(T_f - T_{wb}\right) \tag{27}$$

$$\frac{dH}{dL} = -\mu_{JT} c_{pm}\frac{dp}{dL} + c_{pm}\frac{dT_f}{dL} \tag{28}$$

where

H = specific enthalpy (Btu/lbm)

Q = heat transfer between fluid and surrounding area (Btu/lbm)

v = fluid velocity (ft/sec)

J = mechanical equivalent of heat (778 ft-lbf/Btu)

g_c = conversion factor (32.2 ft-lbm/sec^2-lbf)

g_a = acceleration of gravity (32.2 ft/sec^2)

r_{to} = outside tubing radius (in)

U_{to} = overall heat transfer coefficient (Btu/hr-ft^2-°F)

w_t = total mass flow rate (lbm/sec)

T_f = tubing flowing fluid temperature (°F)

T_{wb} = wellbore (earth interface) temperature (°F)

μ_{JT} = Joule-Thomson coefficient

c_{pm} = specific heat capacity of producing fluid (Btu/lbm-°F)

p = pressure (psi)

The calculation of the tubing fluid temperature for production wells starts at the toe of the producing section and is calculated by increments towards the wellhead. The calculation for injection operations starts at wellhead and it is calculated by increments towards the bottom of the well. The increments must be short enough to ensure that the change in both the inclination and the overall heat transfer coefficients are accounted for. In the casing design model steps of 30 m MD for the length of the well has been used. Solving equation (26), (27) and (28) yields the following equation for tubing fluid temperature:

$$T_f = T_e + A\left(1 - e^{(L_{in}-L)/A}\right)\left(-\frac{g_a \sin\theta}{g_c J c_{pm}} + \phi + g_T \sin\theta + e^{(L_{in}-L)/A}\left(T_{fin} - T_{ein}\right)\right) \quad (29)$$

where

T_e = surrounding earth temperature (°F)

A = coefficient (ft^{-1})

L_{in} = length of well form at start of increment (ft)

L = length of well at the end of increment (ft)

ϕ = coefficient combining Joule-Thomson and kinetic energy effects

g_T = geothermal temperature gradient (°F/ft)

T_{fin} = tubing flowing fluid temperature at start of interval (°F)

T_{ein} = surrounding earth temperature at start of interval (°F)

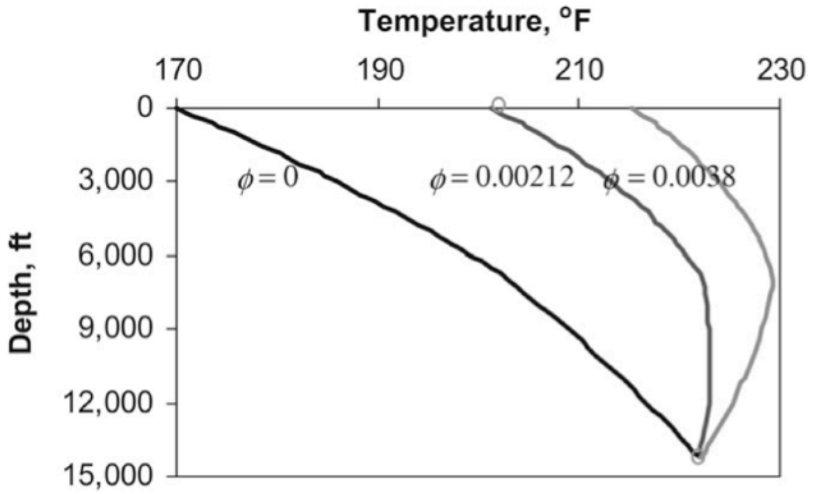

Figure 2-7 The figure illustrates how the temperature varies with ϕ. The tubing flowing fluid temperature has greater heat transfer with the cool surroundings if the ϕ is zero (Hasan, Kabir, and Wang 2009, Fig 4).

The coefficient ϕ is defined, as follows (Hasan and Kabir 1994):

$$\phi = \mu_{JT}\frac{dp}{dL} - \frac{vdv}{g_c J C_{pm}} \tag{30}$$

The correlation factor ϕ is part of the simplified method by Sagar, Doty, and Schmidt (1991), which gave the following empirical factor as a result of a study of 380 wells:

$$\phi = -2.978 * 10^{-3} + 1.006 * 10^{-6}p_{wh} + 1.906 * 10^{-4}w_t \tag{31}$$
$$-1.047 * 10^{-6}R_{gl} + 3.229 * 10^{-5}\gamma_{API} + 4.009 * 10^{-3}\gamma_g - 0.3551 g_T$$

where

p_{wh} = wellhead pressure (psi)

R_{gl} = gas/liquid ratio (scf/STB)

γ_{API} = oil gravity (°API)

γ_g = gas specific gravity

The effect of the values of ϕ is illustrated in Figure 2-7. The simplified method assumes that the Joule-Thomson effect and the kinetic-energy terms, μ and vdv respectively, are small and therefore combined into one term ϕ. The coefficient is approximated to zero when the total mass flow rate is greater than or equal to 5.0 lbm/sec (Sagar, Doty, and Schmidt 1991). The Joule-Thomson and kinetic energy effects are small for wells with low gas content in the

produced fluids, hence ϕ approaches zero. When ϕ is zero the temperature of tubing flowing fluid temperature is smaller.

The equations of total mass flow rate (w_t), the specific heat of produced fluid (c_{pm}), the coefficient A, the surrounding earth temperature (T_e), and the dimensionless temperature (T_D) are defined in Appendix B. The coefficient A depends on the thermal conductivity of earth. The Sagar, Doty, and Schmidt (1991) method suggests a value of the thermal conductivity of earth of 1.4 Btu/hr-ft-°F, which is higher than normal to compensate for the assumption that there is assumed no convection in the fluids in the annuli. It is chosen to use the value of 0.92 Btu/hr-ft-°F in the ILS and in both the methods applied in the casing design model.

The temperatures in the tubing and the casings are calculated using two different methods, namely the method presented by Sagar, Doty, and Schmidt (1991) and the method presented by Hasan and Kabir (1994). The two methods are both based on the theory of heat transfer in wellbores by Ramey (1962) and the detailed theory about the overall heat transfer coefficient in a wellbore by Willhite (1967). Ramey (1962) presents a method to calculate the wellbore temperature during injection of hot and cold fluids, while Willhite (1967) focuses on the details about the overall heat transfer coefficient for steam and hot water injection wells. The theory is also useful for production wells. Sagar, Doty, and Schmidt (1991) developed a model to predict the fluid temperature profile in a two-phase flowing well by using basic thermodynamic principles for deviated wells. They presented a simplified model designed for hand calculations that replaces the Joule-Thomson and the kinetic energy terms with a correlation, expressed in equation (31). In this thesis the temperature is predicted by assuming one phase oil-production, and the Joule-Thomson and kinetic energy effects term is set equal to zero. The model in Hasan and Kabir (1994) is based on the Sagar, Doty, and Schmidt (1991) model, but uses a more accurate method to find the overall heat transfer coefficient based on theory by Willhite (1967).

2.3.2 The Overall Heat Transfer Coefficient

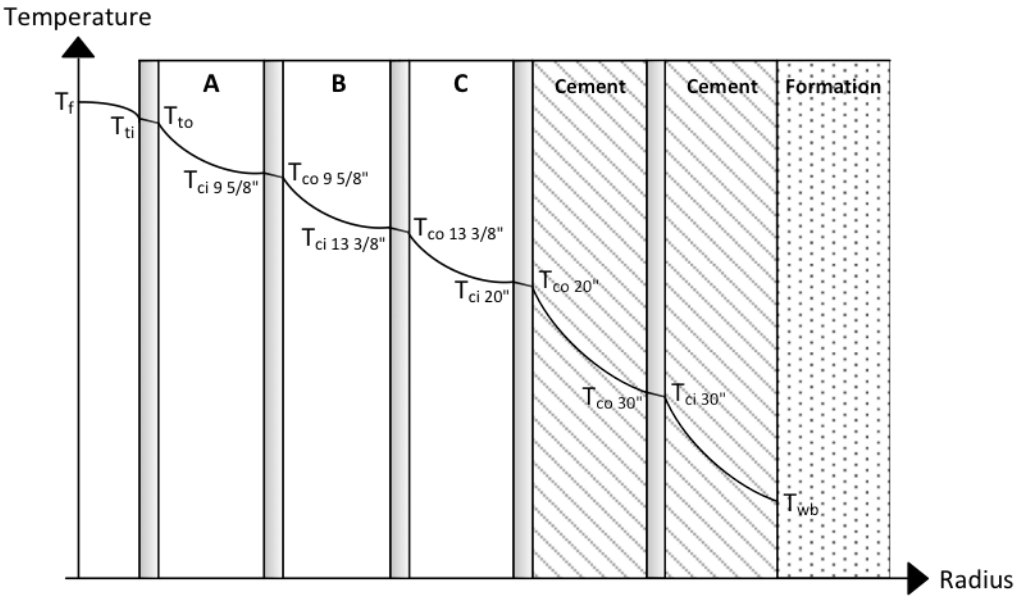

Figure 2-8 The wellbore temperature decreases with the radius. The hot production fluid in the tubing is cooled down by the formation outside the wellbore. To find the tubing and casing temperature the heat loss must be calculated. The figure is based on Willhite (1967, Fig. 6).

The temperature of the tubing and casings depends on the production fluid temperature and the cooling effect of the surrounding undisturbed formation temperature. The radial heat transfer over the wellbore is described by the overall heat transfer coefficient. The temperature profile in the wellbore for a producing well is illustrated in Figure 2-8. The figure shows that the temperature drop is almost negligible over the tubing and casing wall, and that it decreases more in the annuli with fluids. The highest temperature drop occurs in the cement. Willhite (1967) presented an extensive procedure to calculate the overall heat transfer coefficient by evaluating natural convection in fluids, conduction and radiation. Each of the heat transfer processes is described below.

The heat flow through a body is called conduction and is proportional to the temperature difference over the body. The thermal conductivity of steel is high as well as the wall is thin, which leads to that the temperature effect of conduction in the strings is negligible compared to the other heat transfer variables. Sagar, Doty, and Schmidt (1991), Willhite (1967), and Hasan and Kabir (1994) agree that the temperature effect of conductivity in the strings can be neglected when calculating the overall heat transfer coefficient. However, the conductivity in the cement has high effect on the overall heat transfer coefficient.

Fourier´s law gives the heat transfer by conduction as follows:

$$Q = -2\pi r \Delta L k \frac{dT}{dr} \tag{32}$$

where

r = radius (ft)

k = thermal conductivity of material (Btu/hr-ft-°F)

T = temperature (°F)

ΔL = length of increment of well (ft)

The equation can be solved for the temperature change over the cement as follows:

$$T_{ci} - T_{co} = \frac{Q}{2\pi} \frac{\ln(r_o/r_i)}{k_{cem}} \frac{1}{\Delta L} \tag{33}$$

where

T_{ci} = temperature of inner casing wall (°F)

T_{co} = temperature of outer casing wall (°F)

r_o = outer radius (ft)

r_i = inner radius (ft)

k_{cem} = thermal conductivity of cement (Btu/hr-ft-°F)

Natural convection in the annulus is heat transfer as a result of the fluid circling around in the annulus. During production the annulus fluid close to the inner wall will be heated up and have lower density and rise upwards, whereas fluid close to the outer wall will be cooled and denser and thus fall downwards. It causes a circulating flow in the annulus, which transfers heat from the inner string to the outer sting. The heat transfer in fluids in the annulus is a combination of conduction and convection. The conduction in the axial direction is small compared to convection, and is therefore neglected. The heat transfer coefficient for natural convection and conduction (h_c) is derived using the Fourier´s law for conduction and Newton´s law for cooling for convection. The term of convection and conduction in the annulus fluid presented in the casing design model should be used with caution for deviated wells as it is only expressed for vertical wells.

The heat transfer by radiation is radiant energy transferred from one string to another. Hasan and Kabir (1994) states that the radiant heat transfer over the annulus is negligible compared to the natural convection. The forced-convection heat transfer coefficient for flowing fluids in

the tubing (h_f), which is also referred to as film coefficient for heat transfer, is significantly high hence it can be ignored. Sagar, Doty, and Schmidt (1991) claims that both the radiation and convection is negligible and do only account for the heat transfer by conduction in the fluid in the annulus.

Newton´s law of cooling gives the heat transfer by convection as follows:

$$Q = 2\pi r \Delta L h \Delta T \tag{34}$$

where

h = radiative and convective heat transfer coefficient (Btu/°F-hr-ft^2)

The radiative and convective heat transfer coefficient in equation (34) is based on the outer surface area of the tubing or casing on the inside of the current annulus. It is also based on the temperature difference between the two strings. Solving equation (34) for the temperature difference yields:

$$T_{ci} - T_{co} = \frac{Q}{2\pi}\left(\frac{1}{r_i \Delta L (h_c + h_r)}\right) \tag{35}$$

where

h_c = convective heat transfer coefficient (Btu/°F-hr-ft^2)

h_r = radiative heat transfer coefficient (Btu/°F-hr-ft^2)

The convection in the annulus fluid is dependent on the outer and inner radius and the outer and inner temperature of the annulus. As an example the convection (h_c) in A-annulus, called h_{anA}, in Figure 2-8 is calculated by the following equations (Willhite 1967):

$$h_{anA} = 0.049 \frac{(N_{Gr} N_{Pr})^{\frac{1}{3}} N_{Pr}^{0.074} k_{an}}{r_{to} \ln\left(\frac{r_{ci\ 9\ 5/8"}}{r_{to}}\right)} \tag{36}$$

where

$$N_{Gr} = \frac{\left(r_{ci\ 9\ 5/8"} - r_{to}\right)^3 g_A \rho_{an}^2 \dot{T}\left(T_{to} - T_{ci\ 9\ 5/8"}\right)}{\mu_{an}^2} \tag{37}$$

$$\dot{T} = 1/T_{an} \tag{38}$$

$$T_{an} = \frac{T_{to} + T_{ci\ 9\ 5/8"}}{2} \tag{39}$$

$$N_{Pr} = \frac{c_{pa}\mu_{an}}{k_{an}} \tag{40}$$

where

h_{anA} = convective heat transfer coefficient for A-annulus (Btu/ °F-hr-ft^2)

N_{Gr} = Grashof number

N_{Pr} = Prandtl number

k_{an} = conductivity of annulus fluid (Btu/hr-ft-°F)

$r_{ci\ 9\ 5/8"}$ = inside radius of 9 5/8" casing (ft)

g_A = acceleration of gravity (4.17x10^8 ft/hr^2)

ρ_{an} = density of annular fluid (lbm/ft^3)

$\dot{T}$ = coefficient (°R^{-1})

T_{to} = temperature of outer tubing wall (°F)

$T_{ci\ 9\ 5/8"}$ = temperature of inside 9 5/8" casing wall (°F)

T_{an} = annulus temperature (°R)

μ_{an} = viscosity of annular fluid (lbm/ft-hr)

c_{pa} = heat capacity of annular fluid (Btu/lbm-°F)

The Prandtl number, N_{Pr}, is dimensionless and have a value of 7.5 for water (McAdams 1942, 414). For clarity, a full set of equations for temperature prediction for Figure 2-8 is presented in Appendix B.

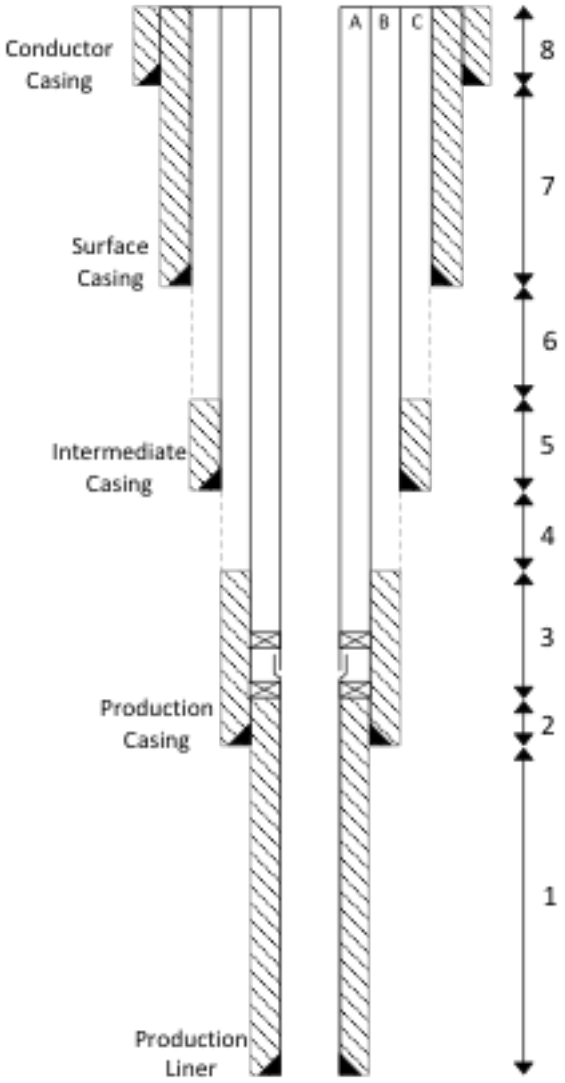

Figure 2-9 The well is divided into eight intervals that have different overall heat transfer coefficients.

The overall heat transfer coefficient varies as illustrated in Figure 2-9. At the top of the well the overall heat transfer coefficient is depending on the following factors: convection in the fluid inside the tubing and in A-, B-, and C-annulus, conduction in the cement in the surface casing and the conductor annulus, and conduction in the tubing and casing walls.

The goal is to find the casing temperatures as it affects the loads in the casing design. The overall heat transfer coefficient and the heat transfer rate are used to find the casing temperatures. The temperatures for the top of the well are illustrated in Figure 2-8. Under the assumptions that the conductivity of steel, the forced-convection in the tubing fluid and the radiative heat transfer can be neglected, the equation of the overall heat transfer coefficient in interval 8 in Figure 2-9 is given as follows (Hasan and Kabir 1994):

$$\frac{1}{U_{to}} = \frac{r_{to}}{r_{to}h_{anA}} + \frac{r_{to}}{r_{co\ 9\ 5/8"}h_{anB}} + \frac{r_{to}}{r_{co\ 13\ 3/8"}h_{anC}} + \frac{r_{to}\ln\left(\frac{r_{ci\ 30"}}{r_{co\ 20"}}\right)}{k_{cem}} + \frac{r_{to}\ln\left(\frac{r_{wb}}{r_{co\ 30"}}\right)}{k_{cem}} \quad (41)$$

where

$r_{co\ 9\ 5/8"}$ = outer radius of 9 5/8" casing (ft)

h_{anB} = convective heat transfer coefficient for B-annulus (Btu/ °F-hr-ft^2)

$r_{co\ 13\ 3/8"}$ = outer radius of 13 3/8" casing (ft)

h_{anC} = convective heat transfer coefficient for C-annulus (Btu/ °F-hr-ft^2)

$r_{co\ 20"}$ = outer radius of 20" casing (ft)

$r_{ci\ 30"}$ = inner radius of 30" casing (ft)

r_{wb} = wellbore radius (ft)

$r_{co\ 30"}$ = outer radius of 30" casing (ft)

The overall heat transfer coefficient based on the theory of Sagar, Doty, and Schmidt (1991) method for the same section is expressed as:

$$\frac{1}{U_{to}} = \frac{r_{to}\ln\left(\frac{r_{ci\ 9\ 5/8"}}{r_{to}}\right)}{k_{an}} + \frac{r_{to}\ln\left(\frac{r_{ci\ 13\ 3/8"}}{r_{co\ 9\ 5/8"}}\right)}{k_{an}} + \frac{r_{to}\ln\left(\frac{r_{ci\ 20"}}{r_{co\ 13\ 3/8"}}\right)}{k_{an}} + \frac{r_{to}\ln\left(\frac{r_{ci\ 30"}}{r_{co\ 20"}}\right)}{k_{cem}} + \frac{r_{to}\ln\left(\frac{r_{wb}}{r_{co\ 30"}}\right)}{k_{cem}} \quad (42)$$

where

$r_{ci\ 13\ 3/8"}$ = inner radius of 13 3/8" casing (ft)

$r_{ci\ 20"}$ = inner radius of 20" casing (ft)

The heat transfer into the formation is driven by heat conduction, and is a transient process. The transient radial heat conduction is given by:

$$Q = \frac{2\pi k_e(T_{wb} - T_e)\Delta L}{T_D} \quad (43)$$

where

k_e = conductivity of earth (Btu/hr-ft-°F)

T_D = dimensionless temperature

The rate of heat flow through a wellbore in equation (27) for steady state is expressed as:

$$Q = 2\pi r_{to} U_{to} (T_f - T_{wb}) \Delta L \tag{44}$$

The wellbore temperature can be calculated by combining the equation (43) and (44):

$$T_{wb} = \frac{T_f T_D + \frac{k_e}{r_{to} U_{to}} T_e}{T_D + \frac{k_e}{r_{to} U_{to}}} \tag{45}$$

The casing temperature with cement in the annulus is calculated by the conduction in the cement using equation (33) and (44):

$$T_{ci} = T_{wb} + \frac{r_{to} U_{to} \ln\left(\frac{r_{wb}}{r_{co}}\right)}{k_{cem}} (T_{to} - T_{wb}) \tag{46}$$

The casing temperature with fluid in the annulus is calculated by convection using equation (35) and (44):

$$T_{co} = T_{ci} + \frac{r_{to}}{r_{co}} \frac{U_{to}}{h_c} (T_f - T_{wb}) \tag{47}$$

Equation (47) is used to find the temperature of the outer casing wall where the annulus is fluid filled. As mentioned, a full set of equations (for the casing temperatures and the convective heat transfer coefficients) and a detailed description of the calculation procedure for the well in Figure 2-8 are presented in Appendix B.

The procedure to predict the tubing fluid temperature requires a comprehensive iterative procedure to find the convective coefficients for the annuli and the overall heat transfer coefficient and then finally calculating the tubing fluid temperature. This procedure is explained in Willhite (1967) and in Hasan and Kabir (1994). The methods in the two papers only apply to wells with only one annulus with fluid, while wells with two or more annuli with fluids causes greater workloads and more iteration to solve the equations to find the tubing fluid temperature. The comprehensive procedure is presented in the following flowchart.

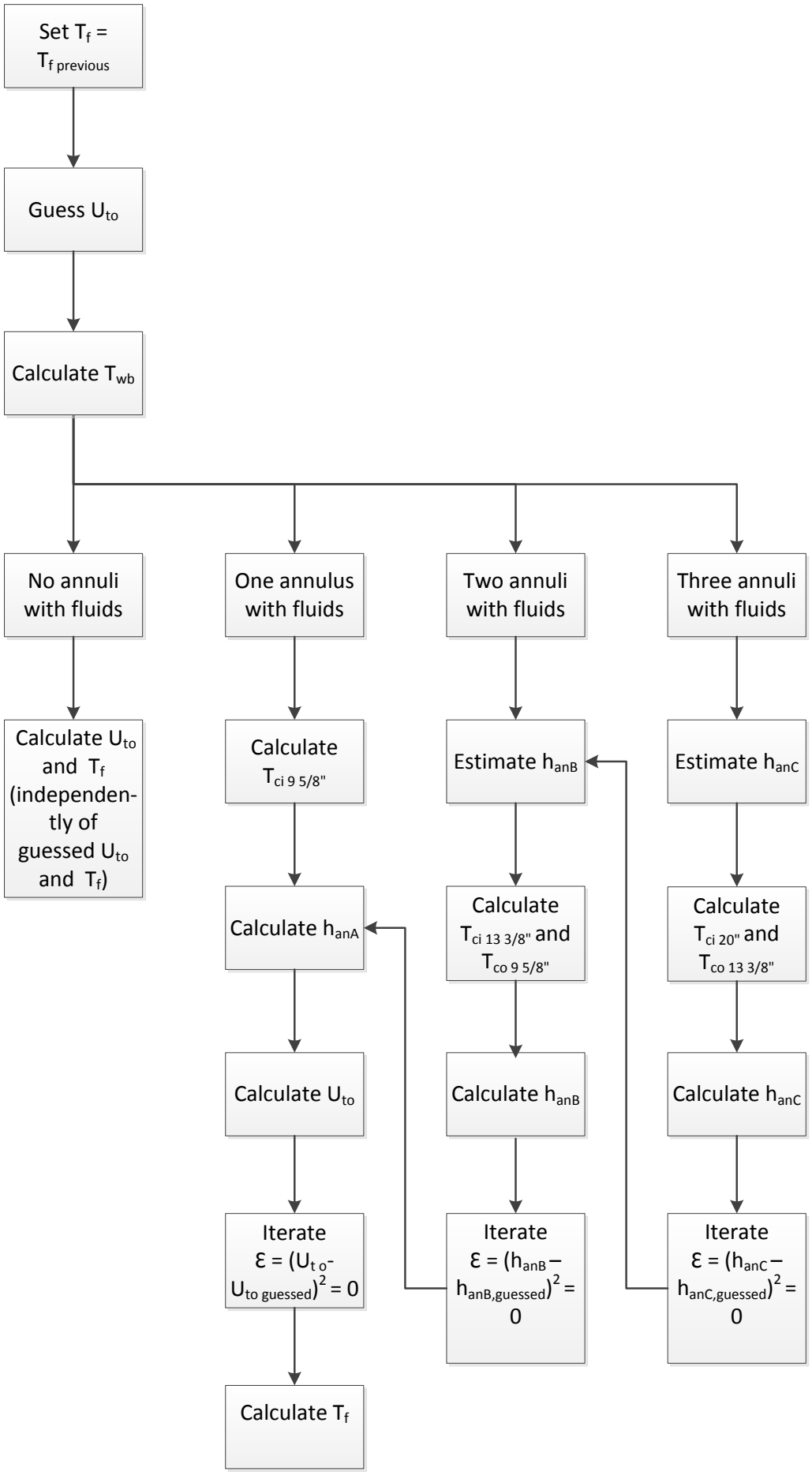

Figure 2-10 The flowchart illustrates the procedure to calculate the tubing and casing temperatures.

The first step in the temperature prediction is to guess an overall heat transfer coefficient for the entire wellbore at the depth of the increment and to assume a tubing fluid temperature. The wellbore temperature and temperature of casing with cement in the annulus can be calculated. The casing temperature of casings with fluids in the annulus is calculated by guessing the convective coefficients of the fluids. The convective coefficient is then calculated based on the casing temperatures. Iterative steps are carried out to find a true solution of the convective coefficient. If there are several annuli with fluids the same procedure is used. Finally, the overall heat transfer coefficient can be calculated based on convection in the annulus fluid and conduction in the cement. The calculated value must be iterated with the guessed value. At last the tubing fluid temperature is calculated. This procedure is performed for each interval until the final temperatures at the top of the well are found.

2.3.3 Friction Effect on Tubing Fluid Temperature

The friction between the tubing wall and the flowing production fluids contributes to a slight increase in tubing fluid temperature. The effect is, according to Çengel and Cimbala (2014), usually considered to have a negligible effect on the final temperature compared to the heat transfer in the well. The theory of simple calculations is included to investigate the actual effect the friction has on the temperature. The temperature rise due to friction is calculated assuming an adiabatic process (which is no heat exchange with the surroundings), which is incorrect, but may be a good approximation for small increments. Temperature rise as a function of the pressure drop due to friction is described in the following equation (Calhoun and Golmanavich 2004, 30):

$$\Delta T = \frac{\Delta P}{\rho c_p} \tag{48}$$

where

P = pressure (Pa)

ρ = density (kg/m^3)

c_p = specific heat capacity of producing fluid (J/kg-°C)

The pressure loss due to friction is given by the Darcy-Weisbach-equation expressed as (Larock, Jeppson, and Watters 2000, 10):

$$\Delta P = f \frac{L_{DW}}{D_i} \frac{\rho u^2}{2} \quad (49)$$

where

f = friction factor

L_{DW} = length of increment (m)

D_i = inside diameter of pipe (m)

u = average flow velocity (m/s)

The friction factor is found using Haaland´s equation (Lienhard and Lienhard 2011, 365):

$$\frac{1}{\sqrt{f}} = -1.8 \log\left(\left(\frac{\varepsilon/D}{3.7}\right)^{1.11} + \frac{6.9}{Re}\right) \quad (50)$$

where

ε/D = relative roughness

Re = Reynolds number

3 Results and Evaluation

3.1 Pressure Loads

The assumptions of load cases are described in section 2.2.2 and the result of the pressure loads are presented in Figure 3-1 to Figure 3-4. The casing design is applied to the production and intermediate casings of a deviated well. The load cases tubing leak, gas migration and full evacuation are evaluated for the production casing, and the gas migration is evaluated for the intermediate casing. The differential pressure is also plotted along with the ILS result. Both methods yields equal results.

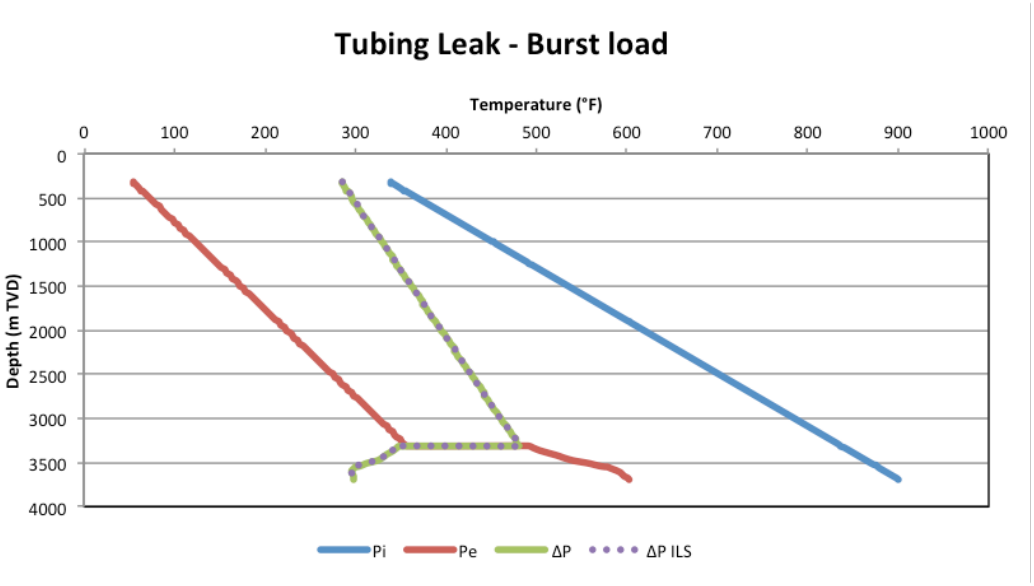

Figure 3-1 Internal and external pressure on the production casing during tubing leak.

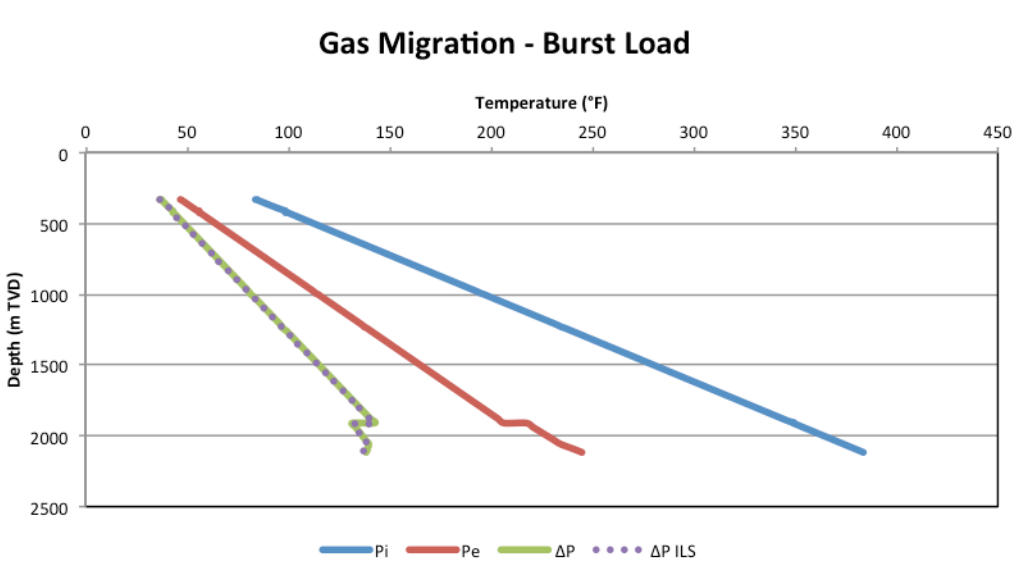

Figure 3-2 Internal and external pressure on the intermediate casing during gas migration.

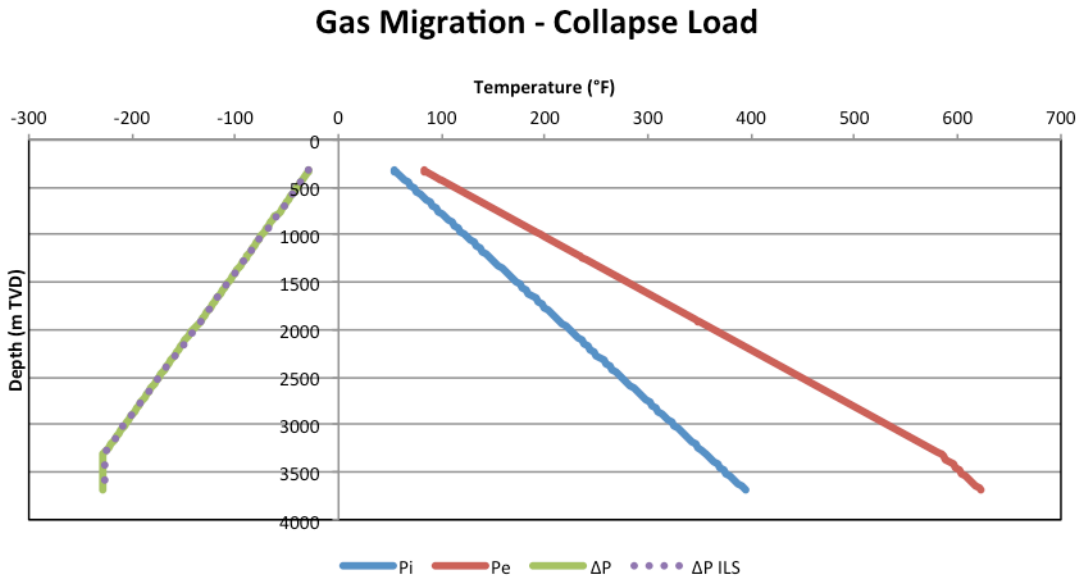

Figure 3-3 Internal and external pressure on the production casing during gas migration.

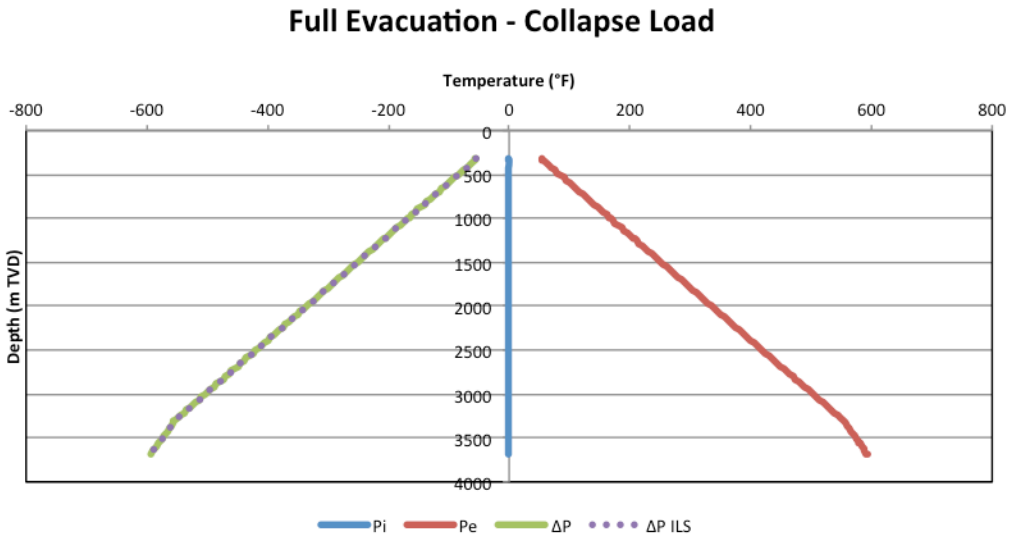

Figure 3-4 Internal and external pressure on the production casing during full evacuation.

3.2 Axial Loads

The axial loads are based on theory presented in chapter 2.2.1. The axial loads for each load case is plotted and commented in this chapter.

The total axial load is a sum of the axial load due to buoyed weight, temperature, ballooning, bending, and buckling. To show how the total axial load is affected by each of these effects, it is chosen to illustrate it with figures where each effect is added on stepwise. Bending and buckling depends on the sum of weight, temperature and ballooning, and is therefore added at last. The tubing leak load case on the production casing is used as an example, and the figure is presented below.

Buoyed weight:

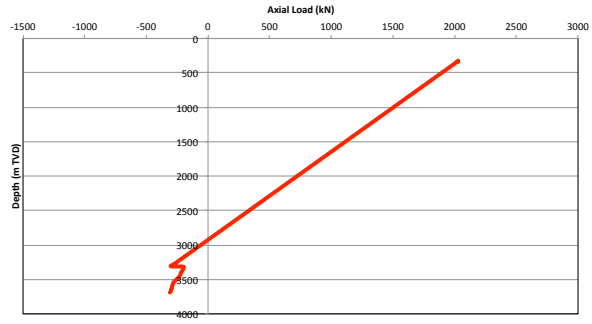

Buoyed weight and temperature:

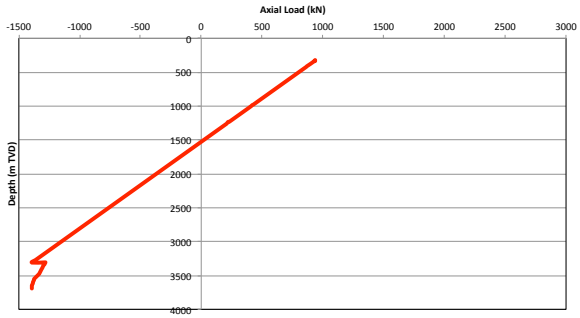

Buoyed weight and ballooning:

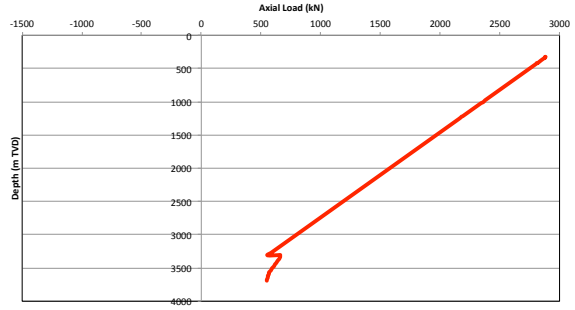

Buoyed weight, temperature and ballooning:

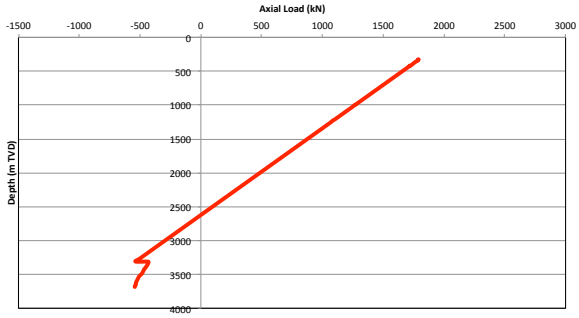

Buoyed weight, temperature, ballooning and bending:

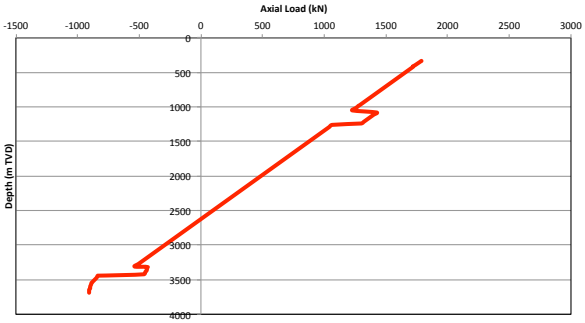

Buoyed weight, temperature, ballooning, bending and buckling:

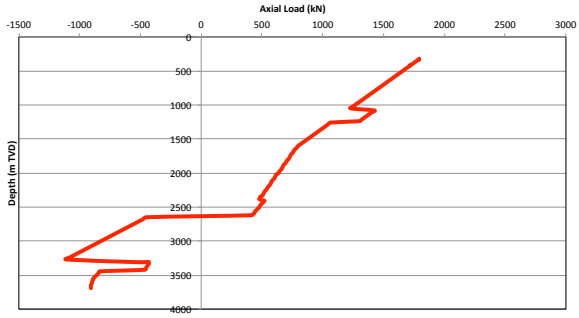

Figure 3-5 The effects of buoyed weight, temperature, ballooning, bending, and buckling are illustrated by adding them together stepwise. The figure at the bottom right is the total axial load.

The last figure at the bottom of Figure 3-5 is the total axial load in the casing as all the effects are added together. The casing design model always assumes worst-case scenario, therefore the axial load of bending and buckling depends on the total axial load. Tension is applied if the total axial load yields tension, and compression is applied if the total axial load yields compression. The effect is clear when observing the buckling that switches between tension and compression when the total axial load (besides bending and buckling) is equal to zero. The total axial load is zero at about 2600 m TVD.

The first plot in Figure 3-5 shows the axial load due to weight only. The axial load due to weight is calculated for initial conditions. It is assumed the casing is fixed at TOC and the

load will not change above that point. Below TOC it is assumed the weight of the casing under new pressure conditions will change. The weight of the casing below TOC in dry air subtracted by the piston force gives the new axial load due to weight in the cemented area. The piston force is calculated using the pore pressure. The piston force during the tubing leak case is smaller than under cementing. Therefore the axial load is reduced compared with the initial conditions.

The tension due to change in temperature is dependent on the temperature during the production and the temperature at initial state. The temperature at initial conditions should be the temperature of the casing when the cement job was finished. During circulation of the well the injected cold fluids will cool the wellbore down, but while the cement settles the casing temperature will be heated up by the formation and reach the undisturbed formation temperature. Undisturbed temperature is chosen as the temperature at initial conditions. To be able to compare the results of the models from the literature with the software all properties are the same. As the temperature model in the casing design model did not lead to the exact same temperature results as the ILS (which will be presented and discussed in chapter 3.4), it is chosen to use the temperatures from the ILS in the casing design model.

The ballooning effect depends on the change in average internal pressure and the change in average external pressure from initial conditions to the conditions of the load case. As explained in the theory and verified in the calculation; the ballooning effect causes tension for the burst loads and compression for the collapse loads. It is assumed the casing can move radially in the event of ballooning. The assumption is also applied in the ILS. The cement and the formation is assumed to be the weakest part and that the casing will push the cement and the formation out of the well.

Bending stresses occur where there are dogleg angles in the wellbore. The effect of bending in this model gives the same result as the software model, which is easy to spot in the plots when comparing the two models. The production and intermediate casing are both affected by the bended wellbore at depth of 1080-1239 m TVD, while the production casing is also affected by the bending at 3448-3692 m TVD.

If the effective buckling force is greater than the critical buckling force it is assumed to occur buckling in the casing. The effective buckling force depends on the total axial load in the

casing string and the internal and external pressure. The effective buckling force for the cemented casing section is calculated differently than the rest of the casing, which will now be described. To calculate whether or not there is buckling in the cemented section, the initial conditions must be considered, as the buckling will not change at that section after it is cemented. The total axial load is only based on the weight of the casing, as the temperature and ballooning effect do not contribute to axial stress under initial conditions. The internal and external pressures applied are the pressures under the initial conditions. For the rest of the casing the total axial loads are a sum of weight, temperature and ballooning stresses, and the pressures used are during the production load case conditions. This leads to no buckling in the cemented area for any of the load cases. In general the buckling stresses in this model correspond well with the software model.

The tension effect of temperature and ballooning are assumed to be constant for the entire casing string. The tension of buoyed weight will always be greatest at the top of the string and decrease further down and cause compression at the bottom. Bending and buckling effect on the casing are local axial loads and does only occur at the local area where there is dogleg due to bending or buckling.

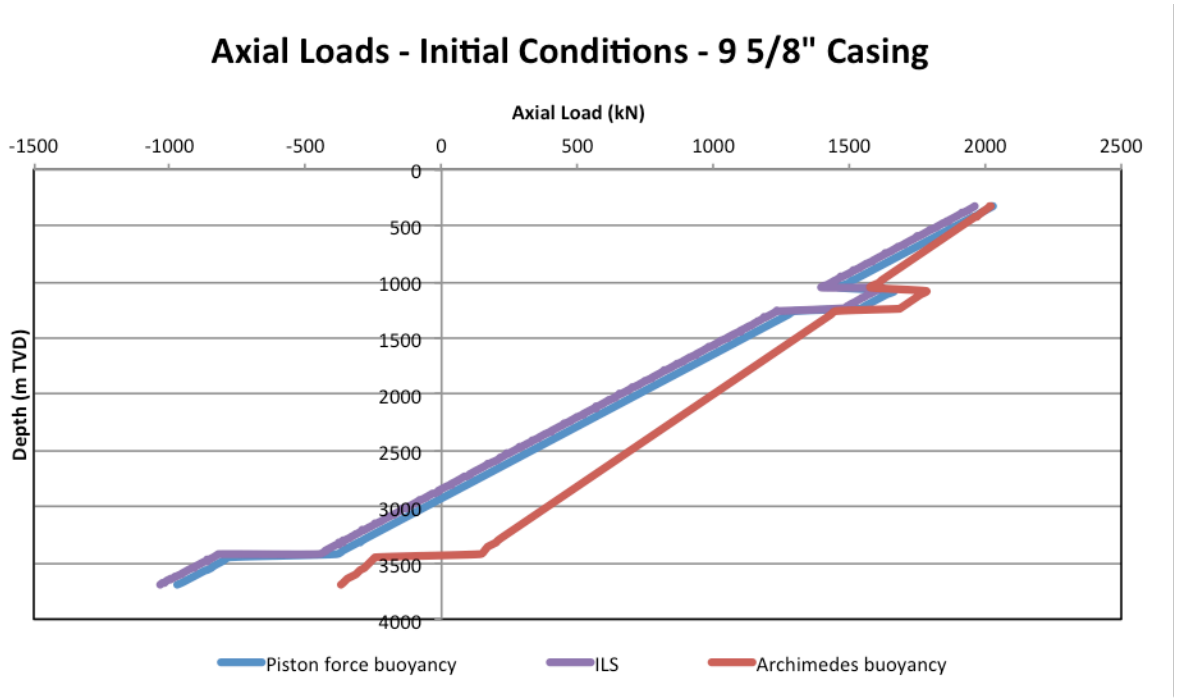

Figure 3-6 Axial load for initial conditions of the production casing illustrates the difference between the two methods of calculating buoyancy. By using the piston force added to the dry weight of the casing the result corresponds well with the ILS result. The Archimedes buoyancy factor multiplied with the dry weight of the casing yields a slightly different result, without any compression in the string. The tension in the string for the two different methods is equal at the top. Bending causes the deviations from the straight lines.

The procedure of calculating the axial load due to weight is, as mentioned in 2.2.1.1, debated. The two different procedures are illustrated in the figure above by calculating the total axial load for initial conditions of the production casing. The axial load due to weight is calculated by using the Archimedes principle and the piston force. The two results are compared with the ILS results. The tension at the top is equal for both methods. At the bottom of the casing the piston force induces compression, while the Archimedes principle causes zero axial load (if excluding the bending stresses).

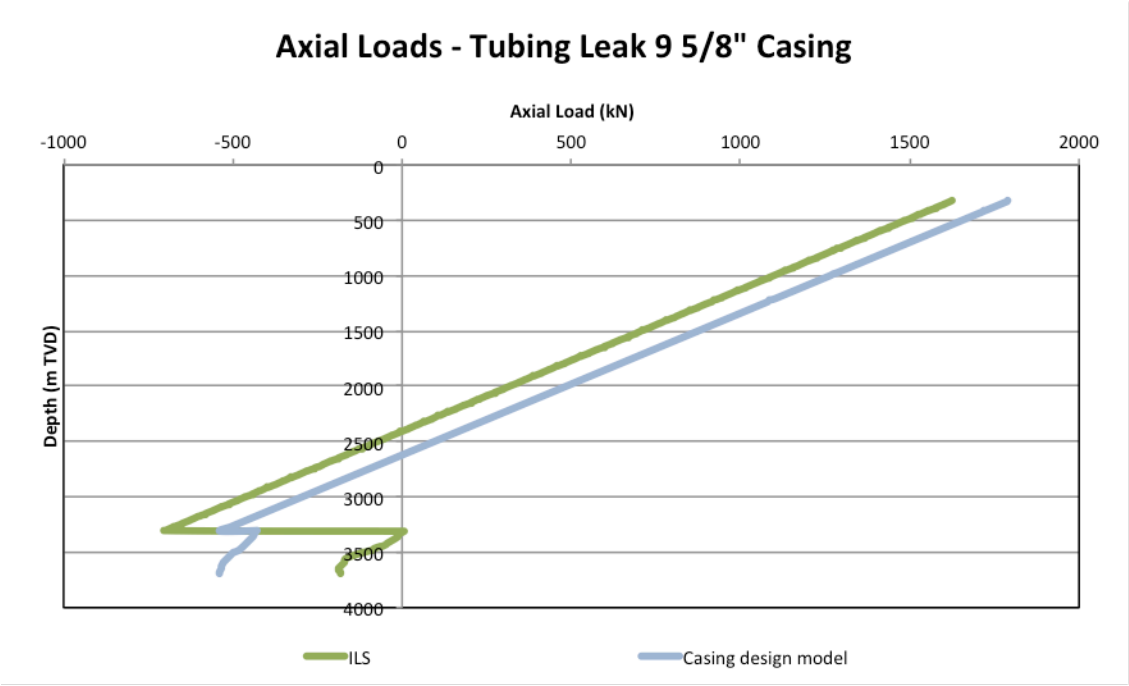

Figure 3-7 Axial loads on the production casing during tubing leak without bending and buckling. The casing design model yields results quite similar to the ILS results.

Figure 3-7 shows the axial load excluded bending and buckling for the tubing leak load case on the production casing. Above TOC the axial load due to weight of the casing for the ILS and the casing design method are equal as shown in Figure 3-6, assuming the ILS use the initial conditions for this calculation. In that case the result indicates that there is a slight difference between the axial load due to the temperature and/or the ballooning effect. If the ILS assumes a constant value of ballooning and temperature over the entire string, as assumed in the casing design model, the axial load due to weight changes below TOC compared with the initial conditions. The method used by the ILS is unknown. The results from the ILS only consist of the total axial load either with or without the bending and buckling loads. Therefore contribution of weight, temperature and ballooning as a separate load is not known.

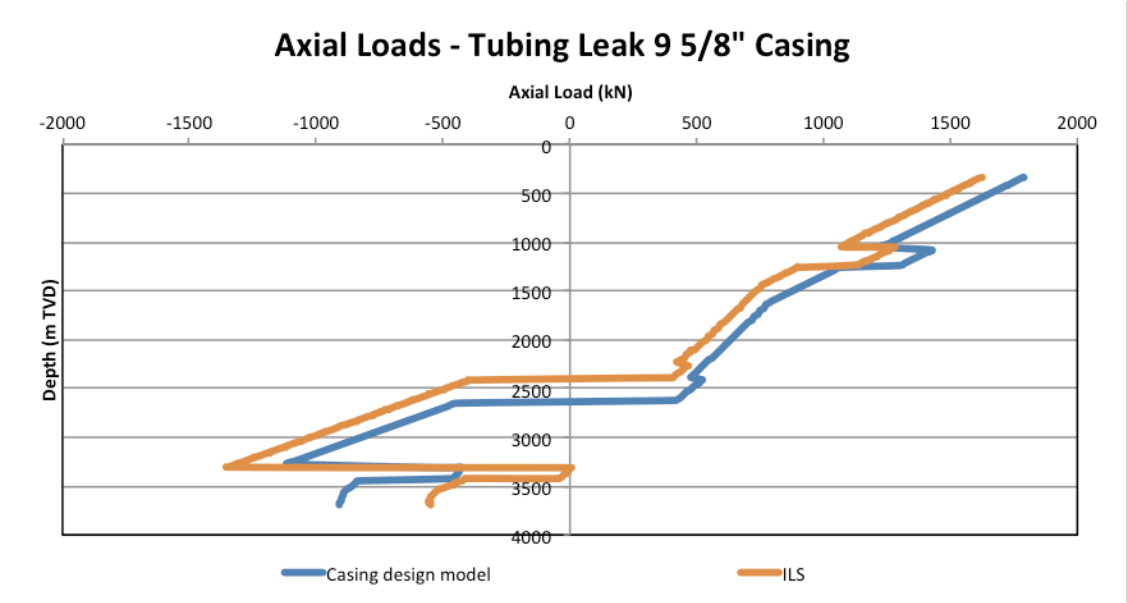

Figure 3-8 Axial loads on the production casing during tubing leak. The casing design model yields results quite similar to the ILS results.

Figure 3-8 shows the results of the casing design model and the ILS for tubing leak on the production casing. Buckling occur at approximately 1500 m TVD for both models. There is tension in the casing at this depth. The buckling occurs at this depth because the buckling pressure overcomes the fact that there is tension in the string, and yields buckling force. The differential pressure is 370 bar at 1600 m TVD where the buckling starts in the casing design model. The buckling gradually increases down the casing.

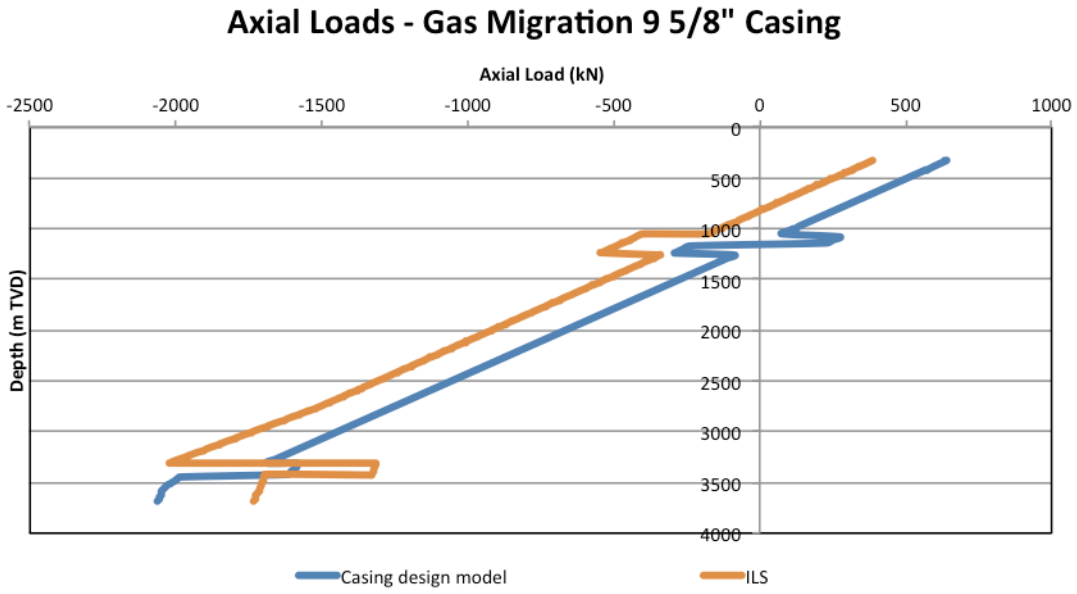

Figure 3-9 Axial loads on the production casing during gas migration.

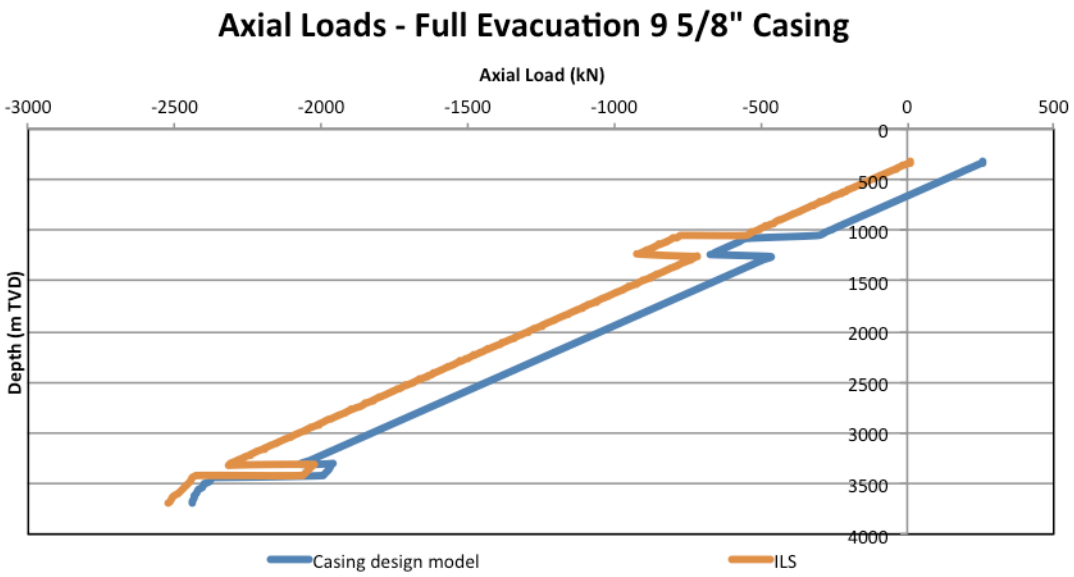

Figure 3-10 Axial loads on the production casing during full evacuation. The result from the casing design model is quite similar to the ILS result.

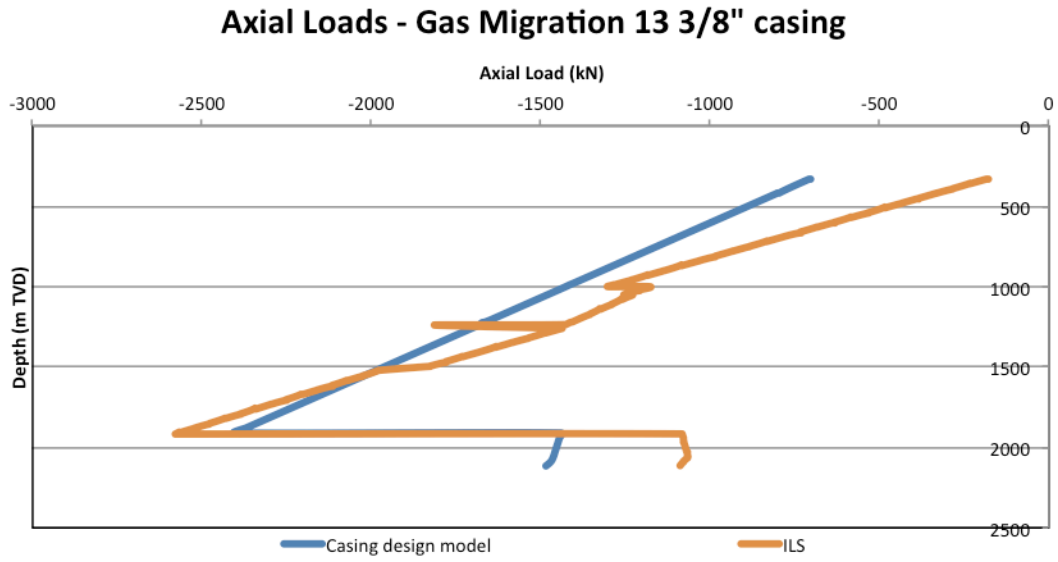

Figure 3-11 Axial loads on the intermediate casing during gas migration. The result from the casing design model does not match the ILS result perfectly.

Figure 3-11 shows the axial load for the intermediate casing during gas migration. The case gives buckling stress in a bended section in the wellbore at 1080-1239 m TVD. Interpreting the results from the ILS in Figure 3-11 shows that the ILS ignores the buckling in the bended section. The casing design has chosen to apply the greatest axial load of either bending or buckling and ignore the smallest in sections where both effects occur.

3.3 Safety Factor Plots and Design Limit Plots

The safety factor plots and the design limit plots are presented below. The safety factor plots are from the casing design model. The safety factor plots for the load cases retrieved from the ILS is included in Appendix C. The design limit plots are applied with the results from both the casing design model and the ILS, as it is easy to compare the two methods in that plot.

The burst and collapse load cases chosen in this study has the greatest differential pressure at the toe of the casing or at TOC. The safety factor is therefore lowest at these depths. The collapse pressure is dependent on the axial load, which will be discussed further in this chapter. The safety factors of gas migration on the production casing and the intermediate casing are greater in the casing design model than in the ILS.

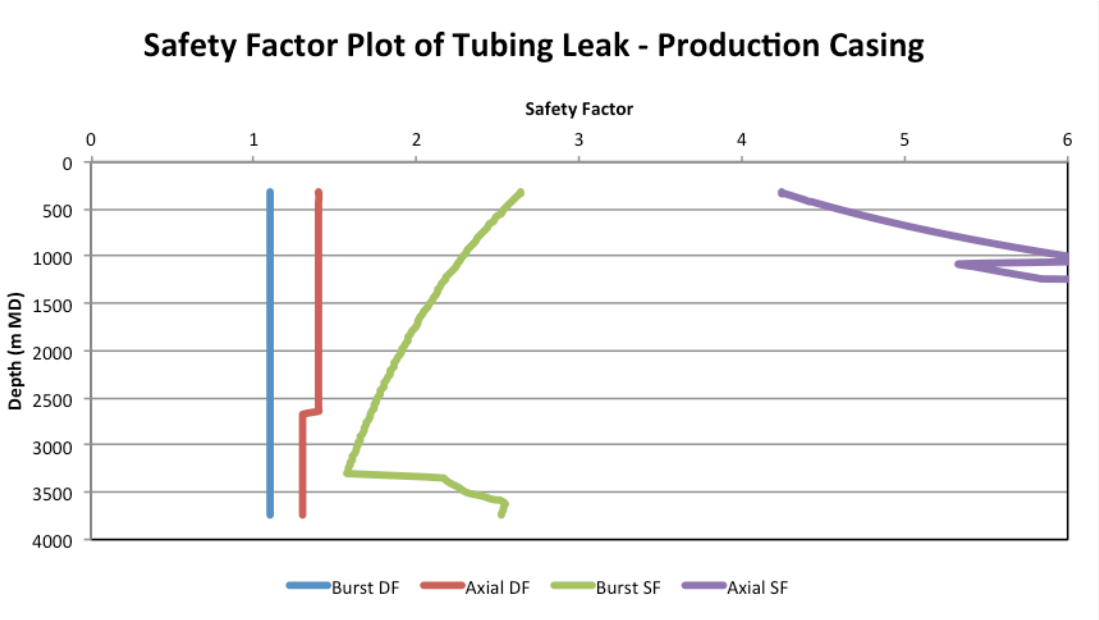

Figure 3-12 Safety factors of tubing leak acting as a burst case on the production casing. The load case does not cause casing failure.

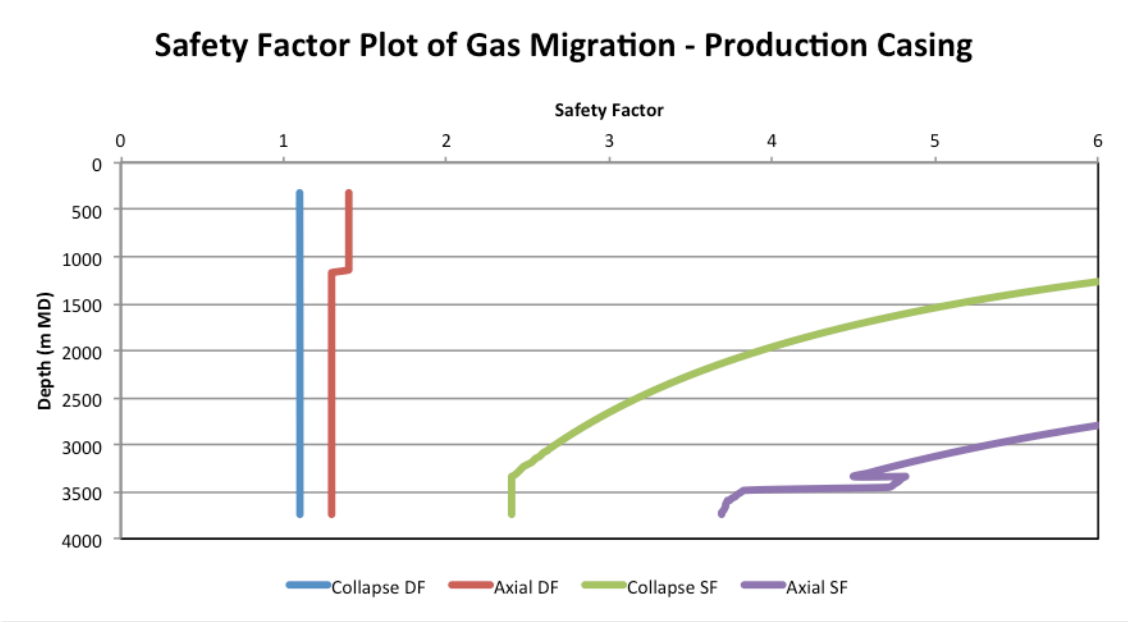

Figure 3-13 Safety factors of gas migration acting as a collapse case on the production casing. The load case does not cause casing failure.

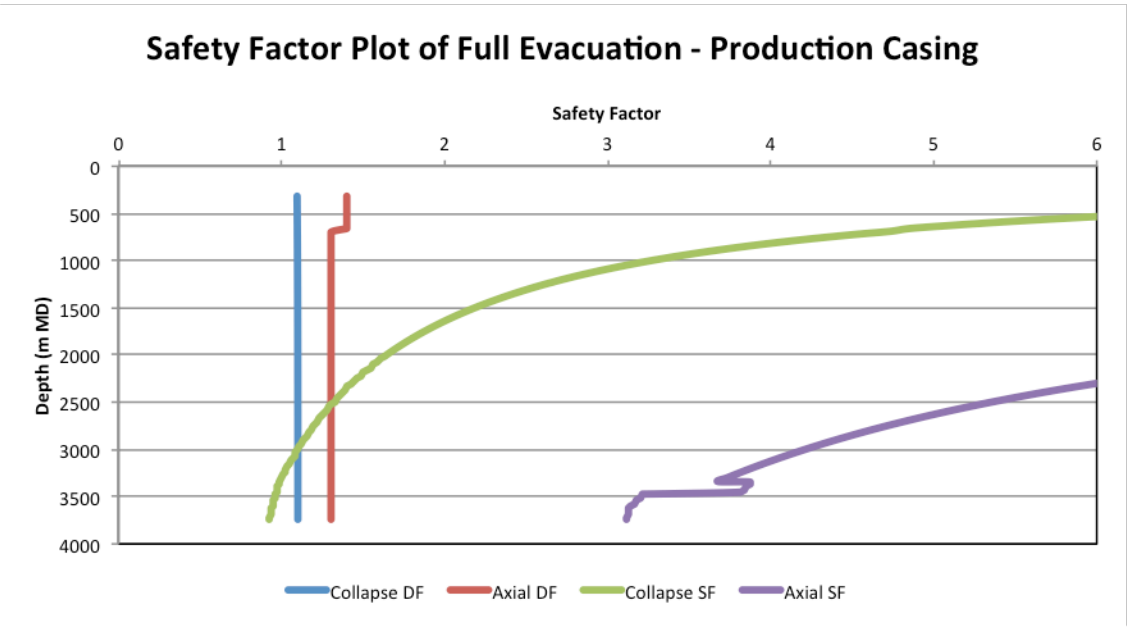

Figure 3-14 Safety factors of full evacuation acting as a collapse case on the production casing. The collapse safety factor is less than one, which induces casing collapse.

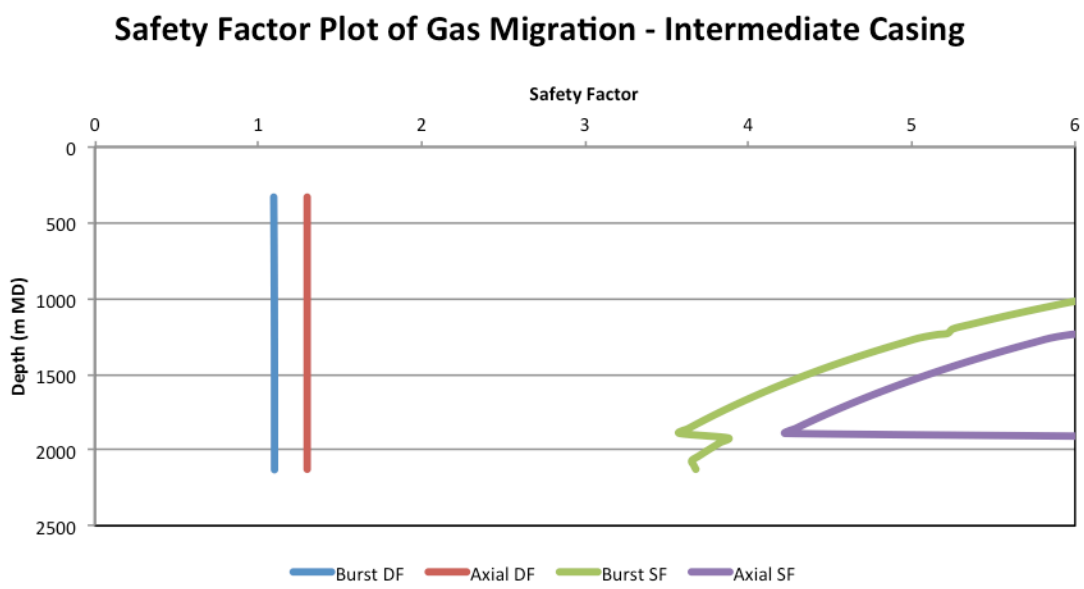

Figure 3-15 Safety factors of gas migration acting as a burst case on the intermediate casing. The lade case does not cause casing failure.

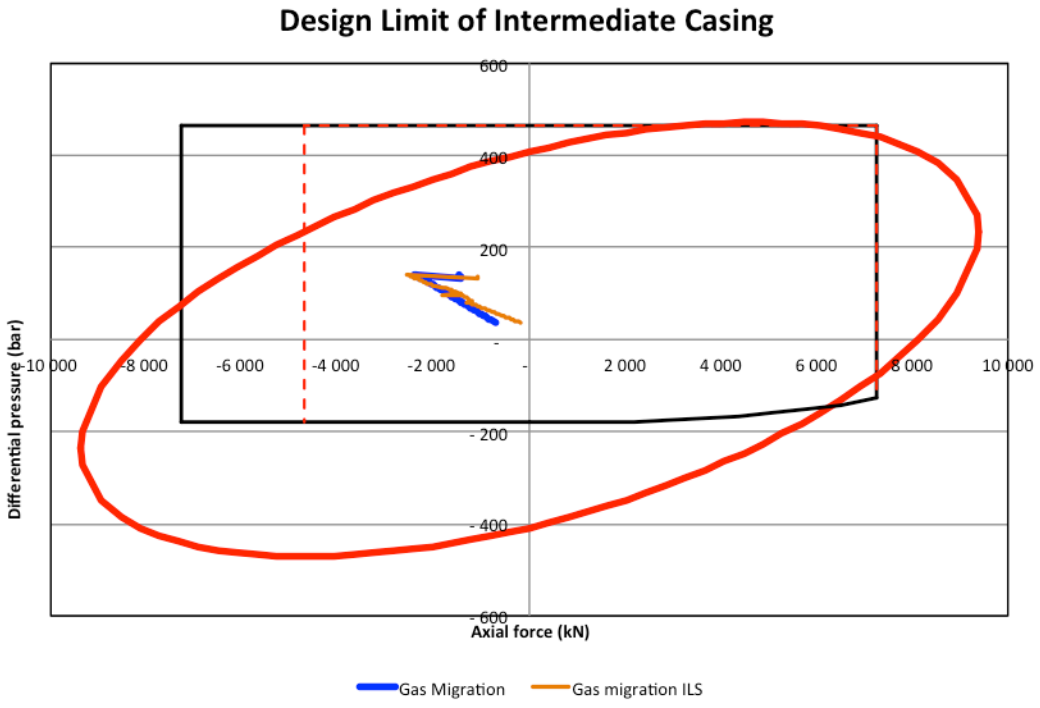

Figure 3-16 Design limit plot for the intermediate casing applied with the gas migration load case. The design limit plot is not indicating any casing failure due to the gas migration load case. The result from the ILS is also included.

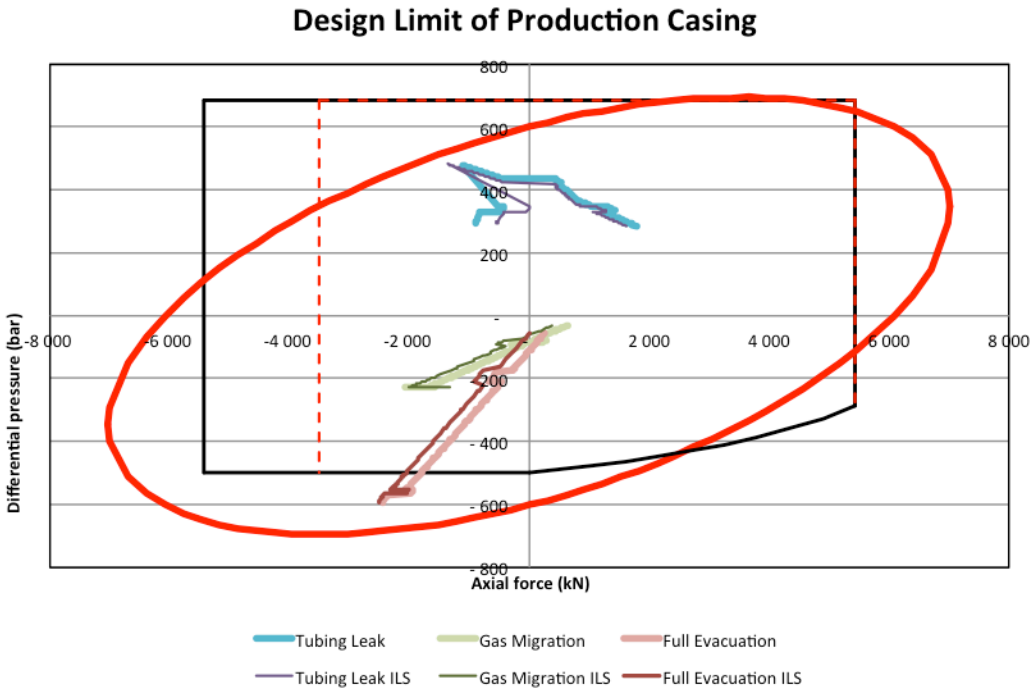

Figure 3-17 Design limit plot for the production casing with tubing leak, gas migration and full evacuation cases plotted. The plot shows that the full evacuation load case is outside the collapse limit and collapse failure is a risk at this stage. The results from ILS are also included.

As discussed in chapter 2.2.1.1 the buoyancy can be calculated in two different ways. The casing design model and the ILS are both calculated by using the piston force. To illustrate the difference between the two methods the Archimedes principle will be used to calculate the buoyancy for one of the loads. The full evacuation load case is a collapse load that has high values of compression in the string, as well as high collapse pressure. As shown in the safety factor plot (Figure 3-14) the load causes failure, as the safety factor is less than one. The collapse limit is reduced if there is tension in the string. It is therefore chosen to calculate the full evacuation over again by using the buoyancy based on the Archimedes principle. This will induce more tension in the string, and the load case may become more significant.

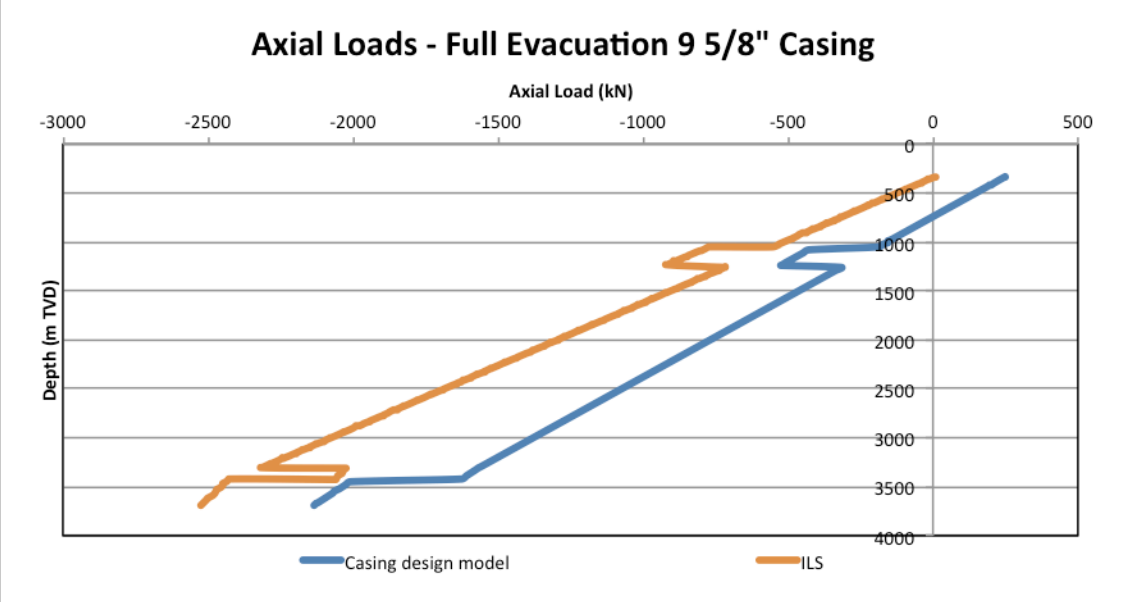

Figure 3-18 Axial loads on the production casing during full evacuation using the Archimedes buoyancy when calculating casing weight. The result deviates from the ILS in greater extent than when using the piston force to calculate buoyancy.

The safety factor plot shows the safety factor for the full evacuation load case when calculating the buoyancy by the Archimedes principle instead of the piston force. The safety factor in Figure 3-19 is slightly smaller at from 720 m TVD and up compared with in Figure 3-14. It is however the safety factor at the bottom of the well that is low, and there is compression in both cases (with buoyancy calculated by the Archimedes principle and piston forces) at the bottom of the casing. Therefore the safety factor that causes failure is not changed between the two methods. In collapse load cases where the total axial load is tension at the depth where the greatest differential pressure occurs, the method of using the Archimedes principle of buoyancy will cause lower safety factors than by using the piston force to calculate buoyancy.

It is chosen not to include the design limit plot, as there is not possible to see any visible changes between the original result of full evacuation and the result using another buoyancy method.

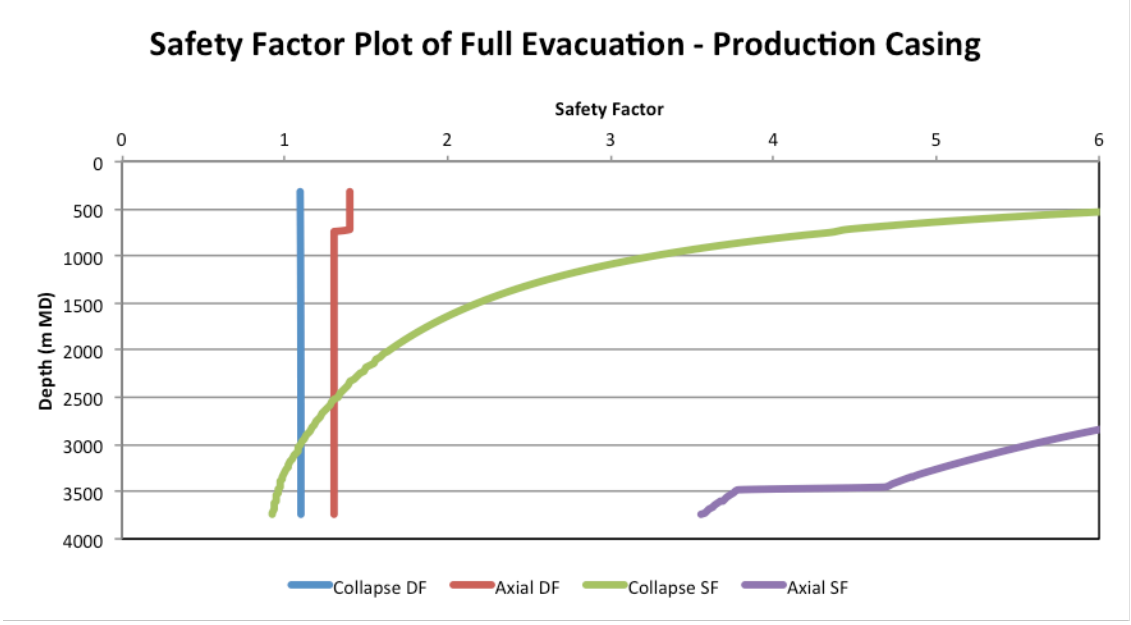

Figure 3-19 Safety factors of full evacuation acting as a collapse case on the production casing using the Archimedes principle to calculate buoyancy. The collapse safety factor is less than one, which induces casing collapse.

3.4 Wellbore Temperature Results

This chapter presents the temperature prediction results from the casing design model and from the ILS. The temperature prediction is modeled by two different methods, namely the Sagar, Doty and Schmidt method and the Hasan and Kabir method. Different assumptions are applied to the methods to study the effects and to achieve the most accurate results.

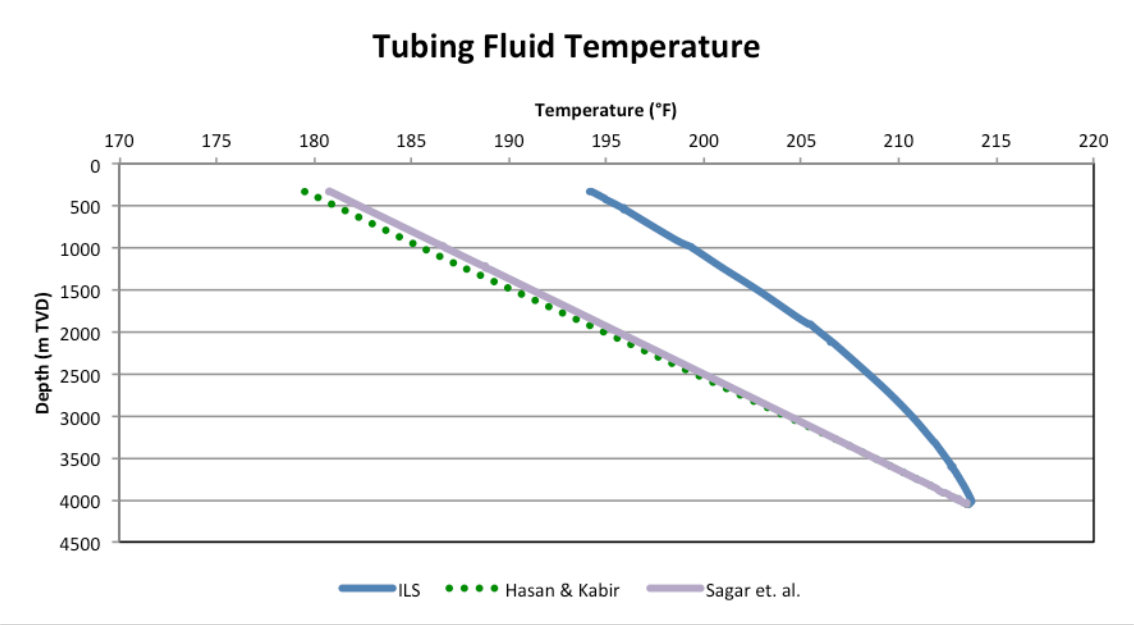

Figure 3-20 Overview of results of tubing fluid temperature by Sagar, Doty, and Schmidt method, Hasan and Kabir method and the ILS. The two methods extracted from the literature, the Sagar, Doty and Schmidt method and the Hasan and Kabir method, yields quite similar results. The results from the ILS have less heat loss in the well, which leads to a greater tubing fluid temperature at wellhead compared with the other two results.

Figure 3-20 is a plot of the tubing fluid temperature result using the Sagar, Doty and Schmidt method, the Hasan and Kabir method and the ILS. The ILS result has less temperature loss than the other two methods. The results are interesting; the two methods used in the casing design model yield very similar results. There is approximately 1 °F for the tubing fluid temperatures at wellhead that separates the two methods from each other.

It was of interest to test the effect of various parameters and assumptions in the temperature prediction to figure out which assumptions or methods the ILS uses to get the results. The initial assumptions are based on early lifetime production temperature and that the conduction in steel is neglected. These assumptions will be discussed further in this chapter. To investigate the effect the assumptions have on the temperature it is chosen to use the Sagar, Doty and Schmidt method. It is easier to use than the Hasan and Kabir method, which demands much iteration. As the two methods are based on the same basic theory and the results in Figure 3-20 are quite similar, it is reasonable to assume the methods will react similarly to changes in parameters and assumptions.

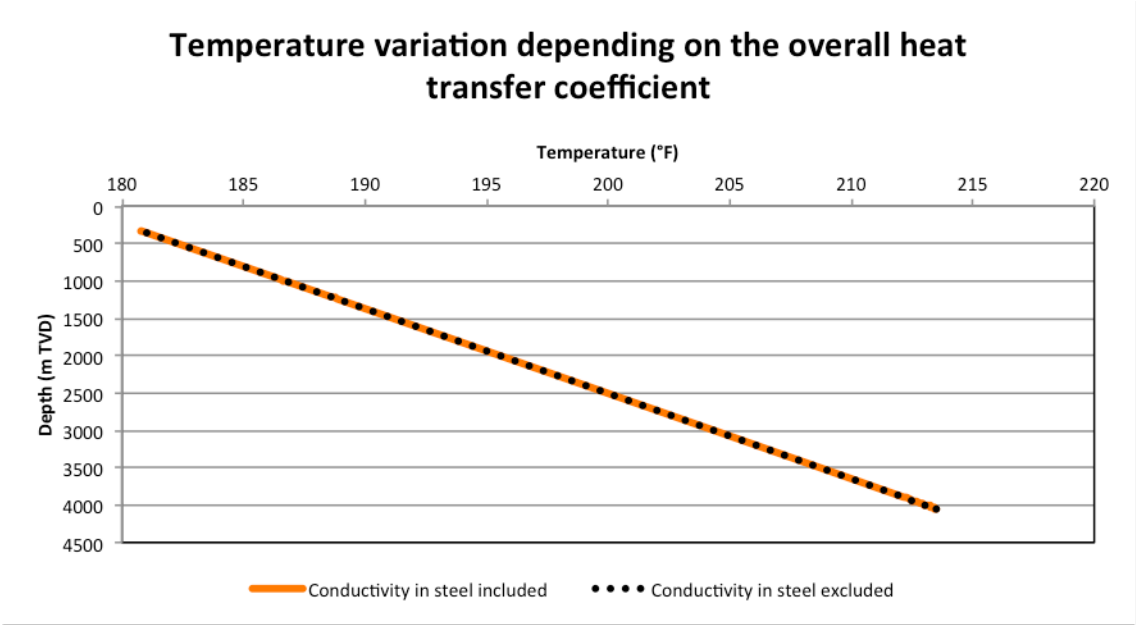

Figure 3-21 The tubing fluid temperature is calculated in two different ways to test the influence of heat transfer over the casing and tubing walls. Sagar, Doty, and Schmidt-method are used to calculate the tubing fluid temperature by including and excluding the conductivity on the steel in the overall heat transfer coefficient. The different assumptions yield similar results of tubing fluid temperature.

Conduction in the steel in the tubing and the casings is assumed to have negligible effect on the overall heat transfer coefficient, hence negligible effect on the temperature in the tubing fluid. The assumption is tested using the Sagar, Doty and Schmidt method. The temperature difference between the two cases when including and excluding the conduction in the pipe walls when calculating the overall heat transfer coefficient is approximately zero. The results are presented in Figure 3-21 .

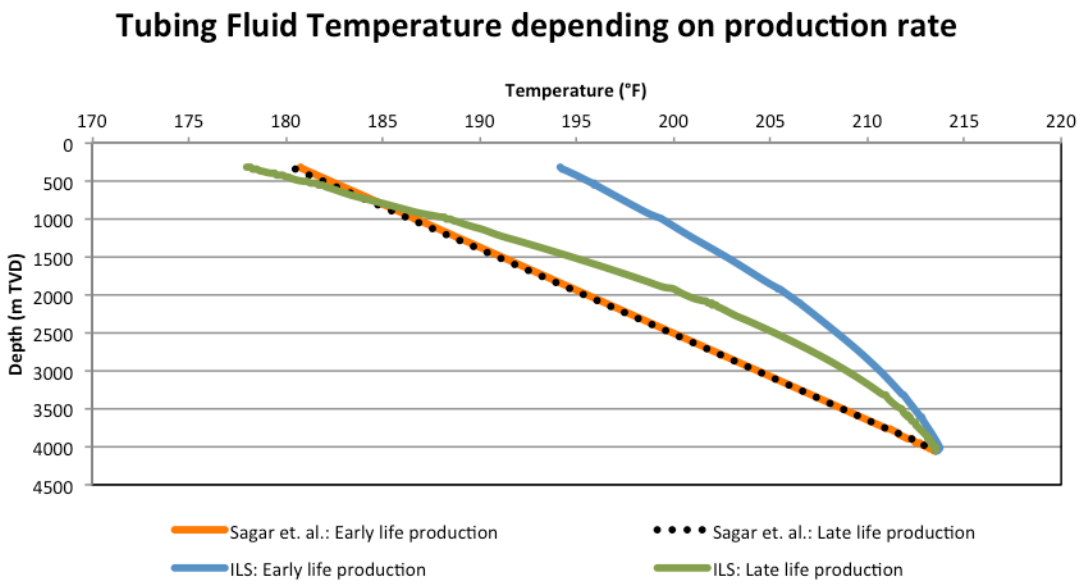

Figure 3-22 The tubing fluid temperature is calculated in two different ways to test the influence of the production rate. At early lifetime of the well the production is 2200m^3/D, while it is 1000m^3/D at late lifetime of the well. The calculation is performed using Sagar, Doty, and Schmidt-method. The tubing fluid temperature at wellhead is reduced with less than 1 °F. The results are compared with the ILS results that show a distinct reduction in temperature at reduced production rate.

The tubing fluid temperature is also calculated to investigate the effect of decline in production rate in Figure 3-22 using the Sagar, Doty and Schmidt method. It is calculated for flowing the well both during early and late lifetime of the well. In late lifetime of the well the production is more than cut in half compared to early lifetime production. The resulting tubing fluid temperature at wellhead is only reduced with less than 1 °F. The ILS results has a clear reduction in temperature when the production rate decreases, the temperature drop is of about 16 °F at wellhead.

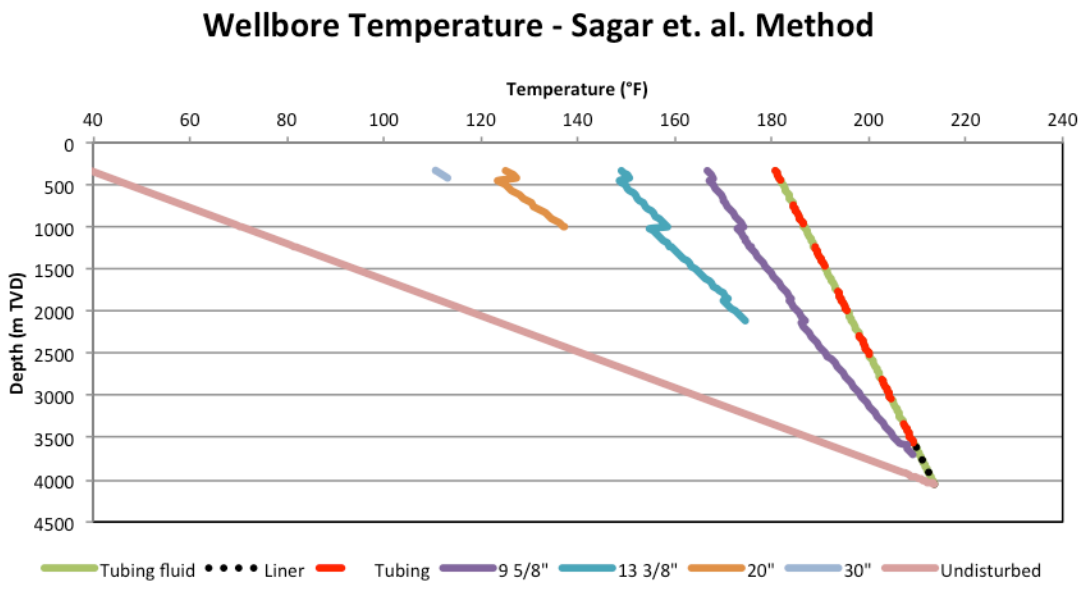

Figure 3-23 Wellbore temperature calculated by Sagar, Doty, and Schmidt-method.

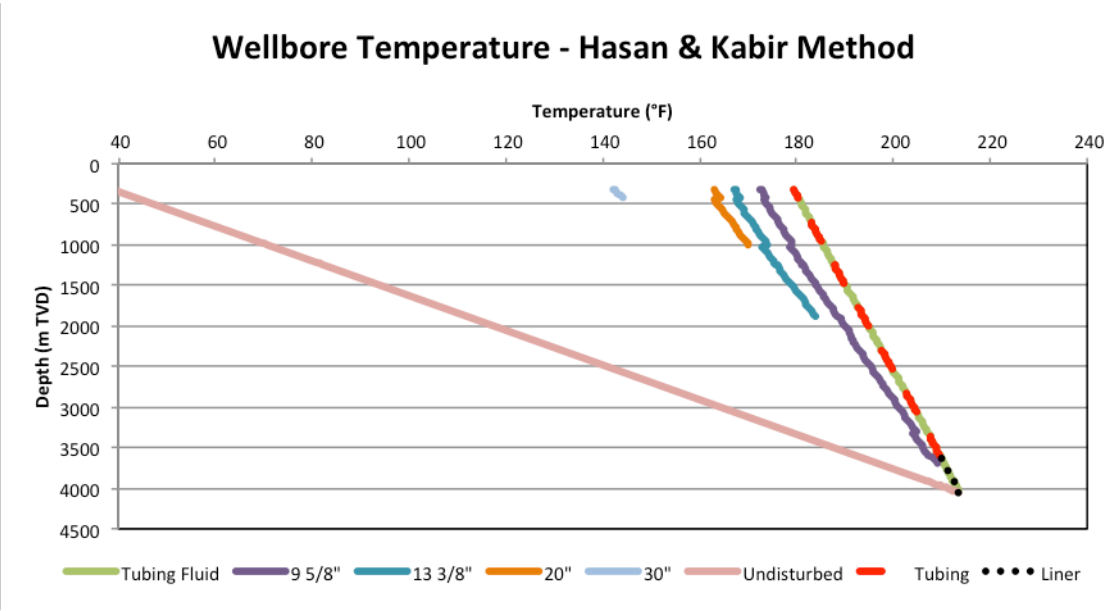

Figure 3-24 Wellbore temperature calculated by Hasan and Kabir-method.

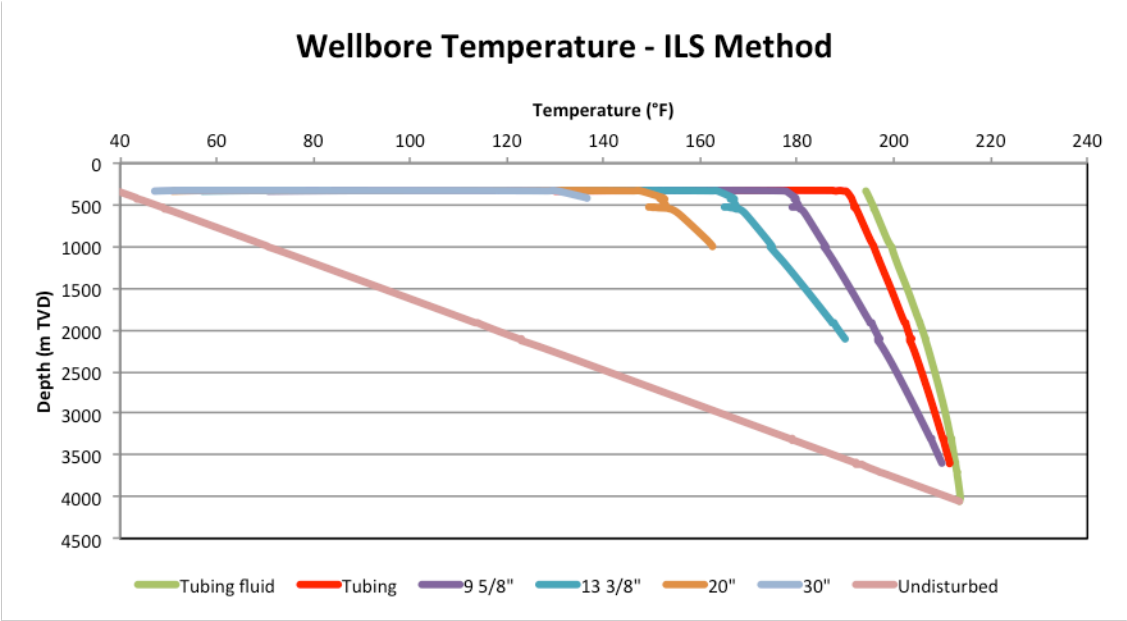

Figure 3-25 Wellbore temperature from ILS.

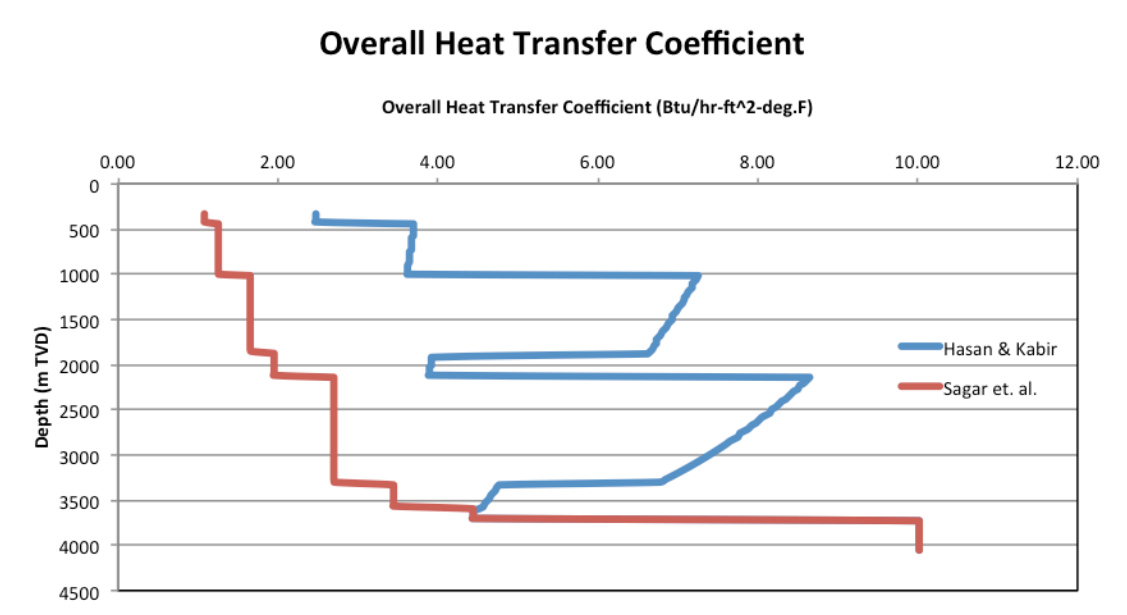

Figure 3-26 The overall heat transfer coefficients calculated by the Sagar, Doty and Schmidt method and the Hasan and Kabir method.

The casing temperature is the desired output after the temperature prediction for casing design. The casing temperatures are dependent on the overall heat transfer coefficient. When comparing the results using different methods it is chosen to view the tubing fluid temperatures to graphically view the results. The entire set of casing temperatures is plotted for the two methods and the ILS in Figure 3-23, Figure 3-24 and Figure 3-25.

Although the Sagar, Doty and Schmidt method and the Hasan and Kabir method yields similar tubing fluid temperature, the wellbore temperature profile is distributed differently, as presented in Figure 3-23 and Figure 3-24. In general, the casing temperatures in Sagar, Doty and Schmidt method are lower than in the Hasan and Kabir method, which is caused by lower overall heat transfer coefficient. The difference in the overall heat transfer coefficient is plotted in Figure 3-26. The overall heat transfer coefficient reduces down the well as the number of annuli is reduced. The difference in temperature between the casings by Saga, Doty and Schmidt method correlates better with the ILS results than the Hasan and Kabir method.

The ILS results in Figure 3-25 show a drastic reduction in temperature at wellhead for all the casings. Over one meter below wellhead the temperature reduction is high compared to the rest of the wellbore where the temperature reduction is approximately constant. It is caused by the cooling effect of the cold seawater at seabed. The temperature reduction will not affect the load cases particularly as it is over such a short interval. The cooling effect at wellhead is ignored in the casing design model.

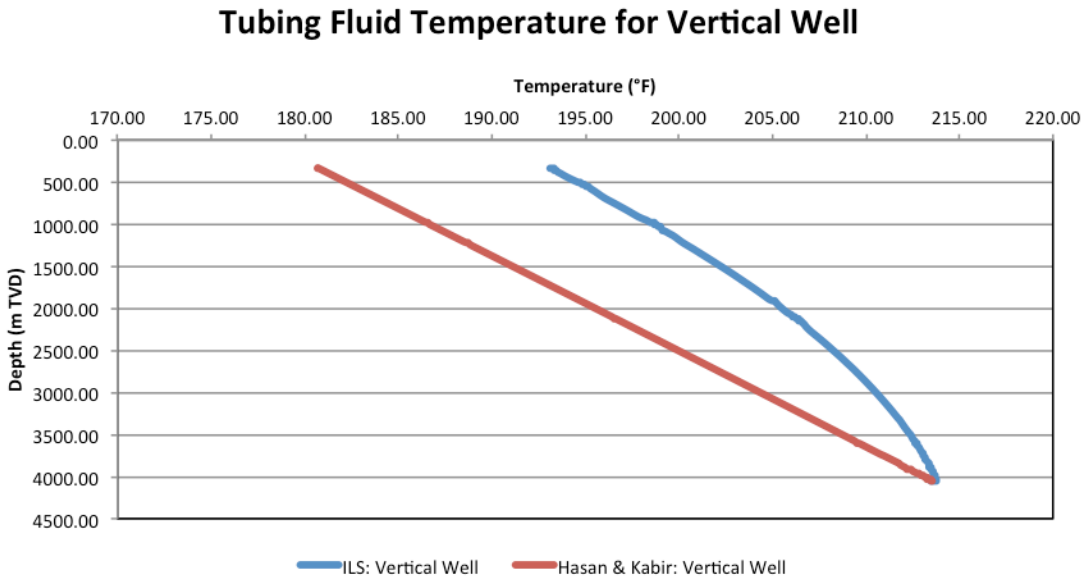

Figure 3-27 Overview of results of tubing fluid temperature by Hasan and Kabir method and the ILS for a vertical well.

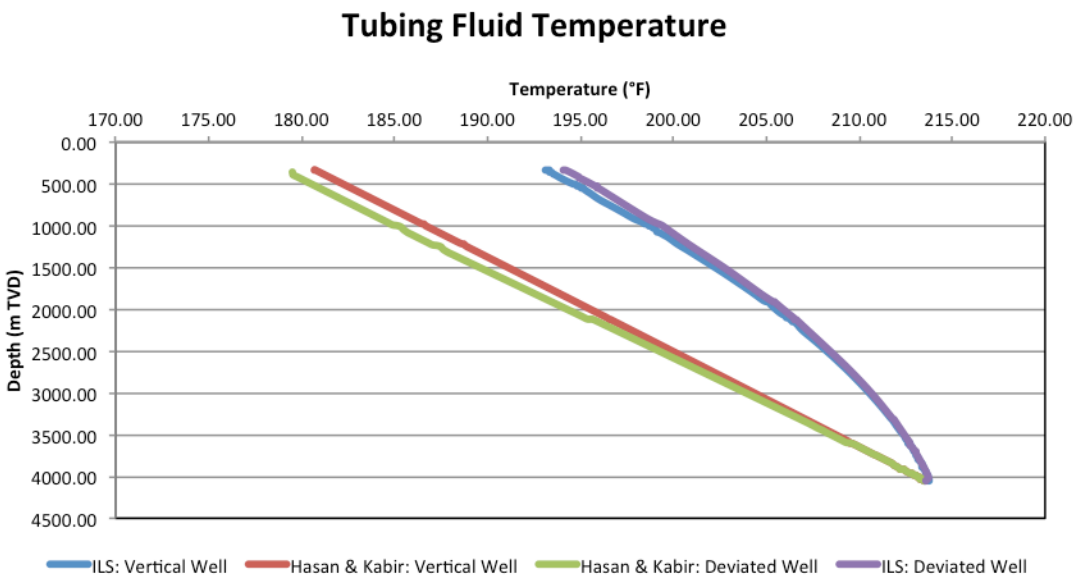

Figure 3-28 Overview of results of tubing fluid temperature by Hasan and Kabir method and the ILS for a vertical and deviated well.

To investigate if the methods calculate the temperature wrong in deviated wells, the well was transformed into a vertical well with only two annuli with fluids to simplify the calculation. The results in Figure 3-27 show the temperature prediction of tubing fluid for a vertical well from both the Hasan and Kabir method and the ILS. Figure 3-28 compare the results with the deviated well although they are not quite comparable as the well composition is slightly different.

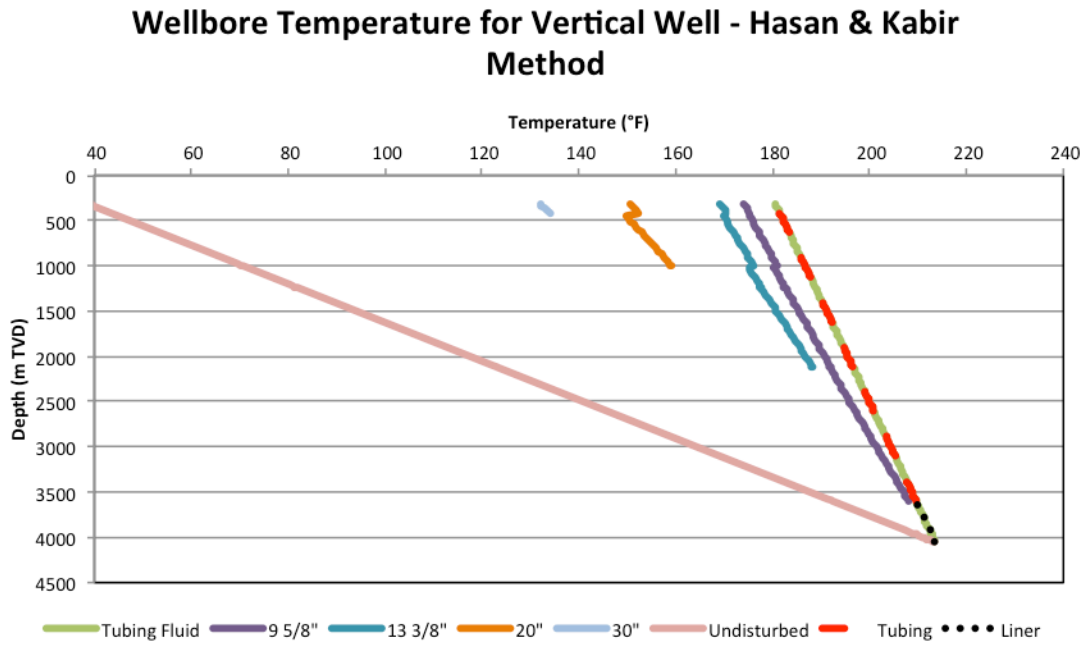

Figure 3-29 Wellbore temperature calculated by Hasan and Kabir method for a vertical well.

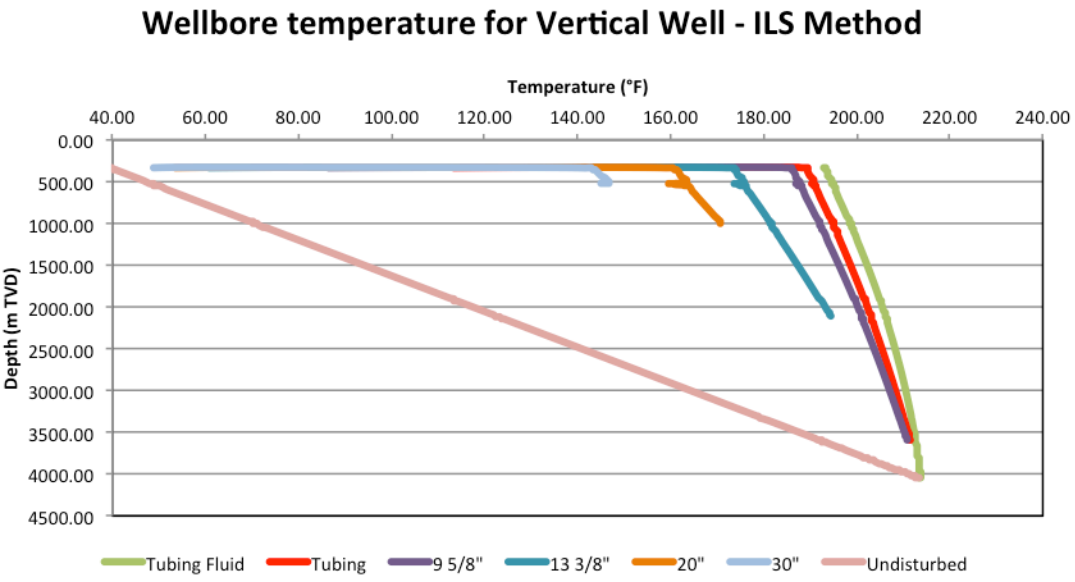

Figure 3-30 Wellbore temperature calculated by ILS for a vertical well.

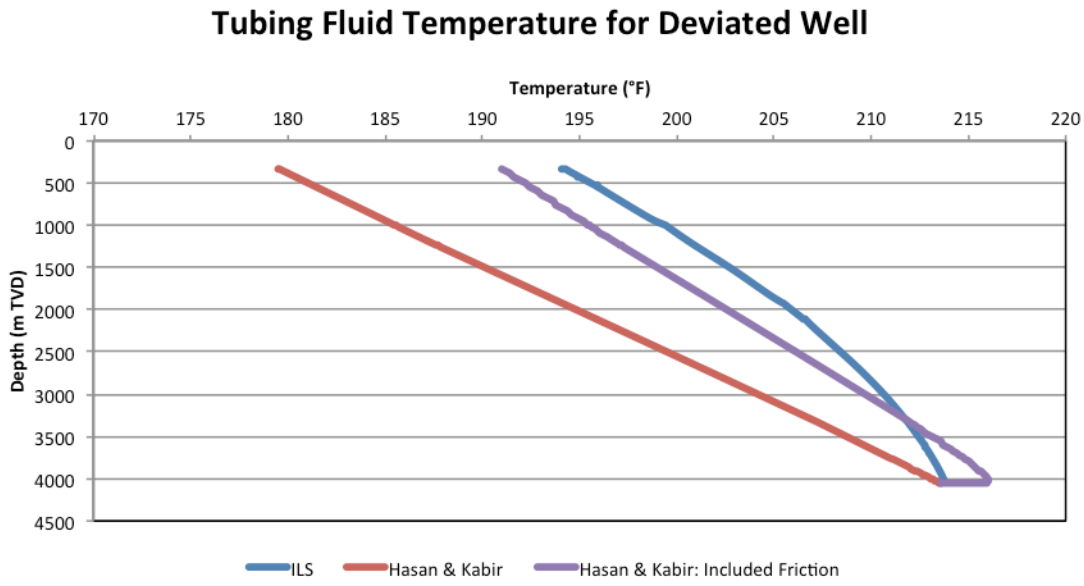

Figure 3-31 Wellbore temperature included and excluded friction in the tubing for the deviated well.

The wellbore temperature from the casing design is lower at wellhead than the ILS wellbore temperature. It is investigated whether the temperature is too low using the Hasan and Kabir method because the friction between the fluids and the tubing is not included. The result is plotted above. The friction contributes to an increase in tubing fluid temperature. For simplicity, all the produced fluids are assumed to flow in at the toe of the well.

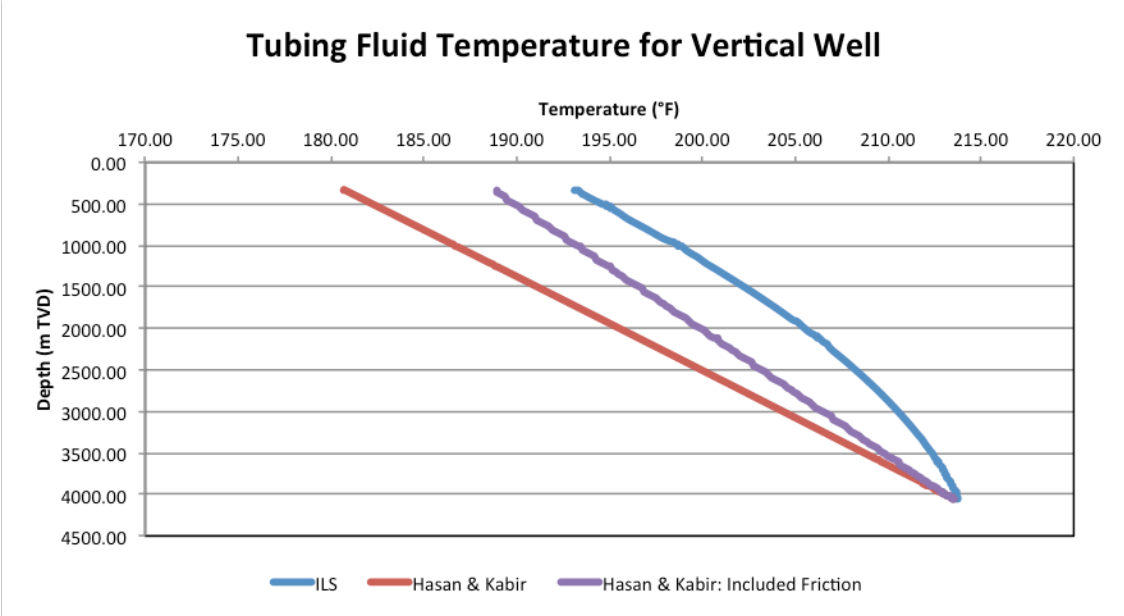

Figure 3-32 Wellbore temperature included and excluded friction in the tubing for the vertical well.

Figure 3-32 is the tubing fluid temperature for a vertical well including the friction in the casing design model The results are compared with the ILS results.

4 Discussion

4.1 Production Pressure and Axial Loads

The external pressure in the load cases are defined in literature to be equal to pore pressure in the cement in burst load cases, while for collapse load cases the external pressure is equal to the hydrostatic pressure of drilling mud above TOC and seawater below TOC. Figure 3-1 and Figure 3-2 show that the differential pressure at the bottom of the string in the burst load cases would be greater if the hydrostatic column of seawater was used in the cemented section instead of pore pressure.

The external pressure during initial conditions in the ILS and the casing design model is based on the column of drilling mud above TOC and of wet cement below TOC. The initial conditions may be argued to be under the transition when the cement is wet and solidified. Right before the casing is properly fixed to the formation by the cement, the cement has changed density. Using this theory the external pressure will depend on the column of density of drilling mud above TOC and of the density of seawater below TOC. The change in external pressure under initial conditions affects the piston force and the axial load under initial conditions, and thereby under the load cases.

Figure 3-11 shows that the ILS ignores the buckling in the bended section. It is discussable whether this is the right way to calculate the total effect of bending and buckling. The buckling induced dogleg angle is slightly greater than the bending dogleg angle. The two effects should not be added together as it is likely to assume the buckling stresses will not increase although there is bending in the wellbore in that section. It may be argued the bending stress should be set to zero instead, as the buckling stress gives greater total axial stress than the bending stress. Therefore the casing design model ignores the bending stresses in the bended section of the casing and buckling stresses are used instead. Consequently this is the opposite of what the ILS does for this section.

The total axial load slightly deviates from the ILS. The bending and buckling loads are assumed to be equal in both the ILS and the casing design model, as the same trends are visible in both models for all the load cases accounted for in present thesis. Above TOC it is argued there might be some differences in the results of temperature and ballooning loads between the two models. The difference is unexpected as the pressures and temperatures are

equal in both models, thus the axial loads should be equal. It may be caused by differences in the mathematical model or by the constants of Young´s elastic modulus and the thermal expansion coefficient of steel.

The axial load due to weight above TOC is assumed to be correct. Below TOC the two models yield different results. The correct axial load in the cemented casing is unknown. All the load cases are calculated with different axial load in the cemented part of the casing, which causes less compression. The axial load due to weight in the load cases is reduced in the cemented section because the piston forces are less than under cementing. Because the casing is fixed in the cement, the axial load above the TOC will remain equal to as during the initial conditions. The ILS results from the load cases show that the axial load due to weight in the cemented casing is not calculated using initial conditions. The method used by the software is unknown. The axial load in the casing that is cemented may be reduced with time in high temperature conditions, which the ILS may account for as a stress-relief. Whether or not the method for calculating the weight in the cement is correct is discussable. The casing design model result does not match perfectly with the ILS results below TOC, but the trends are similar. The non-linear behavior of the axial load below TOC in the ILS result behaves similarly as the results from the casing design model, but the values are shifted. Therefore it is reason to believe the ILS use the pore pressure in the calculations of axial load due to the weight in the cemented casing. Whether or not the method for calculating the weight in the cement in the two models is correct is discussable. Optionally, the axial load due to weight should be based on the conditions under initial conditions for the entire casing.

The two different methods of calculating buoyancy have a noticeable effect on the axial load results for the different load cases. The ILS uses the piston force to calculate the buoyancy of the casing. At the top the methods yields equal results of axial load due to weight, but at the bottom the piston force induce compression, while the Archimedes principle causes zero axial load. The worst-case scenario for load cases that are close to compression failure will be to apply the piston force buoyancy instead of the Archimedes principle of buoyancy. The worst-case scenario for load cases that are close to tension failure or load cases that have great collapse pressure will be to apply the greatest tension possible in the string. In these cases the ILS will not yield the worst-case scenario as the axial load has less tension down the string and compression at the bottom using the piston force buoyancy. Collapse load cases may be aggravated if the Archimedes principle of buoyancy yields the total axial load to be tension at

a depth where the collapse pressure is great. The full evacuation load case was applied with the Archimedes principle to compare the result with result using the piston force. Figure 3-18 and Figure 3-19 shows that there is a difference between the two methods, but the tension is only at the top of the well and the great collapse pressure is at the bottom of the well. The choice of the two different methods does not affect the safety factors of the load case.

The assumption that the axial load due to temperature and ballooning is an average along the entire well length might deviate from the reality. The casing design model has assumed an average for both these effects. The casing design model and the ILS have similar inclination of the total axial load, which indicates that the ILS also assumes average temperatures and pressure when calculating the temperature and ballooning effect on axial load.

4.2 Investigation of the effect of various assumptions and models on wellbore temperature

The Hasan and Kabir method is assumed to be more correct to use rather than the Sagar, Doty and Schmidt method as it takes the convection in the annulus into account. Sagar, Doty and Schmidt simplifies the calculation by assuming the heat transfer in the annulus fluid is by conduction. The two methods yield similar results for tubing fluid temperature, but the casing temperatures in Figure 3-23 and Figure 3-24 are different for the two methods caused by the difference in the overall heat transfer coefficient (Figure 3-26). The Sagar, Doty and Schmidt method yields lower overall heat transfer coefficients due to lower heat transfer in the annuli when assuming only conduction. The results show that the overall heat transfer coefficient does not have a great effect on the resulting tubing fluid temperature, but has a greater effect on the outer casings. The radial temperature drop in the Sagar, Doty and Schmidt method correlates better with the ILS results than the Hasan and Kabir method.

Sagar, Doty and Schmidt method suggests a greater value of the thermal conductivity of earth to compensate for the assumption that there is no convection in the annulus fluids. Ignoring this suggestion causes similar results of tubing fluid temperature for the Sagar, Doty and Schmidt method and the Hasan and Kabir method.

The assumption that conduction in the steel in the tubing and the casings has negligible effect is proven valid in Figure 3-21 by comparing the tubing fluid temperature with and without the conductivity in the steel using the Sagar, Doty and Schmidt method.

The effect of production rate on the tubing fluid temperature was investigated in Figure 3-22. The casing design model yields negligible change in temperature when the production rate is reduced to the half. The ILS has evident temperature loss for the same drop in production rate. As there are no real temperature data for the well, it is not certain whether the casing design or the ILS yields correct temperatures. However, it is expected that the temperature would be affected by changes in production rate.

As mentioned in section 2.3.2 the equations used for the convection in the annulus fluids are defined for vertical wells. The convection in the horizontal part of the well should be ignored entirely. For that section of the well the Sagar, Doty and Schmidt method is more correct to use, as they do not account for the convection in the annulus. The vertical well is based on the deviated well, but the intermediate casing is cemented to the wellhead. The result in Figure 3-28 is therefore not comparable with the deviated well. However, both methods have similar trends for the vertical well as for the deviated well; therefore the convection cannot be the main reason why the tubing fluid temperature is lower than what the ILS yields.

It was tested if the difference between the casing design model and the ILS is due to the friction between the flowing fluids and the tubing wall, since it is not included in the casing design model. The bottom of the well is horizontal. The formation temperature is therefore constant for the entire horizontal section and does not contribute to cooling of the wellbore. The friction in the pipe contributes to an increase in temperature that is greater than the loss to the formation in the horizontal section of the well. The result is presented in Figure 3-31. The same tendency is not seen in the results from the ILS, which argue that the friction is not the main reason why the two results deviates from each other. The friction effect is also added to the vertical well in Figure 3-32. For the vertical well the results from the Hasan and Kabir method when friction is included are close to the results from ILS.

Figure 3-25 shows the wellbore temperature retrieved from the ILS. The tubing temperature is lower than the tubing fluid temperature, which indicates that the ILS has included the convection in the tubing as part of the temperature prediction. The temperature prediction

from the two literature methods used in the casing design model neglect this term, and contributes to different results from the ILS results. The ILS may also account for radiative heat transfer in the annuli with fluids, which the casing design model has neglected.

As mentioned in chapter 2.3.1 the Joule-Thomson and kinetic energy effects, ϕ, has a great effect on the temperature, illustrated in Figure 2-7. ϕ is evaluated to be equal to zero for the well in the casing design model, due to the high total mass flow rate. ILS may calculate with ϕ greater than zero, which causes less heat transfer in the tubing flowing fluid.

4.3 Uncertainty Analysis of Temperature Prediction Model

Several uncertainties for the temperature prediction have been investigated. Some simplifications and uncertainties that are not accounted for are:

- Properties such as density and specific gravity are a function of temperature, and density is also a function of pressure. In this model density is calculated independently of temperature and pressure. No sources has been found on whether or not the ILS model correlates properties as density and specific gravity to the changes in temperature and pressure. The density of water does not change as much as density of gas for various temperatures and pressures. The density of the brine in the annulus in the calculations does not change significantly as it is close to an incompressible fluid.
- Many properties are used, which gives high uncertainty on the result.
- The heat contribution caused by friction between flowing fluids and the tubing wall is calculated by assuming a adiabatic system. The assumption is made for simplification of the calculation, and causes high uncertainty of the friction effect.
- Excluding the convection inside the tubing and the radiative heat transfer in annulus fluid may cause uncertainty.

5 Further Work

- Further investigation of the correct method to calculate the axial load due to weight in the cemented part of the casing. Possibly allow for both methods depending on company philosophy since the literature is split in this question.
- Study the additional compressional stresses the cemented casing is exposed in the case of compaction in the reservoir.
- Study and calculate the axial loads by including the friction between the casings and the wellbore in the deviated section of the well.
- Account for the annular fluid expansion when calculating pressure and axial loads in the well.
- Study and model temperature prediction for two-phase flow.
- Investigate the how the ILS model handle the heat contribution as a result of friction between flowing fluid and the tubing wall. It is calculated for in this thesis, but did not succeed to evaluate the effect in the ILS. Attempts were made by changing the pipe roughness, but there was not discovered any changes in temperature as a result.
- Perform temperature prediction for late lifetime of the well with high content of gas and/or water in the produced fluids and compare the result with results for the early lifetime production.
- Include the effect of convection inside the tubing. The effect is accounted for in the ILS.
- Compare the predicted temperature with real data from a well to see how good the model is when two and three phase flow is implemented.
- The ILS calculates the transient heat flow in the formation differently than the literature examined in the casing design model in present thesis. While the literature uses a transient function of time and wellbore radius, the ILS assumes that half a meter into the formation the temperature will be equal to the undisturbed temperature. The heat flow over the half-meter of formation is calculated by conduction. The temperature prediction should be calculated by using the same assumption as the ILS as an attempt to achieve better match between the results.

6 Conclusion

A casing design model has been developed that predicts wellbore temperature and calculates the differential pressures and axial loads acting on the casings under production. Safety factors have been calculated to compare with the design factors to evaluate if there is risk of casing failure during the lifetime of the well. The following conclusions were drawn from the evaluation of the casing design model:

- The pressure differential under the conditions of the load cases matches perfectly with the ILS results. The axial loads have similar trends and a good match with the ILS axial loads.
- The axial load due to bending and buckling are similar in both the casing design model and the ILS. The temperature and/or ballooning effects on the axial loads are slightly different between the two models, which may be caused by differences in the mathematical model or by the constants in the equations. The ILS and the casing design model disagree on the philosophy behind the calculation of the axial load due to weight in the cemented part of the casing, which causes deviations in the results in this section. It is concluded that the greatest stress obtained from either bending or buckling should be applied if both occur at the same place of the casing. The ILS does not take this into consideration.
- By applying the Archimedes principle of buoyancy instead of the piston force, the safety factors for the tension load cases are reduced. The safety factor for collapse load cases are reduced if the total axial load is tension at the depth of the greatest differential pressure. However, the buoyancy of the piston force and the Archimedes principle are equal at the top of the casing.
- The ILS result has less temperature loss in the well than the casing design model. The differences between the models are not caused by neglecting the steel conductivity or by neglecting the friction between the production fluids and the tubing. In addition, the simplification of convection by assuming a vertical well path is not the cause of the deviation between the two models.
- Changes in the overall heat transfer coefficient have negligible effect on the tubing fluid temperature compared with the casing temperatures in the casing design model.
- The determination of the Joule-Thomson and kinetic energy effect (ϕ) in the casing design model may be a simplification compared with the ILS. The term is assumed to

be negligible with high mass flow rates. Increasing the term causes less heat loss in the well, which would match the results of the ILS better.

The true production temperature in the well is not known, as there is no logging data available. Therefore it is unknown whether the ILS or the casing design model has predicted the correct wellbore temperatures.

7 Nomenclature

Symbols	Description	Oil field unit	SI unit
A	coefficient	ft^{-1}	
A_i	area on the inside of the pipe	in^2	
A_o	area on the outside of the pipe	in^2	
A_s	cross-sectional area	in^2	
c_p	specific heat capacity of producing fluid		J/kg-°C
c_{pa}	heat capacity of annular fluid	Btu/lbm-°F	
c_{pm}	specific heat capacity of producing fluid	Btu/lbm-°F	
c_T	coefficient of thermal expansion	$°F^{-1}$	
D_i	inside diameter of pipe		m
d_i	inside diameter of pipe	in	
d_n	nominal outside diameter of the string	in	
E	Young´s elastic modulus	psi	
f	friction factor		
F_{bal}	ballooning effect force	lbf	
F_c	critical force	lbf	
F_{eff}	effective buckling force	lbf	
F_p	piston force	lbf	
F_T	axial force due to temperature change	lbf	
F_{tot}	total axial load (except bending forces)	lbf	
g	gravity coefficient (9.81 m/s^2)		
g_a	acceleration of gravity (32.2 ft/sec^2)		
g_A	acceleration of gravity ($4.17x10^8$ ft/hr^2)		
g_c	conversion factor (32.2 ft-lbm/sec^2-lbf)		
g_T	geothermal temperature gradient	°F/ft	
h	radiative and convective heat transfer coefficient	Btu/°F-hr-ft^2	
H	specific enthalpy	Btu/lbm	
h_{anA}	convective heat transfer coefficient for A-annulus	Btu/ °F-hr-ft^2	

Symbols	Description	Oil field unit	SI unit
h_{anB}	convective heat transfer coefficient for B-annulus	Btu/ °F-hr-ft^2	
h_{anC}	convective heat transfer coefficient for C-annulus	Btu/ °F-hr-ft^2	
h_c	convective heat transfer coefficient	Btu/°F-hr-ft^2	
h_r	radiative heat transfer coefficient	Btu/°F-hr-ft^2	
I	moment of inertia	in^4	
J	mechanical equivalent of heat (778 ft-lbf/Btu)		
k	thermal conductivity of material	Btu/hr-ft-°F	
k_{an}	conductivity of annulus fluid	Btu/hr-ft-°F	
k_{cem}	thermal conductivity of cement	Btu/hr-ft-°F	
k_e	conductivity of earth	Btu/hr-ft-°F	
L	length of pipe	ft	
L	length of well at the end of increment	ft	
L_{DW}	length of increment		m
L_{in}	length of well form at start of increment	ft	
N_{Gr}	Grashof number		
N_{Pr}	Prandtl number		
P	pressure		Pa
p	pressure	psi	
$P_{frac,\ shoe}$	fracture pressure at casing shoe		Pa
P_i	internal pressure		Pa
p_i	internal pressure	psi	
$P_{i,WH}$	internal wellhead pressure		Pa
P_o	external pressure		Pa
p_o	external pressure	psi	
P_{res}	reservoir pressure		Pa
P_{WH}	wellhead pressure		Pa
p_{wh}	wellhead pressure	psi	
Q	heat transfer between fluid and surrounding area	Btu/lbm	

Symbols	Description	Oil field unit	SI unit
r	radius	ft	
r_c	radial annular clearance	in	
$r_{ci\ 13\ 3/8"}$	inner radius of 13 3/8" casing	ft	
$r_{ci\ 20"}$	inner radius of 20" casing	ft	
$r_{ci\ 30"}$	inner radius of 30" casing	ft	
$r_{ci\ 9\ 5/8"}$	inside radius of 9 5/8" casing	ft	
$r_{co\ 13\ 3/8"}$	outer radius of 13 3/8" casing	ft	
$r_{co\ 20"}$	outer radius of 20" casing	ft	
$r_{co\ 30"}$	outer radius of 30" casing	ft	
$r_{co\ 9\ 5/8"}$	outer radius of 9 5/8" casing	ft	
Re	Reynolds number		
R_{gl}	gas/liquid ratio	scf/STB	
r_i	inner radius	ft	
r_o	outer radius	ft	
r_{to}	outside tubing radius	ft	
r_{wb}	wellbore radius	ft	
T	temperature	°F	
T_{an}	annulus temperature	°R	
T_{ci}	temperature of inner casing wall	°F	
$T_{ci\ 9\ 5/8"}$	temperature of inside 9 5/8" casing wall	°F	
T_{co}	temperature of outer casing wall	°F	
T_D	dimensionless temperature		
T_e	surrounding earth temperature	°F	
T_{ein}	surrounding earth temperature at start of increment	°F	
T_f	tubing flowing fluid temperature	°F	
T_{fin}	tubing flowing fluid temperature at start of increment	°F	
T_{to}	temperature of outer tubing wall	°F	
T_{wb}	wellbore (earth interface) temperature	°F	
$\dot{T}$	coefficient	$°R^{-1}$	
u	average flow velocity		m/s

Symbols	Description	Oil field unit	SI unit
U_{to}	overall heat transfer coefficient	Btu/hr-ft^2-°F	
v	fluid velocity	ft/sec	
w_c	casing contact load	lbf/in	
w_e	distributed buoyed weight of casing	lbf/in	
w_n	nominal weight	lbm/ft	
w_t	total mass flow rate	lbm/sec	
Z	depth of casing		m
Z_{res}	reservoir depth		m
Z_{TOC}	depth of TOC		m
α	dogleg angle	°/100ft	
β	buoyancy factor		
γ_{API}	oil gravity	°API	
γ_g	gas specific gravity		
ΔL	length of increment of well	ft	
Δp_i	change in internal pressure	psi	
Δp_o	change in external pressure	psi	
ΔT	temperature change	°F	
ε/D	relative roughness		
θ	wellbore angle of inclination (radians)		
Θ	wellbore azimuth angle (radians)		
λ	helix angle		
λ_{max}	maximum helix angle		
μ	Poisson´s ratio		
μ_{an}	viscosity of annular fluid	lbm/ft-hr	
μ_{JT}	Joule-Thomson coefficient		
ρ	density		kg/m^3
ρ_{an}	density of annular fluid	lbm/ft^3	
ρ_{cem}	density of cement		kg/m^3
ρ_i	density inside the pipe		kg/m^3
ρ_m	mud density		kg/m^3
ρ_o	density outside the pipe		kg/m^3

Symbols	Description	Oil field unit	SI unit
ρ_{res}	reservoir fluid density		kg/m^3
ρ_s	density of steel (7,83 kg/m^3)		
σ_b	bending stress	psi	
σ_z	axial stress	psi	
ϕ	coefficient combining Joule-Thomson and kinetic energy effects		

8 Abbreviations

ILS	Industry Leading Software
MD	Measured Depth
TOC	Top of Cement
TVD	True Vertical Depth

9 Bibliography

Aadnøy, B.S. 2006. *Mechanics of drilling*. Aachen: Shaker Verlag.

Bellarby, J. 2009. *Well completion design*. Vol. 56. Oxford: Elsevier.

Calhoun, A.R., and Golmanavich, J. 2004. *Plastics Technician's Toolbox*. Brookfield, CT: Society of Plastics Engineers.

Çengel, Y.A., and Cimbala, J.M. 2014. *Fluid mechanics: fundamentals and applications*. Boston, MA: McGraw-Hill.

Hasan, A.R., and Kabir, C.S. 1994. Aspects of Wellbore Heat Transfer During Two-Phase Flow. *SPE Production and Facilities* 9 (3): 211 - 216. SPE-22948-PA http://dx.doi.org/10.2118/22948-PA.

Hasan, A.R., Kabir, C.S., and Wang, X. 2009. A Robust Steady-State Model for Flowing-Fluid Temperature in Complex Wells. *SPE Production and Operations* 24 (2): 269 - 276. SPE-109765-PA http://dx.doi.org/10.2118/109765-PA.

Hearn, E.J. 1997. *Mechanics of materials: an introduction to the mechanics of elastic and plastic deformation of solids and structural materials, 1*. Oxford: Butterworth-Heinemann.

Larock, B.E., Jeppson, R.W., and Watters, G.Z. 2000. *Hydraulics of pipeline systems*. Boca Raton, Fla.: CRC Press.

Lienhard, J.H.I.V., and Lienhard, J.H.V. 2011. *A heat transfer textbook*. 4th ed.: Dover Publication. Available online at: Knovel. http://app.knovel.com/web/toc.v/cid:kpHTTE0007/viewerType:toc/.

Lyons, W.C., and Plisga, G.J. 2011. *Standard Handbook of Petroleum and Natural Gas Engineering*. 2nd ed. Burlington, VT: Elsevier Science.

McAdams, W.H. 1942. *Heat transmission*. 2nd ed. New York, NY: McGraw-Hill.

Mitchell, R.E. 2006. *Petroleum Engineering Handbook - Drilling Engineering*. Vol. 2. Richardson, TX: Society of Petroleum Engineers.

Ramey, H.J., Jr. 1962. Wellbore Heat Transmission. *Journal of Petroleum Technology* 14 (4): 427 - 435. SPE-96-PA http://dx.doi.org/10.2118/96-PA.

Sagar, R., Doty, D.R., and Schmidt, Z. 1991. Predicting Temperature Profiles in a Flowing Well. *SPE Production Engineering* 6 (4): 441 - 448. SPE-19702-PA http://dx.doi.org/10.2118/19702-PA.

Tøien, M. 2014. *Advanced Casing Design - Production Loads*. MS thesis, Norwegian University of Science and Technology, Trondheim, (December 2014).

Willhite, G.P. 1967. Over-all Heat Transfer Coefficients in Steam And Hot Water Injection Wells. *Journal of Petroleum Technology* 19 (5): 607 - 615. SPE-1449-PA http://dx.doi.org/10.2118/1449-PA.

Appendix A: Wellbore properties

This chapter presents some data of the well that is used as an example for the casing design in this thesis.

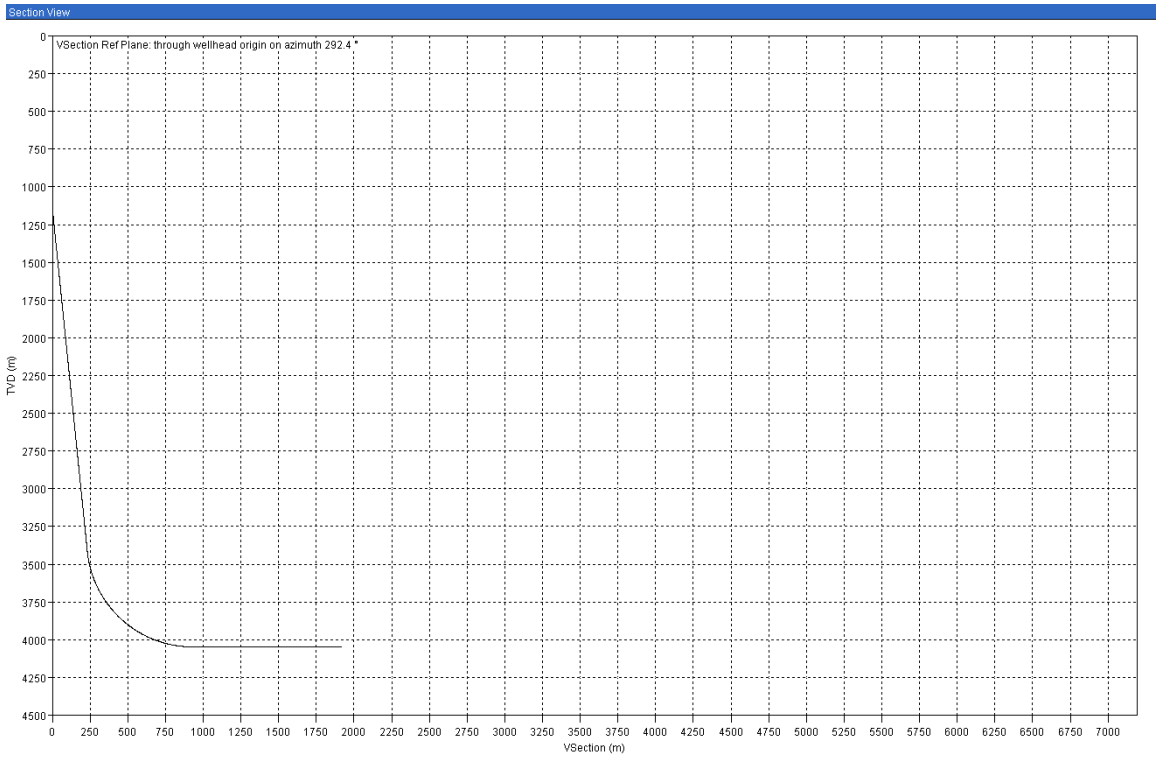

Figure A-1 The well path shows that the well is horizontal in the reservoir.

Table A-1 The properties of the casings in the well.

OD in	ID nominal in	Grade	Nominal weight lbm/ft	d_n/t	σ_{yield} psi	Connection
30	28	X-52	309,7	30	52 000	ST-2
20	18,73	X-56	133	31	56 000	BIG OMEGA
13 3/8	12,347	P-110	72	26	110 000	New VAM
9 5/8	8,535	P-110	53,5	18	110 000	New VAM
7	6,004	13CRS-110	35	14	110 000	VAM Top

Table A-2 Casing shoe depth, TOC and the coherent annulus fluid are given in the table.

OD	Casing shoe depth	TOC	Casing shoe depth	TOC	Mud weight
in	MD	MD	TVD	TVD	sg
30"	420	327	420	327	1,03
20"	1000	327	1000	327	1,03
13,375"	2126	1926	2117	1916	1,45
9,625"	3740	3340	3692	3310	1,71
7" liner	5520	3640	4052	3600	1,70
7" tubing	3640	3590	3600	3555	1,70

Appendix B: Calculating the Wellbore Temperature Profile

This section will illustrate how to calculate the temperature in the well using the Hasan and Kabir (1994) method. First some constants are defined.

The total mass flow rate of produced fluid for a two-phase fluid is given as follows:

$$w_t = \frac{q_g \gamma_g}{1.1309x10^9} + \frac{q_w \gamma_w + q_o \gamma_o}{246.6} \tag{51}$$

where

w_t = total mass flow rate (lbm/sec)

q_g = gas flow rate (scf/D)

γ_g = gas specific gravity

γ_w = water specific gravity

γ_o = oil specific gravity

The specific heat capacity of produced fluid, c_{pm}, is expressed as c_{pl} for liquids. The equation is:

$$c_{pl} = \frac{q_0}{q_0 + q_w} c_{po} + \left(1 - \frac{q_0}{q_0 + q_w}\right) c_{pw} \tag{52}$$

where

c_{pl} = specific heat capacity of liquid (Btu/lbm-°F)

q_o = oil flow rate (STB/D)

q_w = water flow rate (STB/D)

c_{po} = specific heat of oil (Btu/lbm-°F)

c_{pw} = specific heat of water (Btu/lbm-°F)

Typical values of the constants given in equation (52) are c_{po} = 0.485 Btu/lbm-°F and c_{pw} = 1.0 Btu/lbm-°F (Sagar, Doty, and Schmidt 1991).

The undisturbed temperature in the earth is given by:

$$T_e = T_{bh} - g_T L \sin\theta \tag{53}$$

where

T_{bh} = bottomhole temperature (°F)

The coefficients A and the dimensionless temperature (T_D) are defined, as follows (Hasan and Kabir 1994):

$$A = \frac{c_{pm} w_t}{2\pi}\left(\frac{k_e + r_{to} U_{to} T_D}{r_{to} U_{to} k_e}\right) \tag{54}$$

$$T_D = 1.1281\sqrt{t_D}(1 - 0.3\sqrt{t_D}) \quad \text{for } 10^{-10} \leq t_D \geq 1.5 \tag{55}$$

$$T_D = (0.4063 + 0.5 \ln t_D)\left(1 + \frac{0.6}{t_D}\right) \qquad \text{for } t_D > 1.5 \tag{56}$$

$$t_D = \frac{\alpha t}{r_{wb}^2} \tag{57}$$

where

k_e = conductivity of earth (Btu/hr-ft-°F)

T_D = dimensionless temperature

t_D = function of time

α = heat diffusivity of earth (0.04 ft^2/hr)

t = time (hours)

r_{wb} = wellbore radius (ft)

The temperature will be calculated for section eight assuming the temperature for section 1-7 is already calculated, as that is the most comprehensive section. The wellbore temperature is calculated using equation (45). The procedure in the flowchart in Figure 2-10 is used. The temperatures of the different casings are illustrated in Figure 2-8. The first step is to guess the overall heat transfer coefficient (U_{to}). Next, the temperatures are calculated starting from the wellbore wall. Equation (33) is used to find the temperature of the outer conductor wall:

$$T_{co\ 30"} - T_{wb} = \frac{Q}{2\pi\Delta L}\frac{\ln(r_{wb}/r_{co\ 30"})}{k_{cem}} \tag{58}$$

Equation (44) and (58) gives the following equation:

$$T_{co\ 30"} = T_{wb} + r_{to} U_{to}\left(T_f - T_{wb}\right)\frac{\ln(r_{wb}/r_{co\ 30"})}{k_{cem}} \tag{59}$$

For all the casings it is assumed the inner and outer temperature is equal ($T_{ci} = T_{co}$). To find the temperature of the surface casing the similar equation is used, given as:

$$T_{co\ 20"} = T_{ci\ 30"} + r_{to}U_{to}\left(T_f - T_{wb}\right)\frac{\ln(r_{ci\ 30"}/r_{co\ 20"})}{k_{cem}} \tag{60}$$

To find the temperature of the intermediate casing, equation (35) are used to express the following equation:

$$T_{co\ 13\ 3/8"} - T_{ci\ 20"} = \frac{Q}{2\pi\Delta L}\left(\frac{1}{r_{co\ 13\ 3/8"}h_{anC}}\right) \tag{61}$$

Equation (44) and (61) yields:

$$T_{co\ 13\ 3/8"} = T_{ci\ 20"} - \frac{r_{to}}{r_{co\ 13\ 3/8"}}\frac{U_{to}}{h_{anC}}\left(T_f - T_{wb}\right) \tag{62}$$

The temperature at the intermediate casing depends on the convective coefficient in annulus C. The convective coefficient to annulus C is guessed to calculate the temperature in the intermediate casing. Then it is calculated using the temperature of the intermediate casing. The convective coefficient is iterated as described in the flowchart (Figure 2-10).

$$h_{anC} = 0.049\frac{(N_{Gr}N_{Pr})^{\frac{1}{3}}N_{Pr}^{0.074}k_{an}}{r_{co\ 13\ 3/8"}\ln\left(\frac{r_{ci\ 20"}}{r_{co\ 13\ 3/8}}\right)} \tag{63}$$

$$N_{Gr} = \frac{\left(r_{ci\ 20"} - r_{co\ 13\ 3/8"}\right)^3 g_A\rho_{an}^2\dot{T}\left(T_{co\ 13\ 3/8"} - T_{ci\ 20"}\right)}{\mu_{an}^2} \tag{64}$$

$$T_{an} = \frac{T_{co\ 13\ 3/8"} + T_{ci\ 20"}}{2} \tag{65}$$

Similarly the temperature of the production casing is calculated. The inner and outer tubing temperatures are assumed to be equal to the tubing fluid temperature. The convective coefficient of annulus B must also be iterated as with annulus C. The equations for annulus B are expressed as:

$$T_{co\ 9\ 5/8"} = T_{ci\ 13\ 3/8"} - \frac{r_{to}}{r_{co\ 9\ 5/8"}}\frac{U_{to}}{h_{anB}}\left(T_f - T_{wb}\right) \tag{66}$$

$$h_{anB} = 0.049 \frac{(N_{Gr}N_{Pr})^{\frac{1}{3}} N_{Pr}^{0.074} k_{an}}{r_{co\ 9\ 5/8"} \ln\left(\frac{r_{ci\ 13\ 3/8"}}{r_{co\ 9\ 5/8}}\right)} \tag{67}$$

$$N_{Gr} = \frac{\left(r_{ci\ 13\ 3/8"} - r_{co\ 9\ 5/8"}\right)^3 g_A \rho_{an}^2 \dot{T}\left(T_{co\ 9\ 5/8"} - T_{ci\ 13\ 3/8"}\right)}{\mu_{an}^2} \tag{68}$$

$$T_{an} = \frac{T_{co\ 9\ 5/8"} + T_{ci\ 13\ 3/8"}}{2} \tag{69}$$

The convection coefficient for annulus A is described in equation (36), (37) and (39) and does not require any iteration as the temperatures of the tubing and casing sealing the annulus are known. As all the convective coefficients are known, the overall heat transfer coefficient can be calculated using equation (41), which must be iterated by changing the guessed value of U_{to}. At last the tubing fluid temperature is calculated using equation (29).

The following flowchart is based on the flowchart in Figure 2-10, but changed to only apply for interval eight in Figure 2-9. The equation numbers are referred to in the flowchart, some of the calculations are in this chapter, while others are from chapter 2.3.

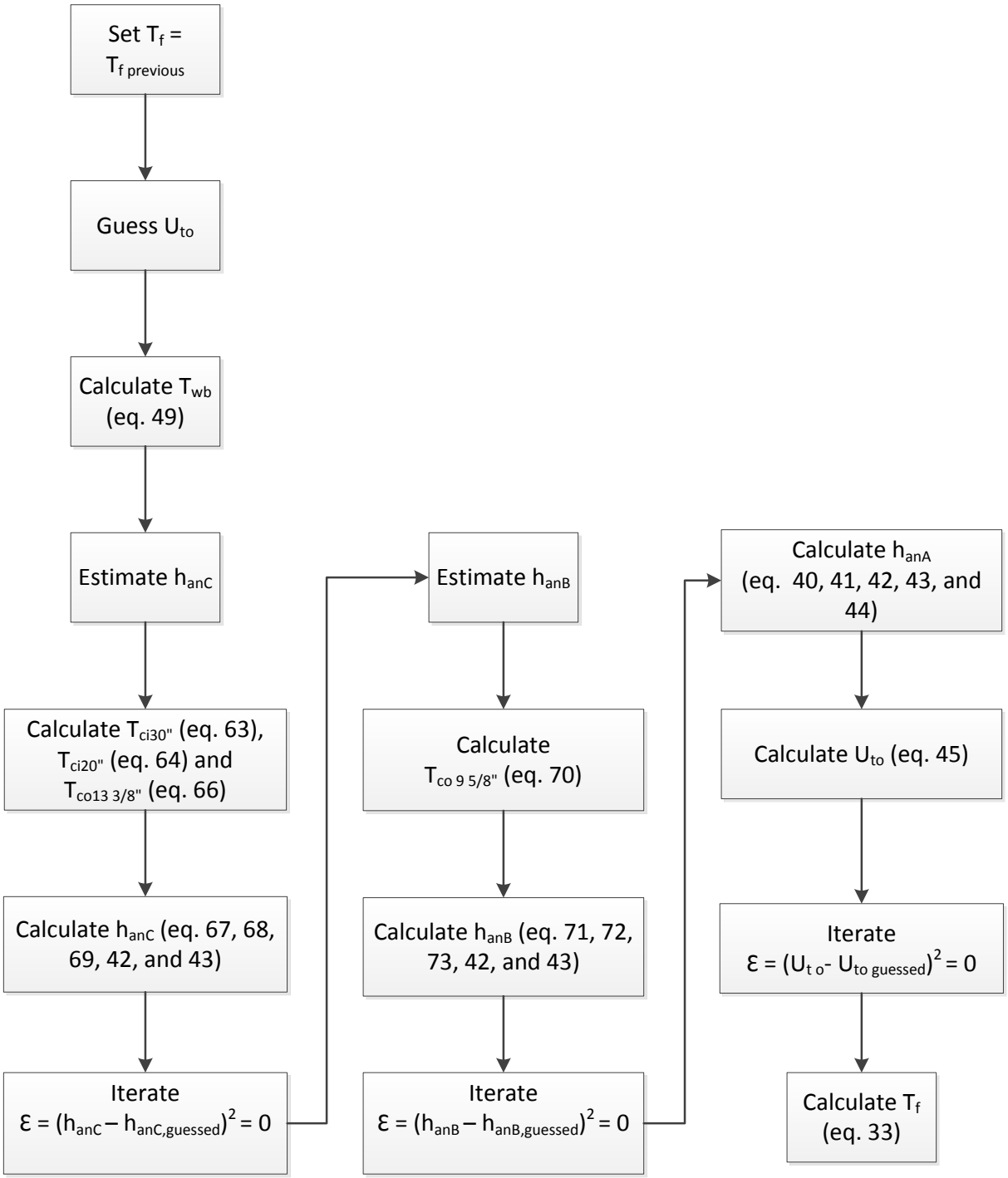

Figure B-1 Flowchart of casing temperature calculation for interval eight from Figure 2-9.

Appendix C: ILS Results

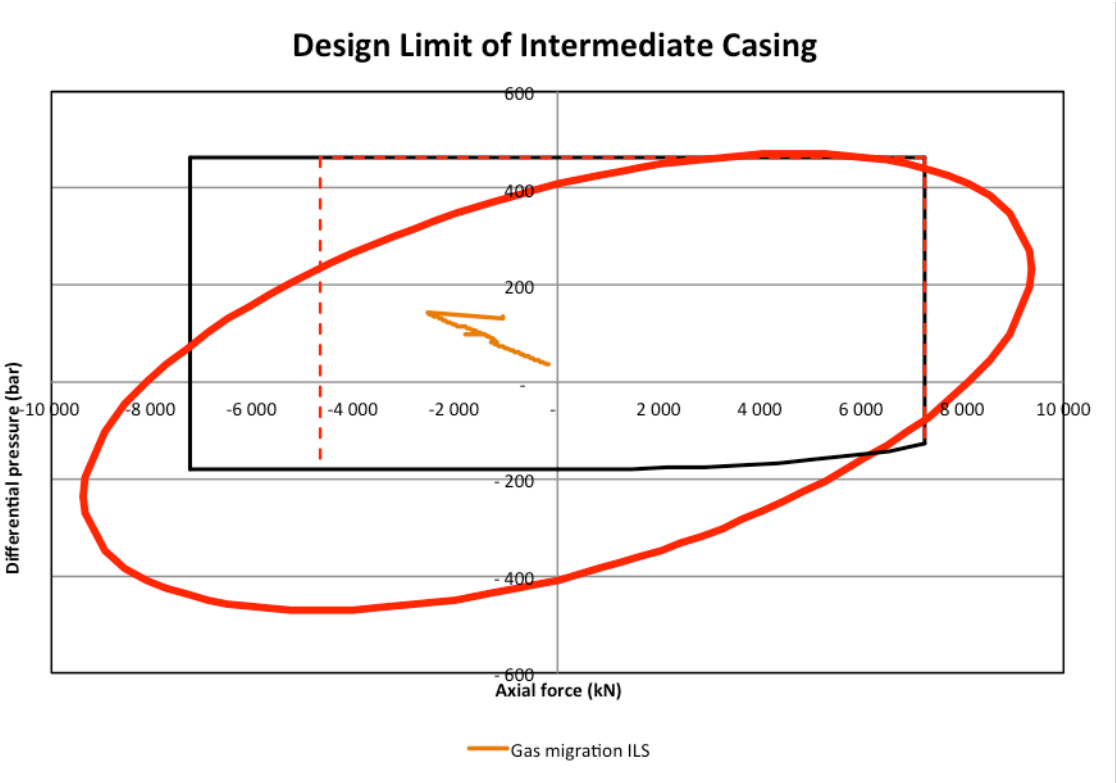

Figure C-1 Design limit plot to the intermediate casing with the gas migration load case applied. The data is extracted from ILS.

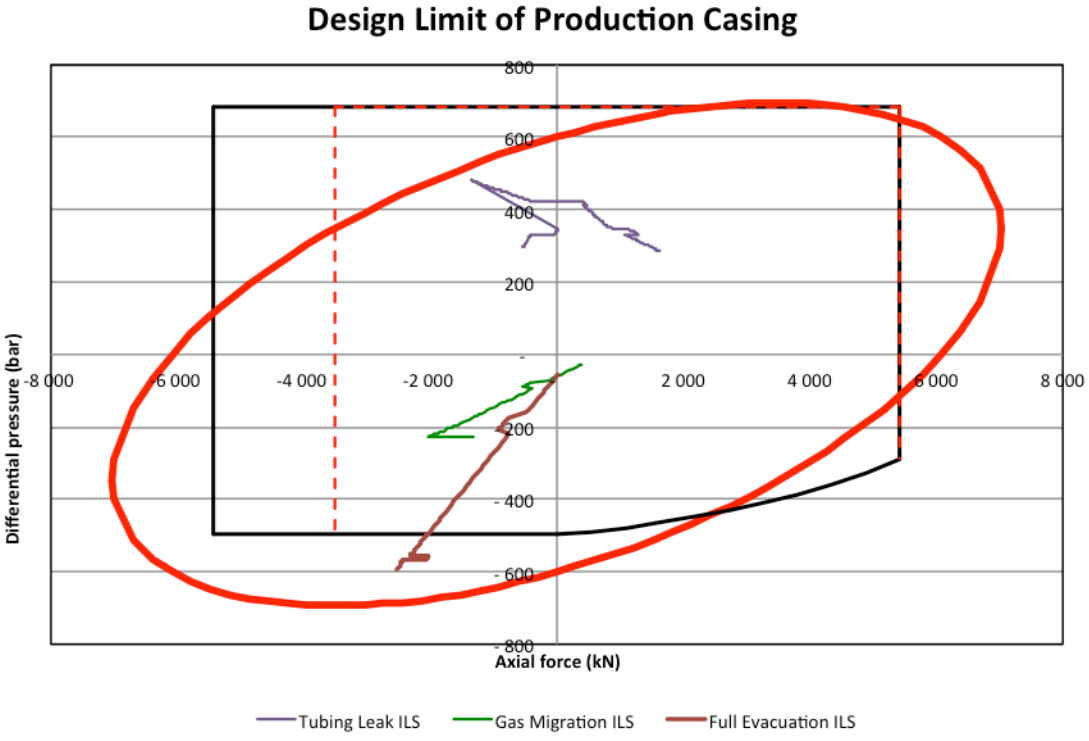

Figure C-2 Design limit plot to the production casing. The loads tubing leak, gas migration and full evacuation are applied to the casing. The data is extracted from ILS.

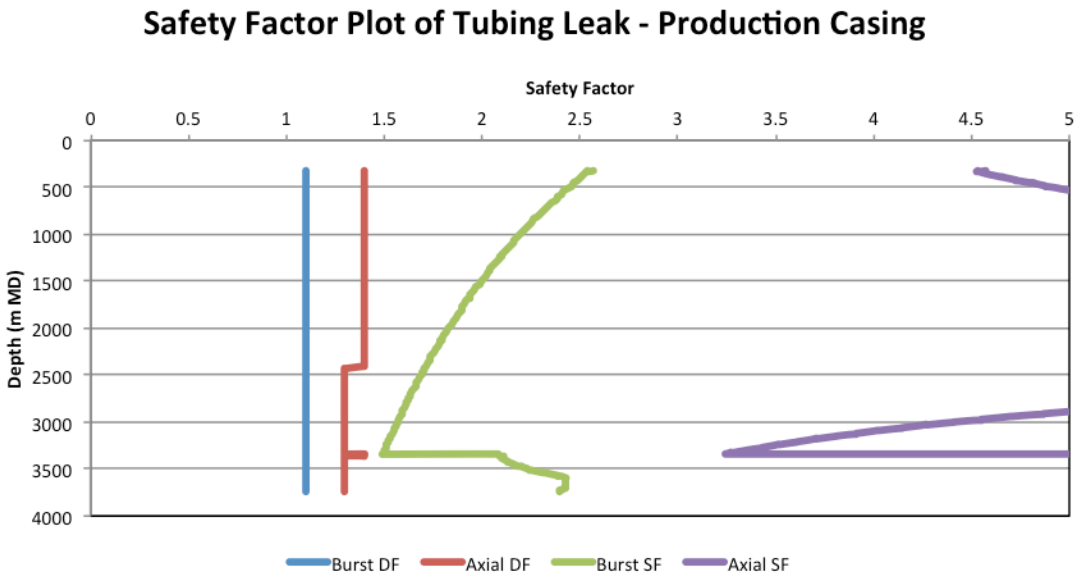

Figure C-3 Safety factors and design factors of the tubing leak case on the production casing.

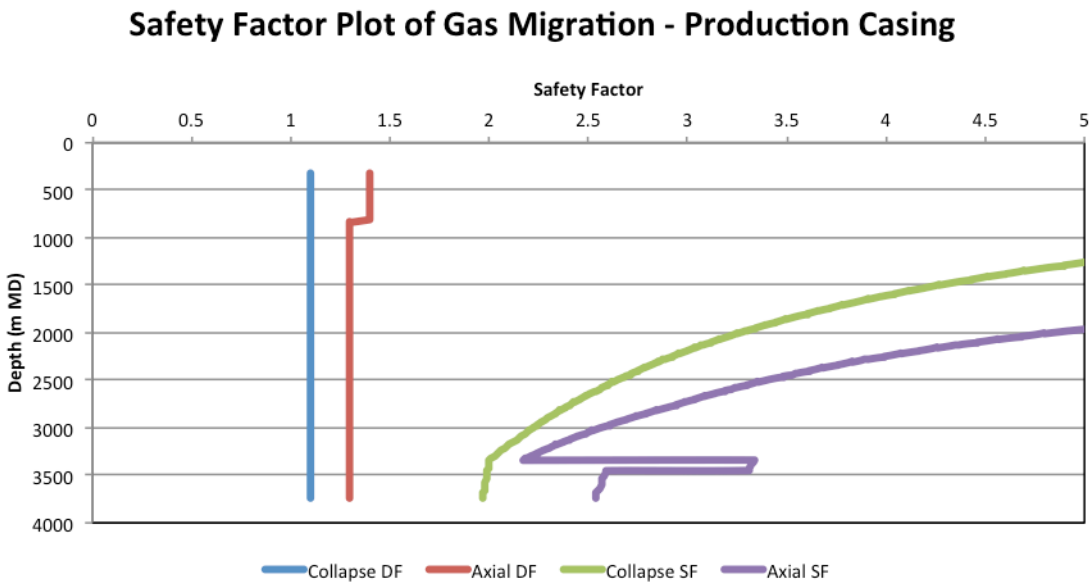

Figure C-4 Safety factors of the gas migration case on the production casing.

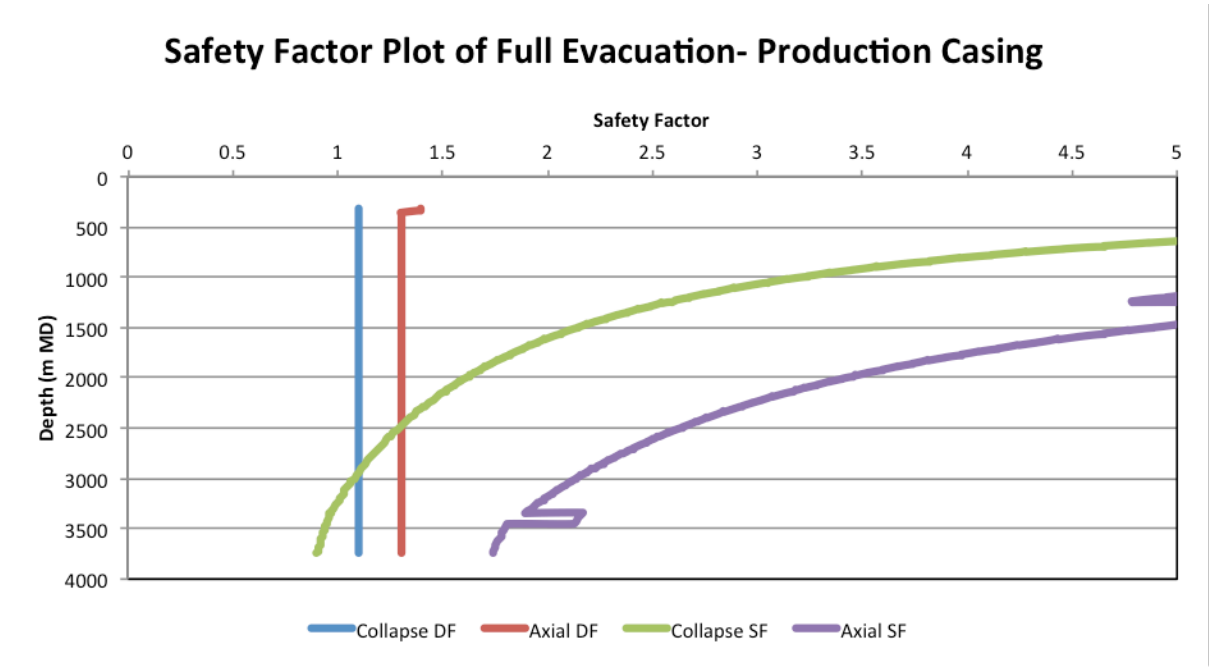

Figure C-5 Safety factors of the full evacuation case on the production casing. The collapse safety factor is less than the design factor of collapse, which indicates casing failure by collapse.

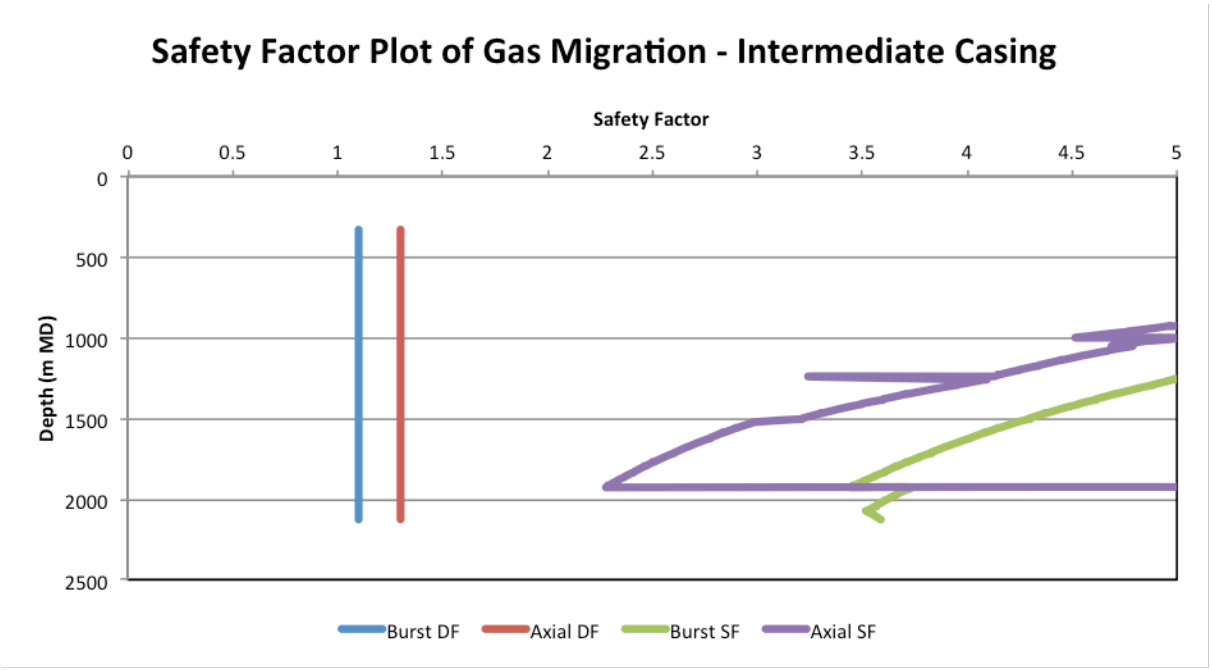

Figure C-6 Safety factors of gas migration on the intermediate casing.

Appendix D: Axial Loads based on Temperature Prediction by Casing Design Model

The following results are used to compare the difference in axial loads when using the temperature obtained in the casing design instead of the temperature from the ILS. The temperature from the casing design model is by using Hasan and Kabir (1994) paper. The temperature is based on a well with water in the annulus, while the ILS temperature used below is for a well with drilling mud in the annulus. The change in axial loads is small.

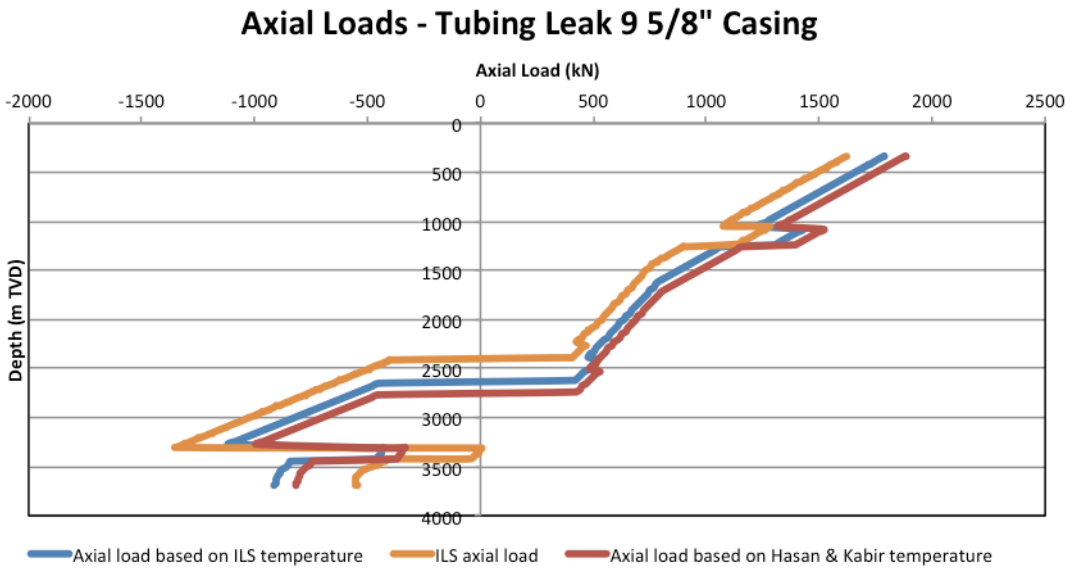

Figure D-1 Tubing leak burst load on the production casing. The axial loads are applied with temperature from the ILS and from the Hasan and Kabir. The axial load from the ILS is plotted for comparison.

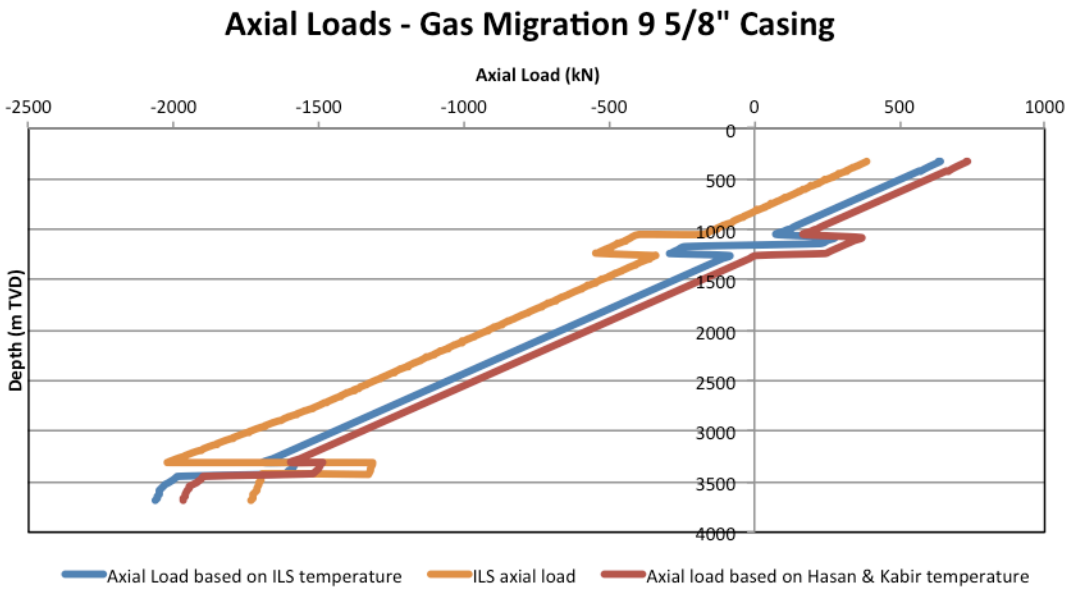

Figure D-2 Gas migration collapse load for the production casing based on the ILS temperature and the Hasan and Kabir temperature.

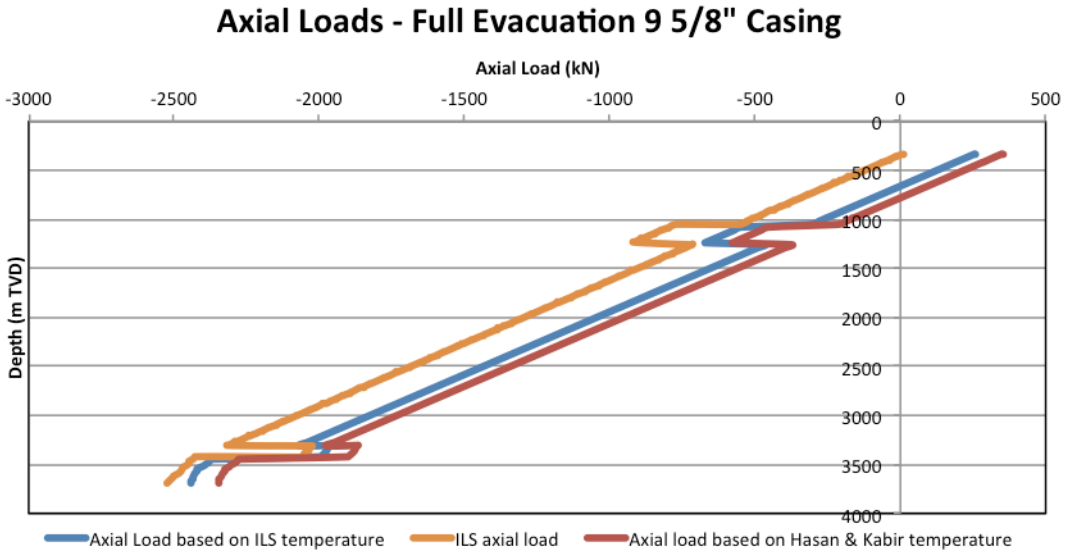

Figure D-3 Full Evacuation collapse load for the production casing. The axial loads are based on the ILS temperature and Hasan & Kabir temperature.

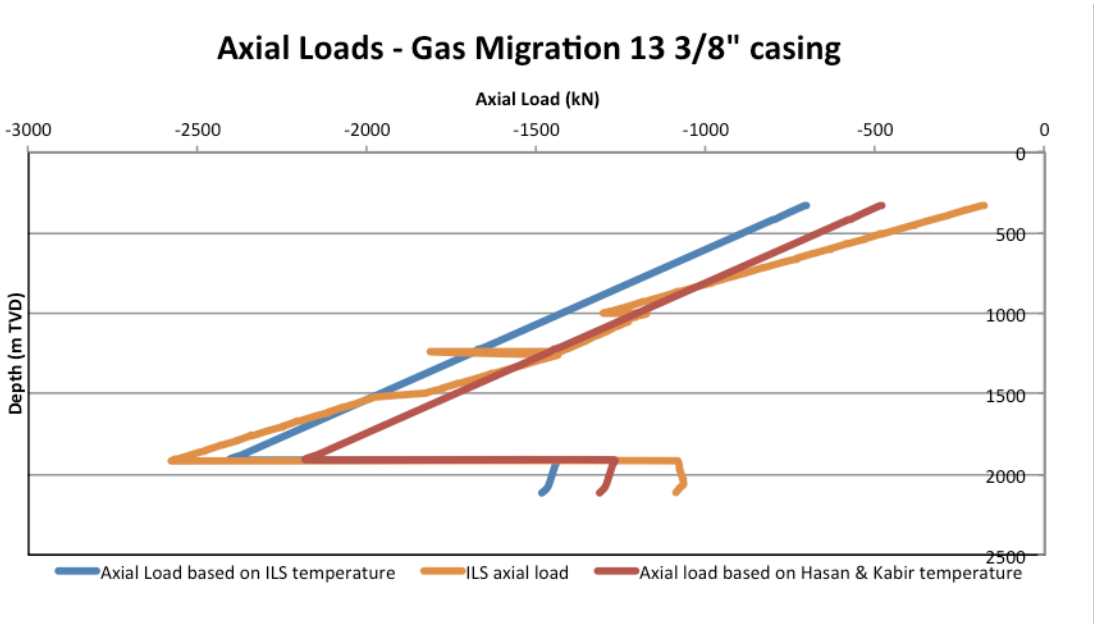

Figure D-4 Gas migration burst load for the intermediate casing based on different temperatures. The axial load by casing design model is based on the ILS temperature and on the temperature from the Hasan & Kabir method.

Appendix E: Overview of Axial Loads in Load Cases

This chapter gives an overview of the resulting load cases working on the intermediate and production casing. The pressure and axial stress are listed for each load case.

Intermediate Casing

Gas Migration

- Burst pressure
- Axial load depending on
  - Weight: the weight at initial condition with tension at the top and compression at the bottom. The cemented part of the casing has reduced compression
  - Temperature: causes compression because the steel expands when exposed to production temperatures
  - Ballooning effect: causes tension in the string because the internal pressure increases and external pressure decreases.
  - Bending: The intermediate casing has bending. The bending of the casing causes compression in the bended area. Buckling occur in the bended section. The buckling causes greater stress than the bending for this particular case, the bending stress is therefore neglected.
  - Buckling: There is helical buckling for the entire length of the casing, except the cemented part. The buckling causes compression.

Production Casing

Tubing Leak

- Burst pressure
- Axial load
  - Weight: the weight at initial condition with tension at the top and compression at the bottom. The cemented part of the casing has reduced compression.
  - Temperature: causes compression because the steel expands when exposed to production temperatures
  - Ballooning effect: causes tension in the string because the internal pressure increases and external pressure decreases.
  - Bending: The production casing has bending. The bending of the casing causes compression at 3448-3692 m TVD and tension at 1080-1239 m TVD.

- Buckling: There is helical and sinusoidal buckling in the casing from 1644 – 3310 m TVD.

Gas migration

- Collapse pressure
- Axial load
  - Weight: the weight at initial condition with tension at the top and compression at the bottom. The cemented part of the casing has reduced compression,.
  - Temperature: causes compression because the steel expands when exposed to production temperatures
  - Ballooning effect: causes compression in the string because the internal pressure decreases and external pressure increases.
  - Bending: The production casing has bending. The bending of the casing causes compression at 3448-3692 m TVD, tension at 1080 – 1140 m TVD and compression at 1140 – 1239 m TVD.
  - Buckling: There is no buckling in the casing.

Full evacuation

- Collapse pressure
- Axial load:
  - Weight: the weight at initial condition with tension at the top and compression at the bottom. The cemented part of the casing has reduced compression.
  - Temperature: causes compression because the steel expands when exposed to production temperatures
  - Ballooning effect: causes compression in the string because the internal pressure decreases and external pressure increases.
  - Bending: the bending causes compression in both of the bended areas in the casing.
  - Buckling: There is no buckling in the casing.

Appendix F: Unit Conversion Factors

Table F-1 The table consists of unit conversion factors used in the casing design model.

From Oil Field Unit	To SI Unit	Multiplication Factor
Btu/lbm-°F	kJ/kg-°C	0.2389
ft	m	0.3048
lbm/ft^3	kg/m^3	16.02
lbf	N	4.448
psi	Pa	$14.50377x10^{-5}$

From Unit	To Unit	Multiplication Factor
ft	in	12
in	m	0.0254

Temperature conversions

$°F = °C \times 9/5 + 32$

$°R = °F + 459.67$